AD-A149 112 PICOSECOND LASER PULSE INTERACTIONS WITH METALLIC AND SEMICONDUCTOR SURFACES(U) HARVARD UNIV CAMBRIDGE MA DIV OF APPLIED SCIENCES N BLOEMBERGEN ET AL. 01 NOV 84 1/2

UNCLASSIFIED N00014-83-K-0030 F/G 20/5 NL

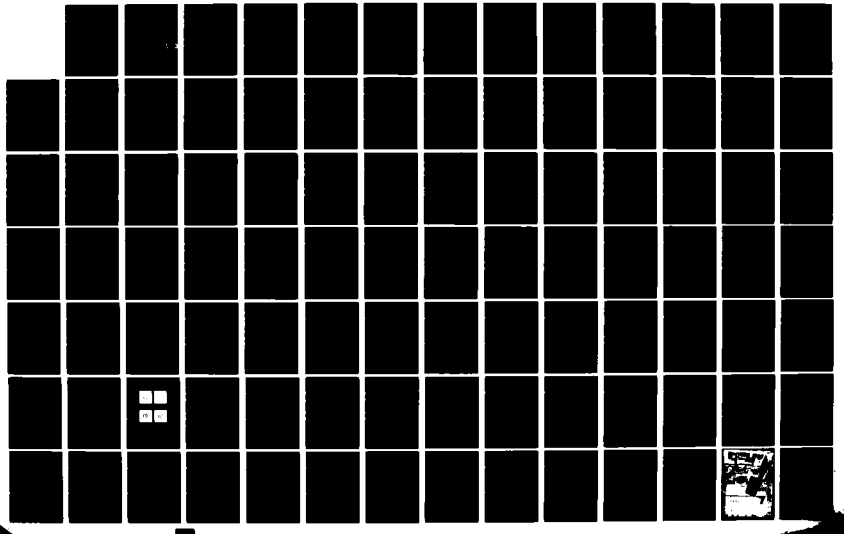

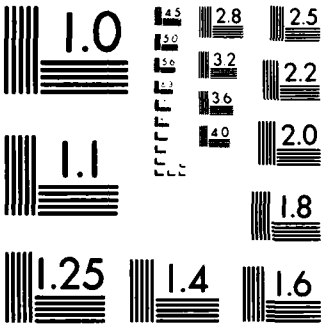

Unclassified
SECURITY CLASSIFICATION OF THIS PAGE (When Data Entered)

AD-A149 112

REPORT DOCUMENTATION PAGE

READ INSTRUCTIONS BEFORE COMPLETING FORM

1. REPORT NUMBER: Annual Progress Report No. 2	2. GOVT ACCESSION NO.: AD-A149 112
3. RECIPIENT'S CATALOG NUMBER:	
4. TITLE (and Subtitle): Picosecond Laser Pulse Interactions with Metallic and Semiconductor Surfaces	5. TYPE OF REPORT & PERIOD COVERED: Annual Technical Report Nov. 1, 1983 - Oct. 31, 1984
	6. PERFORMING ORG. REPORT NUMBER:
7. AUTHOR(s): Nicolaas Bloembergen and Frans Spaepen	8. CONTRACT OR GRANT NUMBER(s): N00014-83-K-0030
9. PERFORMING ORGANIZATION NAME AND ADDRESS: Division of Applied Sciences, Harvard University, Cambridge, MA 02138	10. PROGRAM ELEMENT, PROJECT, TASK AREA & WORK UNIT NUMBERS:
11. CONTROLLING OFFICE NAME AND ADDRESS: Office of Naval Research, 800 N. Quincy Street, Arlington, VA 22217	12. REPORT DATE: November 1, 1984
	13. NUMBER OF PAGES: 5 + 13 appendices = 96 pages
14. MONITORING AGENCY NAME & ADDRESS (if different from Controlling Office)	15. SECURITY CLASS. (of this report): Unclassified
	15a. DECLASSIFICATION/DOWNGRADING SCHEDULE:

16. DISTRIBUTION STATEMENT (of this Report)

This document has been approved for public release and sale; its distribution is unlimited.

17. DISTRIBUTION STATEMENT (of the abstract entered in Block 20, if different from Report)

Approved for public release, distribution unlimited.

DTIC ELECTE JAN 15 1985 S D A

18. SUPPLEMENTARY NOTES

19. KEY WORDS (Continue on reverse side if necessary and identify by block number)

Laser-Materials Interactions, Picosecond Pulses, Metallic and Semiconductor Surfaces, Phase Transitions, Ultrafast Heating and Cooling.

20. ABSTRACT (Continue on reverse side if necessary and identify by block number)

Picosecond heating and cooling experiments on silicon surfaces are reported. The surfaces are probed by a picosecond pulse, following the heating pulse, as a function of wave length, time delay and energy fluence. Picosecond laser-induced transformations of modulated metal films extend the glass formation range. New glassy alloys have been formed.

DD FORM 1 JAN 73 1473 EDITION OF 1 NOV 65 IS OBSOLETE
S/N 0102-014-6601

Unclassified
SECURITY CLASSIFICATION OF THIS PAGE (When Data Entered)

HARVARD UNIVERSITY
Division of Applied Sciences
Pierce Hall, 29 Oxford Street
Cambridge, Massachusetts 02138

Annual Progress Report
ONR Contract N00014-83-K-0030
For Period: November 1, 1983 - October 31, 1984

A. Picosecond Laser Interactions with Semiconductors

The personnel associated with this project during this reporting period consisted of:

Dr. N. Bloembergen, Principal Investigator

Dr. H. Kurz, Senior Research Fellow

Dr. A. M. Malvezzi, Research Fellow

Dr. D. von der Linde, Visiting Scholar (3/1/84-9/30/84)

Dr. G.-Z. Yang, Visiting Scholar (from 1/1/84)

Optical probing with picosecond pulses at various wavelengths of the complex index of refraction of thin semiconducting samples of silicon and germanium, in which energy has been deposited by preceding picosecond pulses, has provided firm quantitative experimental evidence that the energy absorbed by carriers gets transferred to the lattice on time scales shorter than one picosecond. If the energy absorbed per unit surface area is sufficient, melting and superheating of the fluid also occurs on such time scales. These findings have been published or presented at international meetings.

During the past year we have obtained evidence that a GaAs surface layer irradiated by a green pulse (λ = 530 nm) of 20 ps duration also undergoes a transition to the molten phase on a picosecond time scale. In this case a different optical probing technique was used. The incident light pulse, polarized along the (1,1,1) crystallographic direction, creates a second harmonic

reflected ray. The second harmonic energy generated at $\lambda = 265$ nm is proportional to the square of the incident intensity, as long as the sample remains crystalline. When a layer equal to the absorption depth at $\lambda = 265$ nm has melted, the second harmonic generation shows no further increase. The results lead to an energy transfer time between the hot, dense carrier plasma and the lattice vibrations of less than two picoseconds.

A careful observation and analysis of the photoelectric emission induced by $\lambda = 265$ nm picosecond pulses from a silicon crystalline surface has also been completed. The data show, besides the ordinary linear photoelectric effect, an emission proportional to the square of the intensity. This is due to photoemission from the hot, dense carrier plasma created by the same pulse, or by a preceding picosecond pulse. The lifetime of this plasma surface layer is limited by diffusion of the hot carriers out of the shallow absorption depth for $\lambda = 265$ nm radiation. The effect of space charge limitation of the electron emission in an intensity regime before melting occurs has also been demonstrated. After the onset of melting, evaporation of atoms and ions from the superheated fluid silicon takes place. The positive ions reduce the space charge, and the number of emitted electrons equals that of the emitted positive ions.

Further details on this work may be found in the appendices, which are preprints or reprints of technical papers. This material was also presented at several international meetings. Dr. H. Kurz presented invited papers at the International Conference on Quantum Electronics in Anaheim, California, in June 1984, and will also present an invited review of this field at the forthcoming meeting of the Materials Research Society in Boston, Massachusetts, in November 1984.

Recent experiments have focused on the problem of evaporation of neutral

particles from the superheated fluid. It has been established that the silicon readily reaches a temperature over 5000 K at a fluence of 500 mJ/cm^2. Thin film SOS samples are blown off, and the blow-off phenomenon has hampered the study of the rate of evaporation.

Theoretical calculations on the variation of the effective mass of the carriers at high temperatures and densities have been completed. They tend to confirm that the effective mass remains much smaller than the free electron mass up to densities of 10^{21} carriers/cc and up to the melting point.

During the next year attention will be focused on the additional damping or energy transfer which may occur when the plasma frequency of the carrier gas exceeds the band gap energy. It should be possible to investigate this new regime experimentally in germanium. An attempt will also be made to measure the evaporation rate from a superheated surface layer of fluid silicon created on a bulk single crystal of silicon. The evaporated atoms will be collected on a transparent sheet and their density measured by optical means. An additional program element will be the behavior of quantum well structures at high carrier densities, created by picosecond pulses.

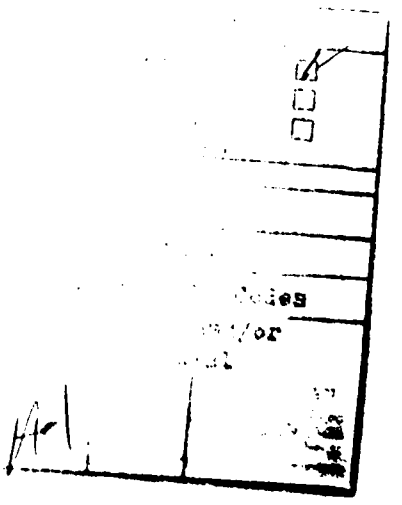

B. Picosecond Pulsed Laser Induced Transformations in Metals and Alloys

The personnel associated with this effort were:

F. Spaepen, Principal Investigator

W.K. Wang, Research Fellow

T. Mizoguchi, Visiting Scientist (summer)

C.A. MacDonald, Graduate Student

S.M. Prokes, Graduate Student (summer)

L.C. Chen, Graduate Student

We have continued the program on the formation of alloys by pulsed laser heating, mixing, and quenching. We have concentrated mainly on the Nb-Si system, which is of interest for its superconducting properties. The starting materials were made by ion beam sputtering, in our recently developed apparatus (see below, and attached report), and consisted of three types:

1. Homogeneous $Nb_{93}Si_7$, which is a microcrystalline Nb(Si) solid solution with lattice parameter a = 3.47 Å.
2. Compositionally modulated $Nb_{75}Si_{25}$ (period 32 Å), consisting of fine grained pure Nb and amorphous Si layers.
3. Compositionally modulated $Nb_{81}Si_{19}$ (period 48 Å), of the same structure as 2 above.

After laser irradiation (30 ps YAG or 30 ns ruby laser pulses), the following structural changes were observed:

1. The composition modulation, observed by x-ray diffraction, decayed as a result of large fluence irradiation.
2. The $Nb_{75}Si_{25}$ modulated films transformed to a bcc Nb(Si) solid solution with lattice parameter a = 3.30 Å after 30 ns irradiation.
3. The $Nb_{81}Si_{19}$ modulated films transformed to an as yet unidentified

phase (in electron diffraction) after 30 ns irradiation.

4. The $Nb_{81}Si_{19}$ modulated films transformed to a bcc Nb(Si) solid solution with lattice parameter a = 3.45 Å after 30 ps irradiation.
5. The $Nb_{93}Si_{7}$ films transformed into a mixture of an a-15 type Nb_3Si, bcc Nba and γ-Nb_5Si_3 after 30 ns irradiation.

Some preliminary investigation of the superconducting properties of these materials has been made. It has become clear that an inductive rather than a resistive method would be preferable for measurements on the small amounts of transformed material available after laser pulse induced transformation.

Glass formation in marginally glass forming alloys, which formed the bulk of last year's work, was continued on the Fe-C system, in which so far no glasses could be made from the melt by conventional quenching methods. Preliminary investigations show that 30 ps laser quenching leads to glass formation in alloys containing 15 and 25 at.% C.

We have continued our study on the direct measurement of the crystal growth velocity and solute trapping in pure metals and simple alloys. The pump-probe technique has been improved to give better statistics. We have also begun to investigate interdiffusion in the liquid and subsequent solute trapping in modulated films, using Auger spectroscopy and x-ray diffraction.

We have made extensive use of the new dual gun ion beam sputtering apparatus developed in this project for the preparation of starting materials. A copy of a technical report on it is attached. It has proved very versatile in producing both homogeneous alloys and various compositionally modulated films.

Appendix 1

OFFICE OF NAVAL RESEARCH

PUBLICATIONS/PATENTS/PRESENTATIONS/HONORS REPORT

for

1 October 1983 through 30 September 1984

for

Contract N00014-83-K-0030

Task No. NR SRO-150

Picosecond Laser Pulse Interactions with Metallic and Semiconducting Surfaces

N. Bloembergen and F. Spaepen
Principal Investigators

Harvard University
Division of Applied Sciences
Cambridge, Massachusetts 02138

a. Papers Submitted to Refereed Journals (and not yet published)

1. A.M. Malvezzi, J.M. Liu and N. Bloembergen, 'Second harmonic generation in reflection from crystalline GaAs under intense picosecond laser irradiation', Appl. Phys. Lett., to be published in November 1984.

2. A.M. Malvezzi, H. Kurz and N. Bloembergen, 'Picosecond photoemission study of laser-induced phase transitions in silicon', to be published in the Proceedings of the Topical Meeting on Ultrafast Phenomena, Monterey, California, June 1984.

3. L.A. Lompré, J.M. Liu, H. Kurz and N. Bloembergen, 'Dynamics of dense electron-hole plasma and heating of silicon lattice under picosecond laser irradiation', to be published in the Proceedings of the Topical Meeting on Ultrafast Phenomena, Monterey, California, June 1984.

4. A.M. Malvezzi, H. Kurz and N. Bloembergen, 'Nonlinear photoemission from picosecond irradiated silicon', submitted for publication in Appl. Phys. A (Springer, Heidelberg).

5. F. Spaepen and C.J. Lin, 'Partitionless crystallization and glass formation in Fe-B alloys during picosecond pulsed laser quenching', Mat. Res. Soc. Symposia Proceedings, in press.

6. F. Spaepen, A.L. Greer, K.F. Kelton and J.L. Bell, 'An ion beam sputtering apparatus for fabrication of compositionally modulated materials', ONR Technical Report and to be published.

Papers 1 and 4 also received partial support from the Joint Services Electronics Program under contract N00014-84K-0465

b. Papers Published in Refereed Journals

1. L.A. Lompré, J.M. Liu, H. Kurz and N. Bloembergen, 'Optical heating of electron-hole plasma in silicon by picosecond pulses', Appl. Phys. Lett. 44, 3-5 (1984).

2. H.M. van Driel, L.A. Lompré and N. Bloembergen, 'Picosecond time-resolved reflectivity and transmission at 1.9 and 2.8 μm of laser-generated plasmas in silicon and germanium', Appl. Phys. Lett. 44, 285-287 (1984).

3. J.M. Liu, L.A. Lompré, H. Kurz and N. Bloembergen, 'Phenomenology of picosecond heating and evaporation of silicon surfaces coated with SiO_2 layers', Appl. Phys. A 34, 25-29 (1984).

4. L.A. Lompré, J.M. Liu, H. Kurz and N. Bloembergen, 'Picosecond time-resolved optical studies of plasma formation and lattice heating in silicon', in Mat. Res. Symp. Proc., Vol. 23, (Elsevier, Amsterdam, 1984), pp. 57-62.

5. A.M. Malvezzi, J.M. Liu and N. Bloembergen, 'Photoelectric emission studies from crystalline silicon at 266 nm', Mat. Res. Symp. Proc., Vol. 23 (Elsevier, Amsterdam, 1984), pp. 135-139.

6. C.J. Lin, F. Spaepen and D. Turnbull, 'Picosecond pulsed laser-induced melting and glass formation in metals', J. Non-Cryst. Solids, 61/62, 767 (1984).

Papers 1, 2 and 3 also received partial support from the Joint Services Electronics Program under contract N00014-84-K-0465

c. Books (and sections thereof) Submitted for Publication

None.

d. Books (and sections thereof) Published

None.

e. Patents Filed

None.

f. Patents Granted

None

g. Invited Presentations at Topical or Scientific/Technical Society Conferences

In January 1984 Professor N. Bloembergen opened the Office of Naval Research Distinguished Speaker Colloquium Series with a presentation, 'Nonlinear Optics and Spectroscopy'.

Dr. H. Kurz presented an invited paper at the International Conference on Quantum Electronics in Anaheim, California, June 1984, on 'Physics of Laser Annealing of Semiconductors'.

i. Honors/Awards/Prizes

Professor Nicolaas Bloembergen was elected a member of the National Academy of Engineering, Washington, D. C., in April 1984.

Professor N. Bloembergen was also elected an honorary lifetime member of the Optical Society of America.

Appendix 2

Dynamics of Dense Electron-Hole Plasma and Heating of Silicon Lattice under Picosecond Laser Irradiation

L. A. Lompré*, J. M. Liu**, H. Kurz and N. Bloembergen

Division of Applied Sciences, Harvard University, Cambridge, MA 02138, USA

Numerous investigations of the mechanisms for pulsed laser-induced phase transition provide ample evidence that the surface of metals and semiconductors undergoes a solid-liquid phase change as soon as a critical laser fluence is exceeded. There is no doubt about the thermal nature of the phase transition as long as nanosecond pulses are being used [1]. It is the main purpose of this contribution to clarify whether under picosecond irradiation the simple thermal melting approach is still valid. This question is focused on the time required to establish thermal equilibrium between carriers and phonons [2].

The conventional picosecond pump and probe technique is applied [3,4]. The highly focused probe beam monitors the transmission and reflectivity of bulk surfaces on thin silicon films on sapphire (SOS), induced by an exciting picosecond pulse at 0.532 μm. The wavelength of the probe pulse is varied between 0.532 and 2.8 μm. By comparing the changes in optical properties at different wavelengths, the contributions due to a variation in lattice temperature T_L and those due to changes in carrier density N are separately determined [5].

At the doubled frequency of a Nd:YAG laser ($h\omega$ = 2.33 eV), the optical properties of picosecond-excited silicon are mainly determined by the indirect gand gap transition. The phonon-assisted indirect absorption α depends strongly on the lattice temperature T_L [6]. In SOS samples multiple reflections from air-silicon and silicon-sapphire interfaces enhance the optical detectivity of changes $\Delta\varepsilon$ in the real part of the dielectric functions considerably. Time-resolved analysis of the reflectivity signatures of SOS samples reveal the interplay between thermal ($\Delta\varepsilon > 0$) and free carrier ($\Delta\varepsilon < 0$) contributions to ε [9]. Due to Auger recombination the plasma density is known to drop below 1.2×10^{20} cm^{-3} after 200 ps. At this time the plasma contributions become negligible at 0.532 μm and the amount of lattice heating can be determined experimentally by comparing samples with different film thicknesses [5].

In Fig. 1 the surface temperature developed 200 ps after the exciting pulse is shown. Picosecond optical probing of lattice temperature reveals significantly higher values than those derived up to now from Raman scattering data using ns pulses. Compared to bulk surfaces (F_{th} = 200 mJ/cm^2), SOS samples exhibit a lower threshold value for surface melting (160 mJ/cm^2). Because of multiple interferences in SOS samples, a larger amount of energy density is absorbed in the silicon film. The absorbed energy density in 0.5 μm thick silicon films is determined by reflectivity and transmission measurements of the pump beam (see top of Fig. 1). The surface temperature increases non-

*Permanent address: C.E.N./Saclay, DPh.G/S.P.A., 91191 Gif-sur-Yvette Cedex, France

**Present address: GTE Laboratories, 40 Sylvan Road, Waltham, MA 02154, USA

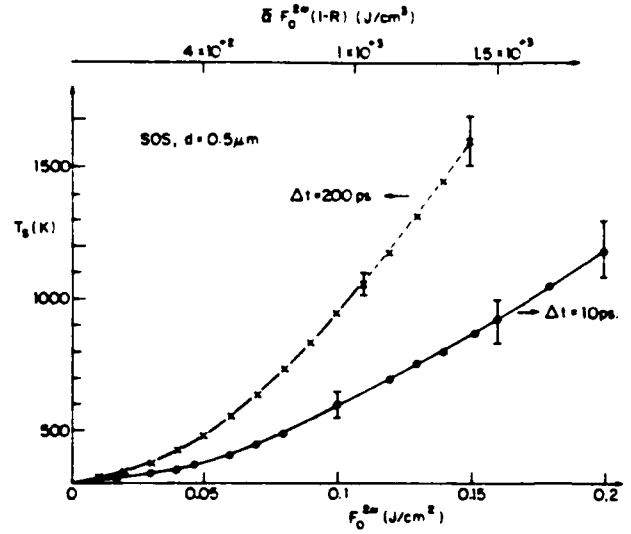

Fig. 1. Surface temperatures T_s versus incident laser fluence at 10 and 200 ps after the heating pulse at 0.532 μm. The data are evaluated from time-resolved reflectivity and transmission measurements on SOS samples using the thermo-optic data of ref. [6]

linearly with the laser fluence $F(2\omega)$ and reaches values close to the melting point of silicon (T_m = 1680 K) at a fluence level (160 mJ/cm^2) where the reflectivity increases rapidly to the liquid state value. Obviously lattice heating and melting occur during the pump pulse. The band gap shrinks nearly instantaneously, resulting in an increase of the pump beam absorbance. This picture is confirmed by measuring the transmission at time delays shorter than the pulse duration. At a time delay of Δt = 10 ps, significant lattice heating already occurs. The result shown in Fig. 1 is obtained by temporal deconvolution of the heating and probing pulse. Plasma contribution has been properly taken into account. Clearly, phonons participating in the indirect absorption process received a significant amount of energy deposited primarily in the electron-hole plasma. The observed transmission changes are in excellent agreement with the optical heating model, where an instantaneous energy transfer to the phonons is assumed.

At a probing frequency below the indirect band gap, free carrier contribution becomes dominant. Drude-like plasma resonances have been observed at 2.8 μm [7]. They have been used for a preliminary estimate of plasma densities far below the threshold for melting. At this probing wavelength the plasma edge is reached at a fluence level of 40 mJ/cm^2 already. Strong free carrier absorption causes transmission drops to zero, preventing a reliable determination of the maximum plasma density at higher fluence levels. For this purpose thin film and bulk crystals are carefully investigated at 1.064 and 1.9 μm. At these probe wavelengths the plasma contributions are less pronounced, and measurements up to the melting point can be performed. This study is completed by a novel three-pulse technique, where the first pulse at 0.532 μm creates carriers, a second pump pulse at 1.064 μm couples energy to the plasma by free carrier absorption without creating new carriers, and a third pulse monitors the induced optical changes [8]. The plasma heating of the second pulse does not affect the susceptibility associated with intraband (Drude) and interband transitions. Neither the reduced mass m* nor the density of electron-hole pairs is changed by additional heating of the plasma. The probability of carrier multiplication by impact ionization is very low [8,9]. The energy loss rate of the carriers to the phonons is faster than the rate for impact ionization, which is expected to be comparable to the Auger recombination rate.

As a selected example, the transmission of bulk silicon at 1.064 μm is plotted versus incident laser fluence for two different time delays Δt in

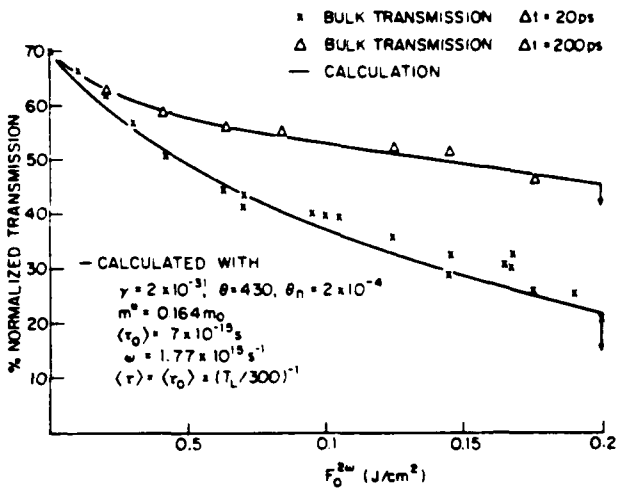

Fig. 2. Transmission of bulk silicon at 1.064 μm versus incident laser fluence at 0.532 μm for two different time delays between pump and probe pulse

Fig. 2. At Δt = 200 ps the plasma density levels off to a constant value above $F(2\omega)$ = 50 mJ/cm^2 due to the nonlinearity of the Auger recombination process. The lattice temperature, however, increases strongly with $F(2\omega)$. Under these conditions the free carrier absorption at 1.064 μm associated with intraband transitions is proportional to $[m^* \langle\tau\rangle (2\gamma t)^{\frac{1}{2}}]^{-1}$, where m^* means the reduced optical mass for electron-hole pairs, $\langle\tau\rangle$ the energy averaged momentum relaxation time of the carriers, and γ the Auger recombination coefficient.

The solid line in Fig. 2 represents calculated transmission values of bulk silicon using $\gamma = 2 \times 10^{-31}$, $m^* = 0.164\ m_0$ and averaged momentum relaxation time $\langle\tau\rangle = 7 \times 10^{-15} \times 300/T_L$, as found in ns experiments [10]. The agreement between measured and calculated data is excellent, indicating a strong phonon participation in the carrier momentum relaxation, even at plasma density levels at which electron-hole scattering dominates the relaxation process. The same calculation provides satisfactory results for the transmission at Δt = 10 ps, where the plasma density depends on the laser fluence $F(2\omega)$. In this case the plasma density has been calculated with the standard equations, including ambipolar diffusion and neglecting impact ionization. The calculated evolution of plasma density and temperature at the surface of silicon irradiated with increasing laser fluence $F(2\omega)$ are finally summarized in Fig. 3. These calculated data are cross checked with experimental data at different probing wavelengths, excitation levels and time delays. They have been used to analyze the dependence of the optical reduced mass on the carrier density in reflectivity measurements. Excellent agreement with the data at 1.064, 1.9 and 2.8 μm has been found up to a fluence level of 150 mJ/cm^2, for a constant optical reduced mass of $(0.16 \pm 0.1)m_0$. The stability of the Drude term indicates a "cold plasma" which is in thermal equilibrium with the lattice. Close to the threshold value for melting, the maximum plasma density is limited to 1.4×10^{21} cm^{-3}, mainly due to Auger recombination. The measured values of lattice temperature and maximum plasma density are consistent with optical heating and thermal melting even on a time scale of picoseconds.

This research was supported by the U.S. Office of Naval Research under contract N00014-83K-0030 and by the Alexander von Humboldt Foundation, F. R. Germany.

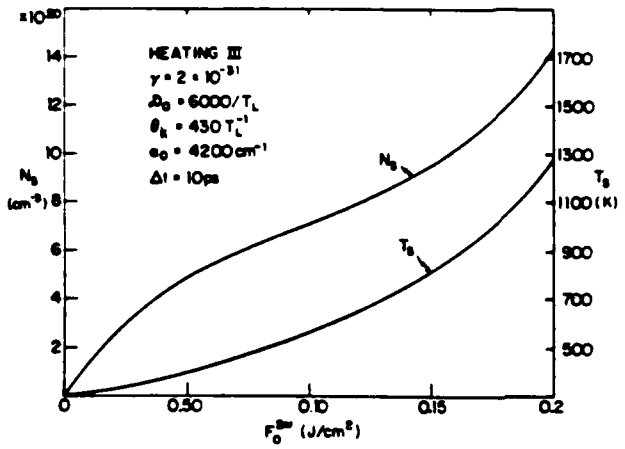

Fig. 3. Calculated plasma densities and temperatures at the surface of bulk silicon versus incident laser fluence at 0.532 μm using the optical heating model with instantaneous energy transfer during the picosecond pulse.

References

1. D.H. Auston, C.M. Surko, T.N.C. Venkatesan, R.E. Slusher, J.A. Golovchenko: Appl. Phys. Lett. 33, 437 (1978)
2. J.M. Liu, R. Yen, H. Kurz, N. Bloembergen: Appl. Phys. Lett. 39, 755 (1981); R. Yen, J.M. Liu, H. Kurz, N. Bloembergen: Appl. Phys. Lett. A 27, 153 (1982)
3. J.M. Liu, H. Kurz, N. Bloembergen: Appl. Phys. Lett. 41, 643 (1982)
4. D. von der Linde, N. Fabricius: Appl. Phys. Lett. 41, 991 (1982)
5. L.A. Lompré, J.M. Liu, H. Kurz, N. Bloembergen: Appl. Phys. Lett. 43, 168 (1983)
6. G.E. Jellison, F.A. Modine: Appl. Phys. Lett. 41, 180 (1982)
7. H. van Driel, L.A. Lompré, N. Bloembergen: Appl. Phys. Lett. 44, 285 (1984)
8. L.A. Lompré, J.M. Liu, H. Kurz, N. Bloembergen: Appl. Phys. Lett. 44, 3 (1984)
9. L.A. Lompré, J.M. Liu, H. Kurz: Proc. Mat. Res. Soc. Symposium, Boston 1983
10. K.G. Svantesson: J. Phys. D, Appl. Phys. 12, 425 (1979)

PHOTOELECTRIC EMISSION STUDIES FROM CRYSTALLINE SILICON AT 266 NM

A. M. MALVEZZI, J. M. LIU,* AND N. BLOEMBERGEN
Division of Applied Sciences, Harvard University, Cambridge, MA 02138; *Present address: Department of Electrical and Computer Engineering, Bell Hall, SUNY at Buffalo, Amherst, NY 14260.

ABSTRACT

Three different photoelectric regimes are observed in the interaction of 15 ps, 266 nm laser pulses with crystalline silicon samples versus light fluence. A superposition of linear and quadratic photoionization is followed by a space charge limited regime up to the critical fluence $F_{th}^{\blacktriangle}$ for the surface amorphization where highly nonlinear ion emission is observed. Ion and electron emissions become equal in magnitude at a fluence $\sim 2F_{th}^{\blacktriangle}$. The absence of observable thermionic effects indicates that thermal equilibrium of the electron-hole plasma and the lattice is reached during the laser pulse duration.

INTRODUCTION

The central question in the investigation of pulsed laser annealing of semiconductors in the picosecond range is related to the time scale of the energy transfer between the hot electron-hole plasma created by the laser pulse and the crystal lattice. In recent times much experimental effort has been devoted to the study of this energy transfer. This goal has been mostly pursued through optical diagnostic methods, either by measuring the optical constants of the semiconducotrs with pump and probe techniques [1] or by direct derivation of the lattice temperature from Stokes and anti-Stokes Raman scattering [2].

Measurements of the electron and ion emission from the semiconductor surface during the interaction with picosecond laser pulses offers an alternative approach to the problem. Here, one probes the material only in its outermost layers, and therefore the data are insensitive to the gradients in the profiles of plasma density or lattice temperature. Thermionic emission is extremely sensitive to the electron temperature. Conversely, the emission of positive ions is an indicator of a hot lattice.

In this paper detailed measurements of the charges emitted by crystalline silicon samples irradiated with 266 nm, 15 ps laser pulses are reported. This work extends the measurements of Liu et al. [3] to laser fluences about four orders of magnitude below the critical value for a surface phase transformation. One of the main results of this analysis is the absence of observable thermionic effects throughout the whole range of laser fluence. Thus, an upper limit to the average electron temperature of $\approx$ 3000 K within the laser pulse can be deduced.

EXPERIMENTAL METHOD

The source of excitation of the silicon samples is a 15 ps, 266 nm laser pulse obtained by frequency quadrupling the output of a Nd:YAG 30 ps laser pulse. The radiation is focused by quartz optics into a vacuum chamber in which the silicon sample is located. The angle of incidence is 48°, and the reflected portion of the beam escapes from the chamber through a second

Mat. Res. Soc. Symp. Proc. Vol. 23 (1984)

window. A 1 mm diameter wire placed at 2.5-3 mm from the sample surface acts as a charge collector. Both sample and wire are electrically insulated from the body of the vacuum chamber and can be independently biased up to $\mp$ 4 kV. Two configurations for the measurements are possible. One can measure either the charges collected on the wire or the ones escaping from the sample. Both methods have been shown to give similar results. Most of the measurements, however, have been performed by measuring the total charges escaping from the target. A charge amplifier connected to the sample collects the charges and provides a signal proportional to the collected charges to the data acquisition system. The calibration of the amplifier has been checked for high charge signals against the charge signal obtained at the oscilloscope through a coaxial cable of known capacitance. The readings agree within a factor 1.5. An absolutely calibrated photodiode and neutral density filters provided the total energy value of each laser pulse. Laser and charge data were directly plotted by an automatic data acquisition system.

Measurements of the spatial beam profile on the target were performed for each experimental run by evaluating the area of the amorphous spots at various laser fluences, as described in reference [4].

The experiments were performed in a vacuum of 5×10^{-7}-5×10^{-8} Torr. The samples were Si (111) and Si (100) lightly doped p-samples with 1-5 Ω-cm and 15-50 Ω-cm, respectively.

RESULTS AND DISCUSSION

The electron and ion emission from Si (111) and Si (100) has been measured in many experimental runs with different focusing conditions. The (1/e) radius ρ of the laser intensity profile on the sample has been varied between 12 and 178 μm. The electron signal does not depend on the contamination of the sample surface. Cleaning procedures such as multiple shot exposure below the fluence for morphological surface damage [5] do not modify the observed features in the collected charges. Contrary to expectation, no qualitative difference in the emission has been found between Si (111) and Si (100) oriented samples, despite the differences in ionization potentials [6,7]. Presumably the surface oxide layer present on the samples exposed to air is not removed by laser pulse cleaning and thus lowers the ionization potential at the surface of the sample [8].

Figure 1 shows the total of collected electron and ion charges versus laser fluence in a typical plot for Si (111). The behavior of the electron emission can be divided into three regimes. At lower fluences (region I) we have a progressively nonlinear departure from a pure linear (slope = 1) relationship between electron signal and laser fluence $F^{4\omega}$. This indicates that the energetically allowed single photon effect is accompanied by a nonlinear photoelectric effect. In a second range of laser fluences (region II), a decrease in the slope of the curve is observed. The collected charge signal is here dependent upon the bias voltage and scales approximately with $V_{bias}^{0.75}$. This behavior is then interrupted at a fluence $F_{th}^{4\omega} = 0.08$ J/cm^2, where amorphous spot formation and positive ion emission occur simultaneously. Above $F_{th}^{4\omega}$ (region III) a steep increase of the electron emission occurs. In this regime each experimental point is obtained on a fresh portion of the sample. Ion emission, on the other hand, is characterized by a very steep behavior. There is no significant amount of ions emitted in regions I and II. The ion signal emerges from the noise at about one quarter of the critical fluence $F_{th}^{4\omega}$. The first part of the ion emission has a relatively low slope. It is followed by a jump-like behavior. Within 25% of the critical value $F_{th}^{4\omega}$ the emission increases by more than two orders of magnitude. At the critical fluence $F_{th}^{4\omega}$ for amorphous formation, the curve bends to a lower slope, and equal amounts of electrons and ions are observed

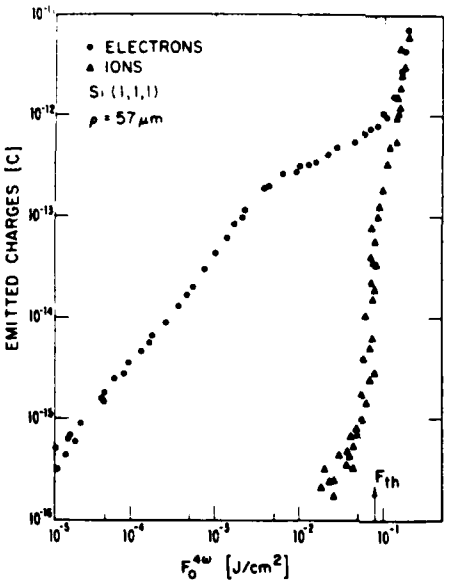

FIG. 1. Emitted charge versus incident laser fluence for (111) oriented silicon samples. The laser spot ρ at 1/e is 57 μm. Full dots, electrons; triangles, ions.

above $2F_{th}^{4\omega}$ in region III.

A more illustrative way of displaying these three regimes of electron emission is shown in Fig. 2, where the ratio Q/E_n of the total electron charge Q to the incident laser energy E_n (in Joules) is plotted versus laser fluence $F(J/cm^2)$. The behavior at low fluences (region I) up to laser fluences $\sim F_{th}^{4\omega}/15$ is linear, as shown on an enlarged scale in Fig. 3. This indicates that a superposition of linear and quadratic ionization processes is effective in this range of laser fluences. The functional dependence of the current density $J(\vec{r},t)$ versus laser intensity $I(\vec{r},t)$ is described by

$$J(\vec{r},t) = k_1 \frac{I(\vec{r},t)e}{h\nu} + k_2\left(\frac{I(\vec{r},t)e}{h\nu}\right)^2$$

where e is the electron charge, hν the photon energy and k_1, k_2 the coefficients for linear and quadratic photoemission, respectively. Integrating this equation over the space and time with the Gaussian beam profile results in

$$\frac{Q}{E_n} = k_1 \frac{e}{h\nu} + \frac{k_2 e^2}{2\sqrt{2}\,(h\nu)^2 \tau} F .$$

Here τ is the laser pulse duration, E_n the total energy of the laser pulse (J) and F its fluence (J/cm^2).

The value of the quantum yield for single photon emission at 4.66 eV, as deduced from the experiment, equals $8(\mp 2) \times 10^{-7}$ electrons per absorbed photon, in agreement with data found in the literature for silicon samples exposed to air [7]. The experimental value for the quadratic effect, $3 \mp 1.5 \times 10^{-32}$ cm² s is consistent with the results obtained by Bensoussan et al. [9], if extrapolated to higher photon energies. This nonlinear process completely dominates the electron emission over a wide range of laser fluences. This can be attributed to a much higher escape probability for the two-photon excited electrons which have an intrinsically higher (up to ~ 4.6 eV) kinetic

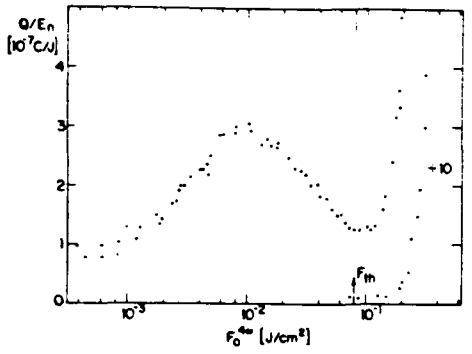

FIG. 2. The data are replotted in terms of the ratio Q/E_n (emitted negative charge over incident laser energy) versus incident laser fluence for Si (111).

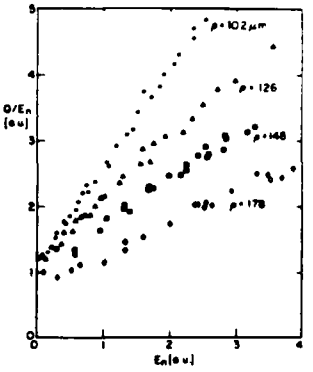

FIG. 3. Ratio Q/E_n of emitted negative charge to incident laser energy versus incident laser energy at different focusing conditions on a Si (111) sample. The values of the laser spot radii are shown for each curve.

energy than the electrons emitted by a single photon process, which have about 0.06 eV kinetic energy.

The nonlinear behavior at fluences higher than $\sim F_{th}^{4\omega}/15$ is masked by space charge limitations. This regime of emission depends on the bias voltage on the collecting electrode and cannot be neutralized at the highest bias voltages permissible in our experimental conditions. Space charges rapidly neutralize the applied fields at the surface. The electron emission is limited to the leading edge of the picosecond pulse.

Simultaneously with the observation of amorphous spot formation at the critical laser fluence $F_{th}^{4\omega}$, sharp rises in ion and electron emission occur. The ion emission has a step-like behavior, and the electron space charge limitation is suddenly released. These discontinuities show that the surface conditions of the sample are suddenly modified at this fluence, as one would expect for a phase transition to the molten state of silicon.

Thermionic emission is a very steep function of the electron temperature T_e. Therefore, it should manifest itself with a highly nonlinear behavior even in region I. In Fig. 3 the ratio Q/E_n versus incident laser energy E_n for various laser spot sizes in region I shows that the behavior is strictly linear. Thus the thermionic contribution below the saturation equals at most the accuracy of the data. Application of the Richardson-Dushman equation gives an upper limit of $\sim$ 2200 K for the average electron temperature during the laser pulse in region I. In region III the equal amounts of electrons and ions observed above $2F_{th}^{4\omega}$ reduce the possible thermionic emission contribution to less than 10^{-12} Coulombs in this regime. This gives an upper limit of $\sim$ 3000 K for the average electron temperature during the phase transition.

CONCLUSIONS

The results of our measurements can be summarized as follows. The electron charges collected at lower laser fluences must be attributed completely

to the superposition of single-photon photoemission and a quadratic photoelectric effect. No experimental evidence for thermionic emission is found in our measurements. This provides an upper limit of 3000 K to the average electron temperature $\bar{T}_e$ during the laser pulse duration. The data are consistent with the establishment of equilibrium between the carrier and the lattice temperature during the laser pulse (15 ps). A space charge limited regime is observed for the electron emission at fluences between $F_{th}^{4w}/15$ and F_{th}^{4w}. Sufficient charge densities (Coulombs/cm^3) can build up to screen the applied field in a fraction of the laser pulse duration. At the critical fluence for the phase transformation, melting resulting in subsequent formation of an amorphous pattern, the sudden release of the space charge regime and the appearance of positive charges are consistent with the notion of surface melting during the laser pulse [10].

REFERENCES

1. J.M. Liu, H. Kurz, and N. Bloembergen, Appl. Phys. Lett. 41, 693 (1982).
2. A. Compaan, M.W. Lee, A. Aydinli, and C.M. Lee, Mat. Res. Soc. Symp. Proc. 13, 35 (1983).
3. J.M. Liu, R. Yen, H. Kurz, and N. Bloembergen, Mat. Res. Soc. Symp. Proc. 4, 23 (1982).
4. J.M. Liu, Optics Lett. 7, 196 (1982).
5. R.T. Yen, Thesis, Harvard University (1981).
6. F.G. Allen and G.W. Gobeli, J. Appl. Phys. 35, 597 (1970).
7. R.M. Broudy, Phys. Rev. B 1, 3430 (1970).
8. R.M. Broudy, Phys. Rev. B 3, 3641 (1971).
9. M. Bensoussan, J.M. Moison, B. Stoesz, and C. Sebenne, Phys. Rev. B 23, 992 (1981).

10. This research was supported by the U.S. Office of Naval Research under contract N00014-83-K-0030.

Appendix 4

PICOSECOND TIME-RESOLVED OPTICAL STUDIES OF PLASMA FORMATION AND LATTICE HEATING IN SILICON

L. A. LOMPRÉ,* J. M. LIU,** H. KURZ AND N. BLOEMBERGEN
Division of Applied Sciences, Harvard University, Cambridge, MA 02138; *C.E.N. Saclay, DPH.G./S.P.A.S., 91191 Gif-sur-Yvette, France; **Department of Electrical and Computer Engineering, Bell Hall, SUNY at Buffalo, Amherst, NY 14260

ABSTRACT

Time-resolved studies of reflectivity and transmission at 0.532 μm, 1.064 μm and 2.8 μm of thin silicon films following irradiation with ps pulses at 0.532 μm have been performed. The formation of the electron-hole plasma and the evolution of lattice temperature is investigated as a function of pump fluence and time delay. Quantitative determination of the plasma densities and lattice temperature up to the melting temperature shows that the maximum plasma density is limited to $\sim 1 \times 10^{21}$ cm^{-3} by Auger recombination even on a time scale of picoseconds at fluences sufficient to cause the phase transition. The thermal nature of the phase transition is confirmed.

Numerous investigations of the change in optical properties of silicon have been carried out as a function of picosecond irradiation fluence [1-4]. These data indicate melting of the surface when the pulse fluence exceeds a critical threshold value. This paper shows that more quantitative information about the lattice temperature and the electron-hole plasma kinetics can be obtained by varying the wavelength of the probing beam and its time delay with respect to the heating pulse.

The real part of the dielectric function at a probing frequency ω below the direct bandgap,

$$\varepsilon' = n_L^2(T,N)[1 - k^2(T,N)] - AN \qquad (1)$$

where

$$A = \frac{4\pi e^2}{\omega^2}\left(\frac{1}{m_e} + \frac{1}{m_h}\right),$$

increases with the lattice temperature T due to indirect interband transitions and decreases with the number of electron-hole pairs N. The optical reduced mass, $m^* = (m_e^{-1} + m_h^{-1})^{-1}$ may depend on the structure in the vicinity of the conduction band minimum and valence band maximum covered by the energetic distribution of the carriers during the time of observation.

The imaginary part of the dielectric function

$$\varepsilon'' = 2n_L^2(T,N)k_L(T,N) + BN \qquad (2)$$

where

$$B = \frac{4\pi e^2}{\omega^3}\left(\frac{1}{m_e\langle\tau_e\rangle} + \frac{1}{m_h\langle\tau_h\rangle}\right)$$

increases with the temperature T and plasma density N. As a third unknown parameter, the scattering times of the carriers (τ_e and τ_h) averaged over their energy distribution come into play.

At a wavelength of 532 nm the real part ε' reveals the opposing effects

Mat. Res. Soc. Symp. Proc. Vol. 23 (1984)

of increasing lattice temperature and increasing plasma density. The imaginary part depends mainly on the lattice temperature, while plasma absorption is negligible at 532 nm [5,6]. By contrast, at 2.8 μm and 1.9 μm both ε' and ε" are dominated by plasma effects [7].

Careful comparison between the time-resolved spectra of the reflectivity and transmission at these wavelengths permits the quantitative determination of the lattice temperature and plasma density during and after ps excitations by photons whose energies are about twice as large as the indirect band gap of Si.

To avoid undesirable diffusion phenomena and obtain uniform temperature and plasma profiles within the penetration depth of the exciting pump laser, the measurements have been performed on thin (0.5 μm) films of silicon on sapphire (SOS). In addition, the multiple interferences between air-silicon and silicon-sapphire interfaces increase the sensitivity to changes of the dielectric function.

Further understanding of the picosecond dynamics of semiconductor carriers and lattice has been obtained by a novel three-pulse technique. The first pulse at 532 nm creates carriers. A second pump pulse at 1.064 μm of 30 ps duration adds energy to the plasma by free carrier absorption, without changing its density. The effect of this additional plasma heating is studied by a third probing pulse at 532 nm, at different time delays with respect to the first two heating pulses [8]. If the excess energy is retained in the plasma for times comparable to Auger recombination time, the temperature of the electron-hole plasma is increased above the band gap. Impact ionization and, consequently, a lowering of the dielectric function are expected.

The experimental set-up for all these measurements is similar to that described in reference [3]. Due to Auger recombination the electron-hole plasma density drops below 1×10^{20} cm^{-3} after 150 ps, and the plasma contribution to ε' and ε" becomes negligible for 532 nm light. At a time delay of 200 ps the lattice temperature can be directly measured by transmission changes of silicon film at various fluence levels. The SOS sample is heated by a 20 ps pulse with a diameter of 300 μm. The probe pulse at the same wavelength is focused to 30 μm and aligned directly at the center of the pump spot. The polarization of the two beams is orthogonal to suppress undesirable interferences. The fluence of the probe pulse is kept at 0.1% of the pump fluence to avoid reheating phenomena.

As shown in Fig. 1, the SOS film exhibits significant changes of reflectivity and transmission with increasing fluence level of the pump pulse $F_{2\omega}$. The reflectivity increases gradually from 15% to 40%, followed by a flat level up to 0.16 J/cm^2. Above this level a sharp rise to 69% occurs, which corresponds to the metallic reflectivity of liquid silicon at an angle of 26° as used in this experiment. The flat level portion reflects the conditions of bulk reflectivity because of the nearly complete suppression of the multiple interferences by the strong increase of the film absorbance.

The transmission drops continuously from an initial value of 48% to the detection limit of 1% at 0.2 J/cm^2. This limit corresponds to an average optical absorption $\alpha = 4\pi nk/\lambda \geq 7 \times 10^4$ cm^{-1}, nearly one order of magnitude above the room temperature value of $\alpha \sim 10^4$ cm^{-1}. According to the measurements of Jellison and Modine, the absorption coefficient α increases exponentially with temperatures $\alpha = \alpha_0 \exp(T/\theta)$, where $\theta = 430 \mp 30$ K and α_0 is a constant factor [9]. We determined $\alpha_0 = 4200$ cm^{-1} for the SOS sample at room temperature. From the transmission data of Fig. 1 we extract the surface and average temperatures in the following way. We calculate the temperature profile T(x) after 200 ps for various laser fluences, taking into account the temperature dependence of optical absorption, thermal conductivity and heat capacity. These T(x) profiles are converted into absorption profiles $\alpha(x) = \alpha_0 \exp(T(x)/\theta)$ and compared with the optical densities $\bar{\alpha} = d^{-1} \int_0^d \alpha(x)dx$

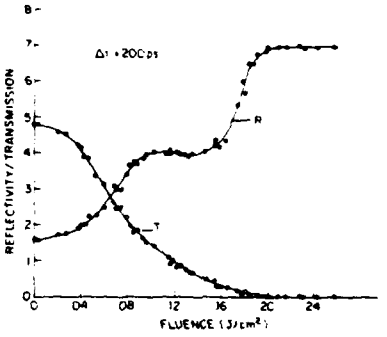

FIG. 1. Reflectivity and transmission at λ = 532 nm, probed with a delay Δt = 200 ps after the pump pulse at λ = 532 nm, versus incident fluence in a 0.5 μm thick SOS sample.

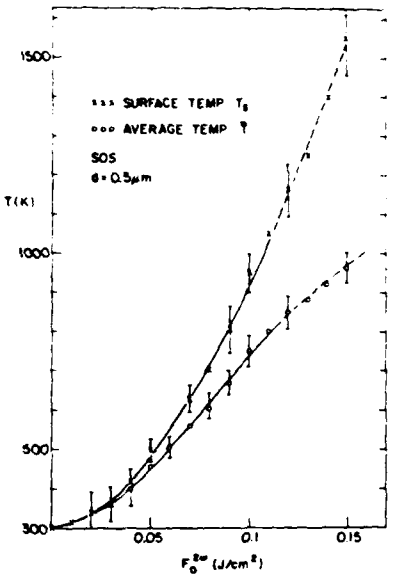

FIG. 2. Average temperature $\bar{T}$ and surface temperature T_s in SOS sample, obtained from the transmission data versus incident fluence.

obtained from the transmission data. The corresponding surface temperatures T_s and average temperature $\bar{T} = d^{-1} \int_0^d T(x)dx$ of SOS are plotted in Fig. 2 versus the incident laser fluence $F_0^{2\omega}$. It should be noted that the multiple interferences of SOS lead to rapidly varying spatial modulation of the energy absorption during the ps irradiation. Therefore, we measured in addition the reflectivity R and transmission T at a time delay Δt = 0. From the fraction of absorbed energy A = 1 - R - T, we calculated the expected temperature rise using the simple thermal model. There is excellent agreement between the two approaches.

This optical probing of the lattice temperature reveals significantly higher values than those derived from Raman scattering [10]. When our data are extrapolated to higher fluence levels along the dashed lines in Fig. 2, the melting temperature of 1680 K is reached at the surface of SOS for a laser fluence above 160 mJ/cm^2. It is precisely at this fluence level that the reflectivity of SOS starts to rise to the liquid state value, as shown in Fig. 1.

At shorter time delays Δt between pump and probe pulses, the negative plasma contribution ($-\Delta N = -(4\pi e^2/\omega^2 m^*)N$) competes with the positive contribution from the increased lattice temperature. The complete time-resolved spectra of reflectivity and transmission of SOS shown in Fig. 3 reveals the temporal change of the dielectric constants ε' and ε" by the formation of electron-hole plasma and evolution of the lattice temperature. The transmission drop is obviously terminated immediately after the excitation pulse, indicating that the lattice heating is completed at this time and the phonons contributing to the indirect absorption process have reached a steady state temperature.

The reflectivity, however, rises to a maximum at Δt ~ 0 ps and passes through a minimum where the plasma contribution ΔN is compensated by the temperature-induced increase of $n_L(T)$. The slow recovery of the reflectivity to the final value of 22% is clearly due to decay of the plasma density via

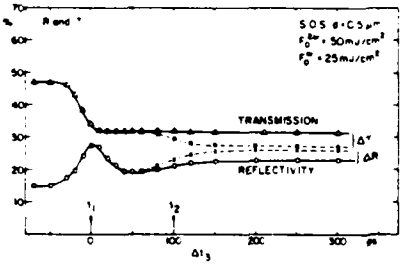

FIG. 3. Time-resolved reflectivity and transmission in SOS induced by a pump pulse at 532 nm with 50 mJ/cm² and probed at the same wavelength at different time delays (solid line). The dotted line indicates changes induced by a second pump beam at 1064 nm with 25 mJ/cm² applied with the time delay Δt_{21} = 100 ps after the first pump pulse at 532 nm (50 mJ/cm²).

Auger recombination. To calculate the plasma density, the role of the impact ionization during the laser irradiation has to be clarified.

A first pulse at 532 nm with 50 mJ/cm² creates a carrier plasma and elevates the lattice temperature (full line in Fig. 3). A second pulse with 30 ps duration at 1.064 μm adds around 1 eV excess energy to the plasma at a time delay Δt_{21} = 100 ps. A third pulse at 532 nm probes the resulting changes in reflectivity ΔR and transmission ΔT at a time delay Δt_{31}. The dotted line in Fig. 3 shows the effect of the second heating pulse (25 mJ/cm²). A further increase of lattice temperature is observed, but no evidence for a change in the plasma term $4\pi e^2N/\omega^2m^*$ can be deduced. Obviously neither the reduced mass m^* nor the density of electron-hole pairs is changed by the additional heating of the plasma. As in the case of 532 nm excitation, the optical input energy is immediately transferred to the phonon system. The plasma cools off so rapidly that the probability for the creation of new electron-hole pairs is very low.

Thus the electron-hole plasma kinetics is mainly governed by the optical generation rate G, the Auger recombination rate γN^3 and the diffusion rate $\nabla N D_a$ where D_a is the ambipolar diffusion coefficient.

The three-pulse plasma heating technique permits a precise determination of the temporal dependence of the free carrier absorption $\alpha_{FCA} = N\sigma_{FCA}$, by measuring the additional amount of lattice heating at different delay time Δt_{21}. In Fig. 4 the probing pulse is set at a time delay of Δt = 400 ps, monitoring the relative change of reflectivity ΔR and transmission ΔT. Clearly the additional heating of the lattice is proportional to the number of electron-hole pairs N. The heating peaks at a time delay Δt_{21} of 10 ps, indicating the moment when the plasma density reaches a maximum.

The decrease of ΔR and ΔT at larger Δt_{21} reflects again the decay of the plasma density via Auger recombination. This thermometric determination of plasma relaxation is by far more sensitive than direct optical measurements. The solid line in Fig. 4 shows the calculated relative reflectivity and

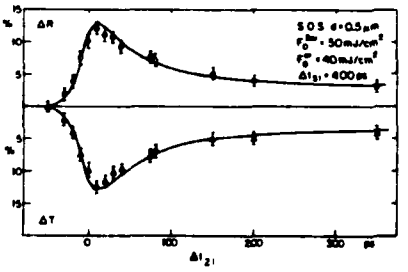

FIG. 4. Relative changes of reflectivity (ΔR) and transmission (ΔT) probed at a delay fixed at 400 ps induced by a second pulse at 1064 nm with a fluence of 40 mJ/cm² as a function of its time delay Δt_{21}.

transmission changes of SOS. The plasma density N(x,t) has been calculated numerically with $\gamma = 4 \times 10^{-31}$ cm^6/sec, $D_a = 6 \cdot 10^3 T_L^{-1}$ cm^2/s (20 - 300 T_L) and $\sigma_{FCA} = 5 \times 10^{-18} T_L/300$ cm^2 [11]. The calculation assumes that the absorbed laser energy is distributed immediately to the lattice. The relative changes of R and T are evaluated by using conventional thin film optics expressions at a fluence level of $F_o^{2\omega} = 50$ mJ/cm^2. The plasma density reaches a maximum of $\sim 4 \times 10^{20}$ cm^{-3} at $\Delta t = 10$ ps and drops to 6.5×10^{19} cm^{-3} at 300 ps, exactly reproducing the relaxation by Auger recombination.

By changing the probe wavelength to 2.8 μm, the contribution of the lattice temperature to ε' and ε" becomes negligible compared to the plasma effects. The transients in reflectivity and transmission of SOS are exclusively dominated by the plasma terms AN and BN at this wavelength. Probed at a time delay of 10 ps, where the plasma density reaches a maximum, the transmission of SOS drops to zero for 2.8 μm already at low laser fluences of the excitation beam, as shown in Fig. 5. The initial rise in the transmission below 20 mJ/cm^2 is solely due to interference effects in SOS samples.

The reflectivity exhibits a plasma resonance, indicating that the plasma density exceeds $N_c = m^* \pi \varepsilon_a (c/e\lambda)^2 = 2.5 \times 10^{20}$ cm^{-3} where $\varepsilon_a = 11.8$ is the high frequency dielectric constant and $m^* = (m_e^{-1} + m_h^{-1})^{-1} = 0.15\ m_o$ is the optical reduced susceptibility masses of electron-hole plasma in equilibrium with the lattice phonons. As soon as the plasma edge is reached, the transmission drops to zero and no further probing of the plasma kinetics is possible.

To determine the plasma densities at higher fluence levels close to the threshold for the phase transition, probing at 1.064 μm is preferable. At this wavelength the reflectivity does not exhibit a Drude-like resonance. The density appears to be limited below the critical density $N_c = 1.76 \times 10^{21}$ cm^{-3} for this wavelength. The transmission remains measurable up to the threshold fluence for melting. Again, the slight increase of the transmission at low fluences is due to multiple interferences of the probing light between the SOS interfaces. Around $F_o^{2\omega} = 0.160$ J/cm^2, where the SOS sample starts to melt, transmission drops to 34%. With the free carrier absorption $\sigma = 5.1 \times 10^{-18}$ T/300 cm^2 reported in the literature and with our numerically calculated distribution functions for N(x) and T(x), a density at the surface $N_s \simeq 1 \times 10^{21}$ cm^{-3} is derived. This value is in good agreement with theoretical calculations of the spatial and temporal development of the plasma density N(x,t) based on thermal equilibrium between plasma and lattice phonons.

In conclusion, time-resolved measurements of reflectivity and transmission of SOS samples as a function of pump fluence, time delay and of probing wavelength provide quantitative data about the lattice temperatures and plasma density during and after the irradiation with picosecond pulses. Close to fluence threshold for phase transitions at the sample surface, the lattice temperature reaches the melting point and the plasma density peaks to

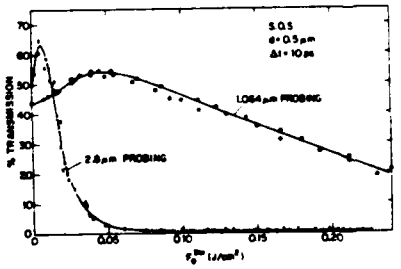

Fig. 5. Time-resolved transmission in SOS (0.5 μm) induced by a pump pulse at 532 nm at different fluences and probed at 1.064 and 2.8 μm at a time delay of 10 ps.

10^{21} cm^{-3}, limited by Auger recombination. There is no evidence for impact ionization throughout the range of laser fluences, indicating a fast energy loss of the electron-hole plasma via phonon emission. The characteristic energy transfer time is less than a few picoseconds, in agreement with the theoretical expectations based on deformation potential scattering. The lattice reaches the melting point during the picosecond pulse, if the energy fluence exceeds the threshold value necessary to observe a phase transition.

This research was supported by the United States Office of Naval Research under contract N00014-83-K-0030.

REFERENCES

1. D.H. Auston, C.M. Surko, T.N.C. Venkatesan, R.E. Slusher, and J.A. Golovchenko, Appl. Phys. Lett. 33, 437 (1978).
2. J.M. Liu, R. Yen, H. Kurz, and N. Bloembergen, Appl. Phys. Lett. 39, 755 (1981); R. Yen, J.M. Liu, H. Kurz, and N. Bloembergen, Appl. Phys. Lett. A 27, 153 (1982).
3. J.M. Liu, H. Kurz, and N. Bloembergen, Appl. Phys. Lett. 41, 643 (1982).
4. D. von der Linde and N. Fabricius, Appl. Phys. Lett. 41, 991 (1982).
5. L.A. Lompré, J.M. Liu, H. Kurz, and N. Bloembergen, Appl. Phys. Lett. 43, 168 (1983).
6. A. Lietoila and F. Gibbons, Appl. Phys. Lett. 40, 624 (1982).
7. H. van Driel, L.A. Lompré, and N. Bloembergen, Appl. Phys. Lett., to be published.
8. L.A. Lompré, J.M. Liu, H. Kurz, and N. Bloembergen, Appl. Phys. Lett., to be published (Jan. 1984).
9. G.E. Jellison and F.A. Modine, Appl. Phys. Lett. 41 (2), 180 (1982).
10. A. Compaan, M.C. Lee, H.W. Loo, G.J. Trott, and A. Aydinli, J. Appl. Phys. 54 (10), 5950 (1983).
11. K.G. Svantesson, J. Phys. D 12, 425 (1979).

Appl. Phys. A 34, 25–29 (1984)

Appendix 5

Applied Physics A Solids and Surfaces

Phenomenology of Picosecond Heating and Evaporation of Silicon Surfaces Coated with SiO_2 Layers

J. M. Liu*, L. A. Lompre**, H. Kurz, and N. Bloembergen

Gordon McKay Laboratory, Division of Applied Sciences, Harvard University, Cambridge, MA 02138, USA

Received 12 January 1984 Accepted 25 January 1984

Abstract. Picosecond time-resolved reflectivity measurements on bare silicon surfaces and silicon surfaces with oxide layers reveal very fast heat diffusion and material evaporation on subnanosecond time scales. With a thick oxide layer resolidification of a molten silicon surface can take place in a few hundred picoseconds. At high laser fluences, vaporization processes take only a couple of 100 ps.

PACS: 64.70.Fx, 44, 79.20.Ds

Recent experimental results [1, 2] on ultrafast pulsed laser interactions with silicon have demonstrated that thermal equilibrium between the dense photo-excited electron-hole plasma and the silicon lattice is established on a picosecond time scale. Experiments with femtosecond laser pulses [3] indicated subpicosecond energy transfer times from the carriers to the lattice and subsequent structural changes of the silicon lattice in a few picoseconds. Our earlier experiments [4] measured on picosecond time scales the temperature rise of a silicon lattice induced by 20-ps laser pulses. When the laser pulse has sufficient fluence to induce melting, heating rates can be as high as 10^{14} °C/s. Transient lattice heating, melting, and overheating of the melt are observed during the 20-ps pulse duration [5]. The extremely high heating rates on the surface create very steep gradients in the temperature profiles which then induce very high cooling rates through fast diffusion of the heat into the bulk substrate after the pulse. These ultrafast heating and cooling processes induced by picosecond pulses provide a unique opportunity to study the thermodynamics of transient phase transitions and the kinetics of crystal regrowth and phase transformation under extreme conditions [1, 2].

Previously, we have reported that at higher fluences, evaporation of material from the irradiated surface can take place. The morphologies of evaporation or removal of material induced by a 20-ps laser pulse under various conditions have been studied [6]. When a silicon surface covered by a layer of SiO_2 is irradiated with a picosecond pulse at a fluence above certain threshold value, the oxide layer can be removed after the pulse. The sharp, reproducible threshold laser fluences to induce melting of the silicon surface, cracking of the SiO_2 layer, and complete removal of SiO_2, for samples, with oxide layers of different thicknesses are reported in this paper. We also describe picosecond time-resolved reflectivity measurements on silicon surfaces covered by oxide layers of known thickness in comparison with data taken on bare silicon surfaces to demonstrate the very fast processes of heat diffusion and material evaporation in different laser fluence regimes.

Experimental

Silicon wafers of (100) and (111) surfaces were used in this experiment. However, the data do not depend on the surface orientation except that the amorphous

* Permanent address: GTE Laboratories Incorporated, 40 Sylvan Road, Waltham, MA 02254, USA

** Permanent address: C.E.N./Saclay, DPh.G/S.P.A.S., F-91191 Gif-sur-Yvette Cedex, France

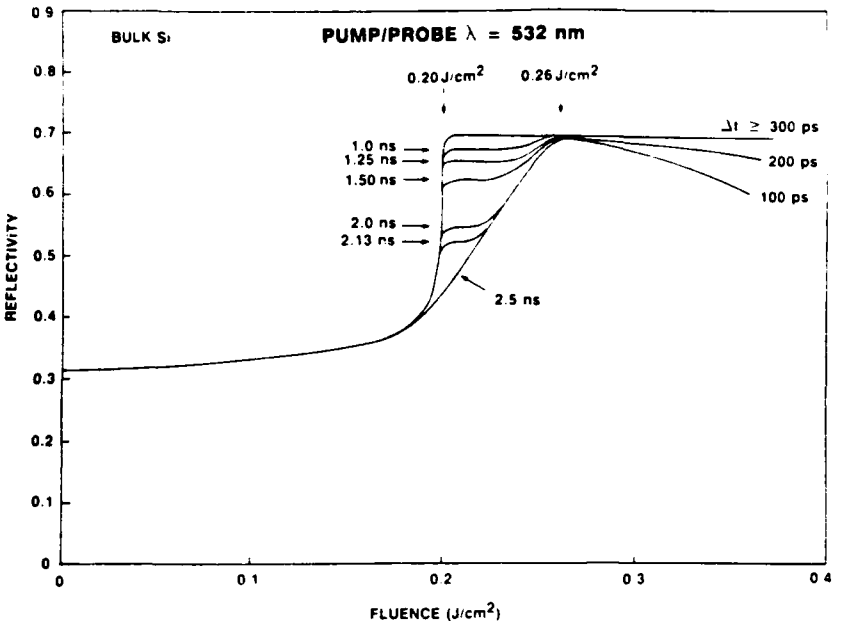

Fig. 1. Reflectivity of a bare silicon surface vs. pump fluence at various probe time delays. Both pump and probe are 20-ps pulses at 532-nm wavelength

patterns induced by the 20-ps pulses at $\lambda = 532$ nm are easier to observe on a (111) surface. The oxide layers of well-controlled thickness characterized with an argon laser [7] were grown by heat treatment in dry O_2, at 960° or 1100 °C, respectively, for appropriate time durations. In this experiment, we exclusively used the 20-ps pulses at 532-nm wavelength from the second harmonic of a mode-locked Nd : YAG laser. The time-resolved reflectivity measurements were performed with the same experimental setup described in [4]. Briefly, the sample is heated by a pump pulse focused to a diameter of 300 μm at the (1/e) intensity contour of its Gaussian spatial profile. The probe pulse at the same wavelength ($\lambda = 532$ nm) focused to a diameter of 30 μm at the exact center of the pump spot is incident at 26° to the normal of the sample surface. The variable time delay of the probe pulse with respect to the pump pulse can be extended from -50 ps to 2.5 ns.

Results

Here, we discuss the results on three different samples: bare (111) silicon, (111) silicon with a thin SiO_2 layer of 410 Å thickness, and (111) silicon with a thick SiO_2 layer of 2100 Å. Figure 1 shows the reflectivity of a bare silicon surface as a function of pump fluence at various probe delays longer than 100 ps when the pump and probe pulses are temporally completely separated. A sharp rise of the reflectivity to 69%, characteristic of the metallic reflectivity of molten silicon at an incident angle of 26°, indicates the occurrence of melting at a threshold fluence of 0.2 J/cm² [4, 5]. At lower fluences, the reflectivity increases from an initial value of 31.5% gradually with increasing pump fluence because of heating of the silicon surface below the melting threshold. At higher fluences, the decrease of the reflectivity with increasing pump fluence at 100 and 200 ps probe delays indicates overheating of the molten surface with excess fluence above the melting threshold. This reduced reflectivity recovers to the 69% level as the overheated liquid silicon surface cools down. This process takes about 300 ps at a fluence below 0.5 J/cm². Cooling and resolidification of the molten silicon surface are driven by diffusion of heat into the bulk substrate. At fluences just above the melting threshold, these processes may take place right after the pulse. When the resolidification front reaches the optical penetration depth of molten silicon (about 90 Å at 532 nm), the reflectivity starts to drop. This explains the gradual drops of the reflectivity after 1 ns probe delay at fluences between 0.2 and 0.26 J/cm². Without the precise knowledge of the initial melt depth at various pump fluences, we cannot derive an accurate value of the upper limit of the regrowth speed. However, if we estimate a conservative melt depth of 400 Å, the regrowth speed in the initial stage of resolidification may well be above 30 m/s. This high regrowth speed results in amorphization of the silicon surface observable at fluences between 0.2 and 0.26 J/cm² [6, 8]. At fluences above 0.26 J/cm² cooling takes longer times as indicated by the long-lasting high reflectivity. The slower regrowth speeds then allow the liquid surface to resolidify into crystalline phase at a threshold fluence of 0.26 J/cm².

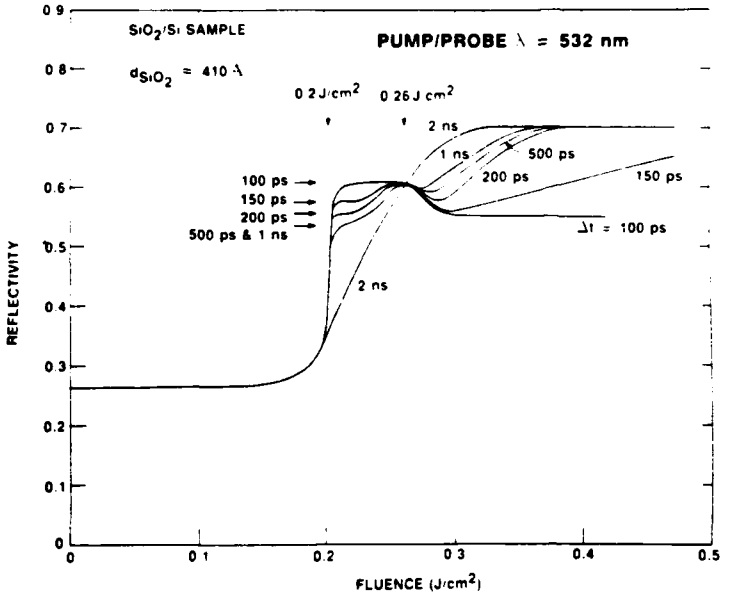

Fig. 2. Reflectivity of a silicon surface with a SiO_2 layer of 410 Å thickness vs. pump fluence at various probe time delays. Both pump and probe are 20-ps pulses at 532-nm wavelength

When a silicon surface has a SiO_2 layer, the optical reflectivity can be changed drastically due to multiple interferences in the oxide layer [7] although SiO_2 does not absorb light at 532 nm. In our experiment, the sample with a thin SiO_2 layer has an initial reflectivity of 26.5% at 532 nm and the one with a thick SiO_2 layer has an initial $R = 30\%$, which are both very close to the bare silicon reflectivity of 31.5%. For the sample with a thin oxide layer, melting also occurs at a threshold fluence of 0.2 J/cm^2 as indicated by the sharp rise in the plot of reflectivity vs pump fluence at various probe delays in Fig. 2. At fluences below 0.2 J/cm^2 heating of the silicon surface also increases the reflectivity gradually with increasing pump fluence. However, no change in the behavior of multiple interferences as a function of probe time delay was observable. At a very reproducible threshold fluence of 0.26 J/cm^2, we started to observe cracking and partial removal of the SiO_2 layer. Complete, clean removal of the SiO_2 layer occurs at a threshold of 0.3 J/cm^2. Because SiO_2 softens at 1853 and melts at 1983 K [9] which are both higher than the melting point of silicon at 1685 K and because SiO_2 does not absorb light at 532 nm, at fluences between 0.2 and 0.26 J/cm^2 the silicon surface melts under the solid oxide layer and resolidifies into amorphous phase afterwards. In this fluence regime, the high reflectivity level rises during the pulse and reaches a maximum value of 61% at 100 ps delay, which is lower than the reflectivity of the bare molten silicon surface because of the multiple interferences in the oxide layer. However, the reflectivity does not stay at the maximum value, but it keeps on changing and starts to drop after 100 ps when heat diffusion from the molten silicon surface into the SiO_2 overlay changes the optical property of SiO_2 gradually. This drop of reflectivity then stops at 500 ps and the reflectivity stays constant with time until the resolidification front under the molten silicon layer comes within one optical absorption depth from the surface after about 1 ns, as discussed previously. The temperature dependence of the heat diffusivity in SiO_2 is not available to us. If we take the only available value $D = 0.006$ cm^2/s at room temperature [10], we estimate a time duration on the order of 1 ns for the heat to diffuse across the 410 Å-thick SiO_2 layer. Presumably, the time-resolved reflectivity data show that heat diffusion establishes a uniform temperature profile in the SiO_2 layer within 500 ps. Then heat diffusion into the bulk silicon substrate is solely responsible for further cooling of the hot silicon surface and the SiO_2 layer afterwards.

At higher fluences, heating of the SiO_2 layer through heat diffusion from the overheated molten silicon surface may raise the temperature to the softening point or even the melting point of SiO_2. Meanwhile, the vapor pressure of the overheated silicon surface also increases with increasing pump fluence. The softened or molten SiO_2 may react with the molten silicon to form SiO which then evaporates [8]. At even higher fluences, direct evaporation of SiO_2 or blow-off of SiO_2 by silicon vapor pressure can take place. After the SiO_2 layer is completely removed, the surface then shows the high reflectivity $R = 69\%$ of the bare molten silicon surface. The reflectivity plots in Fig. 2 then demonstrate the time scale of the evaporation processes. At fluences between 0.26 and 0.3 J/cm^2 where the removal of SiO_2 is never complete and

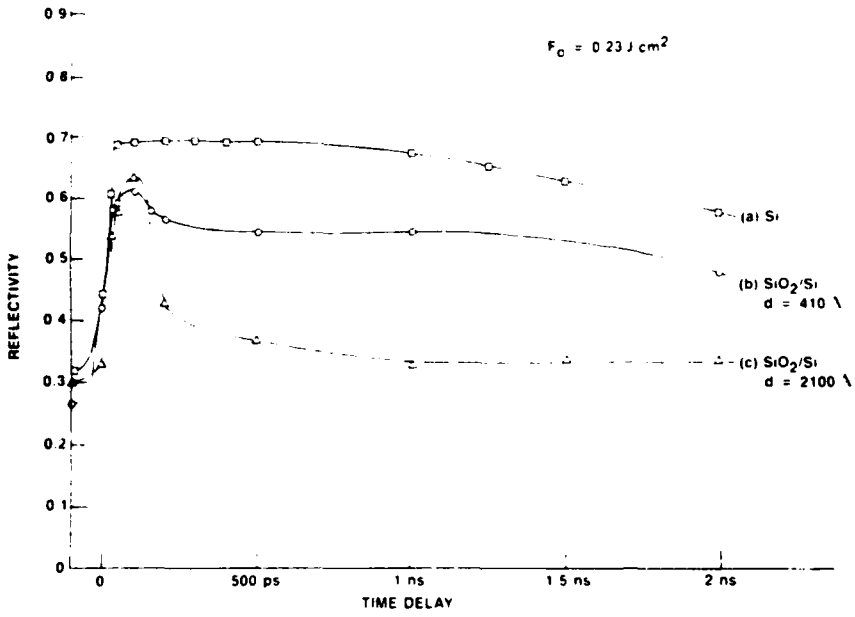

Fig. 3a–c. Reflectivity changes as a function of the probe time delay at three different sample surfaces irradiated with a 20-ps, 532-nm pulse at a fluence of 0.23 J/cm²: (a) bare silicon surface, (b) silicon surface with a SiO_2 layer of 410 Å thickness, (c) silicon surface with a SiO_2 layer of 2100 Å thickness

clean, the reflectivity recovers gradually to higher levels that never reach 69%. In this fluence regime all the processes of heating, softening, cracking, and partial removal of SiO_2 can happen and the changes in the reflectivity are very complicated. Above 0.3 J/cm² where complete removal of the SiO_2 layer is observed, the reflectivity eventually reaches the 69% level after certain time delay which depends on the pump fluence. At fluences just above 0.3 J/cm² the evaporation process may take 2 ns. At fluences above 0.4 J/cm² it takes 150 to 200 ps to complete the evaporation.

The data on the sample with a thick SiO_2 layer of 2100 Å thickness also demonstrate very interesting features of the heat diffusion and evaporation processes. However, because of the larger thickness of the SiO_2 layer, multiple interferences and heat diffusion together make the reflectivity strongly dependent upon probe time delay. The data became too complicated for a plot as in Fig. 1 or 2. In this sample, the threshold fluence for melting is increased to 0.22 J/cm² presumably because more heat is diffused into the thicker SiO_2 layer during laser heating of the silicon surface. At fluences below this threshold, the reflectivity increases gradually with increasing pump fluence. In contrast to the trace in Fig. 2 for the sample with a thin SiO_2 layer, the reflectivity now changes with time delay even below the melting threshold because the 2100 Å SiO_2 layer thickness is closer to the probe wavelength of 5320 Å so that changes in the optical property in this layer due to heating induce observable effects from multiple interferences. At higher fluences, removal of the SiO_2 layer is also observed with reproducible thresholds of 0.33 J/cm² for cracking and partial removal and 0.39 J/cm² for complete removal. Although the layer is much thicker, the process of evaporation and removal also takes only a few hundred picoseconds to about 2 ns, depending on the pump fluence. At a time delay of 1–1.5 ns, the reflectivity data become very scattered due to scattering of the probe light by the evaporated SiO_2 particles in front of the sample surface. The data become clean again after a longer delay when these particles are completely removed.

At a fluence between 0.22 and 0.33 J/cm², the reflectivity data of the sample with a thick oxide layer show early cooling of the molten silicon surface due to diffusion of heat into the SiO_2 layer before the heat diffusion into the bulk silicon substrate starts to cool down the molten silicon layer. This phenomenon is particularly obvious at fluences just above the melting threshold of 0.22 J/cm².

For the purpose of comparison, the reflectivity changes of the three samples pumped at the same fluence of 0.23 J/cm² are shown in Fig. 3 as a function of probe time delay. The reflectivity of the bare silicon surface rises abruptly to the reflectivity of molten silicon during the pulse, stays until resolidification front driven by heat diffusion into the bulk substrate reaches an optical depth from the molten surface after 1 ns, and then drops gradually as the whole molten layer resolidifies. For the sample with a thin SiO_2 layer, the reflectivity also rises during the pulse as the silicon surface melts under the solid SiO_2 layer. It reaches a maximum of 61% at 100 ps time delay and falls as the SiO_2 layer is heated by the heat diffusion. The reflectiv-

ity then stays constant from 500 ps to 1 ns time delay after the oxide layer acquires a uniform temperature profile and before resolidification of the underlying molten silicon layer starts to reduce the reflectivity. The reflectivity trace of the sample with a thick SiO_2 layer reveals a completely different process of cooling. It rises somewhat more gradually to its maximum value of 63% at 100 ps time delay, indicating that more heat is being taken away by diffusion into the thick SiO_2 overlay during the pulse. After it reaches the maximum value, it drops quickly and reaches a very low value after 500 ps. Because of the thickness of the oxide layer, a uniform temperature profile can never be established in the layer through heat diffusion in a few nanoseconds. This thick layer also has enough capacity to absorb the heat released by the molten silicon layer during cooling and resolidifying. Therefore, this reflectivity trace shows that the molten silicon layer is now cooled and resolidified mainly by heat diffusion into the thick SiO_2 layer in less than 500 ps, rather than being cooled by heat diffusion into the bulk substrate which should happen later. The final reflectivity at a level of 33% simply demonstrates the reflectivity of a warm amorphous silicon layer covered by a warm SiO_2 layer with a nonuniform temperature profile, after the molten silicon layer has resolidified into the amorphous phase.

This example shows that the behavior of coated surfaces can give additional information about heating and evaporation processes. Transparent layers with lower melting and boiling points than the melting point of the substrate may also be useful, as would a time-resolved mass-spectrographic study of the evaporating species.

Acknowledgement. This work was supported by the U.S. Office of Naval Research under contract No. 00014-83K-0030.

References

1. J. Narayan, W.L. Brown, R.A. Lemons (eds.): *Laser-Solid Interactions and Transient Thermal Processing of Materials* (North-Holland, New York 1983)
2. J.C.C. Fan, N.M. Johnson (eds.): *Energy Beam-Solid Interactions and Transient Thermal Processing*, Materials Research Society Conference Proceedings (1983)
3. C.V. Shank, R. Yen, C. Hirliaman: Phys. Rev. Lett. **50**, 454 (1983); also in [1, 2]
4. L.A. Lompre, J.M. Liu, H. Kurz, N. Bloembergen: Appl. Phys. Lett. **43**, 168 (1983)
5. J.M. Liu, H. Kurz, N. Bloembergen: Appl. Phys. Lett. **41**, 643 (1982)
6. J.M. Liu: Ph.D. Thesis, Harvard University (1982)
7. R.H. Hendel, D.D. Casey, C.U. Bickford: J. Vac. Sci. Technol. **18**, 818 (1981)
8. J.M. Liu, R. Yen, H. Kurz, N. Bloembergen: Appl. Phys. Lett. **39**, 755 (1981)
9. H.F. Wolf: *Silicon Semiconductor Data* (Pergamon Press, Oxford 1969) pp. 642–644
10. H.F. Wolf: *Semiconductors* (Wiley, New York 1971) p. 375

Note added in proof: 1. In order to avoid interference of pump and probe, the pump beam is s-polarized, whereas the probe is p-polarized.

2. The error limits on the R values are $\pm 0.5\%$ at zero or very low pump fluences and $\pm 1\%$ at higher pump fluences close to or above the melting threshold.

Optical heating of electron-hole plasma in silicon by picosecond pulses

L.-A. Lompré,[a] J.-M. Liu,[b] H. Kurz, and N. Bloembergen
Gordon McKay Laboratory, Division of Applied Sciences, Harvard University, Cambridge, Massachusetts 02138

(Received 12 September 1983; accepted for publication 11 October 1983)

Using a novel three-pulse technique, essential information about the density, optical effective mass, and kinetics of laser-generated plasmas in silicon has been obtained.

PACS numbers: 72.30. + q, 79.20.Ds, 71.35. + z

Numerous investigations of the change in optical properties of silicon induced by a strong pump or "heating" pulse have recently been carried out.[1-4] By varying the wavelength of the probing pulse and its time delay with respect to the picosecond pump pulse, the contributions due to a variation in lattice temperature and those due to changes in carrier density have been separately determined.[5]

The real part of the dielectric function at a probing frequency ω

$$\epsilon' = n_L^2(T)[1-\kappa^2(T)] - \frac{4\pi e^2 N}{m^*\omega^2} \tag{1}$$

increases with the lattice temperature $T (dn/dT > 0, \kappa^2 < 1)$ and decreases with the number of electron-hole pairs N. As long as there is no reliable information about the modification of the optical reduced mass $m^* = (m^{*-1}_e + m^{*-1}_h)^{-1}$ at high densities and carrier temperatures T_e available, the reflectivity data of laser-generated plasmas in silicon allow only the determination of N/m^*.

The imaginary part of the dielectric function

$$\epsilon'' = 2n_L^2(T)\kappa_L(T) + \frac{4\pi e^2 N}{\omega^3}\left(\frac{1}{m^*_e\langle\tau_e\rangle} + \frac{1}{m^*_h\langle\tau_h\rangle}\right) \tag{2}$$

increases with N and T; however, as a third unknown parameter, the scattering times of the carriers (τ_e, τ_h) averaged over their energy distribution come into play. Thus the experimental determination of ϵ' and ϵ'' does not provide sufficient information to solve separately for N_e, N_e, and m^*.

In this letter results obtained with a three-pulse tech-

[a] Permanent address: C.E.N./Saclay, DPh. G/S.P.A.S., 91191 Gifsur-Yvette Cedex, France.
[b] Permanent address: Department of Electrical and Computer Engineering, Bell Hall, SUNY at Buffalo, Amherst, New York 14260.

 0003-6951/84/010003-03$01.00

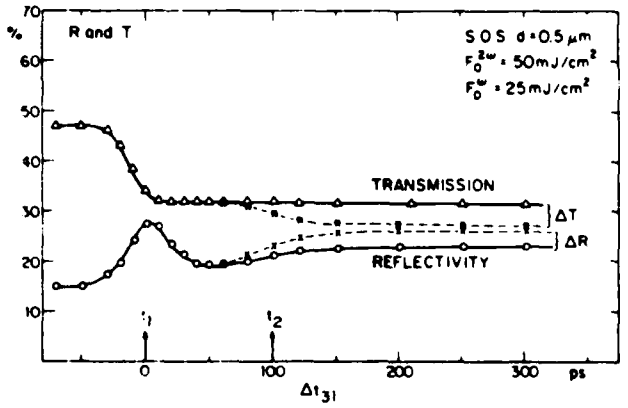

FIG. 1. Time-resolved reflectivity and transmission in SOS induced by the first pump pulse at 532 nm with 50 mJ/cm² and probed at the same wavelengths at different time delays (full line). Changes induced by the second pump beam at 1064 nm with 25 mJ/cm² (dotted line).

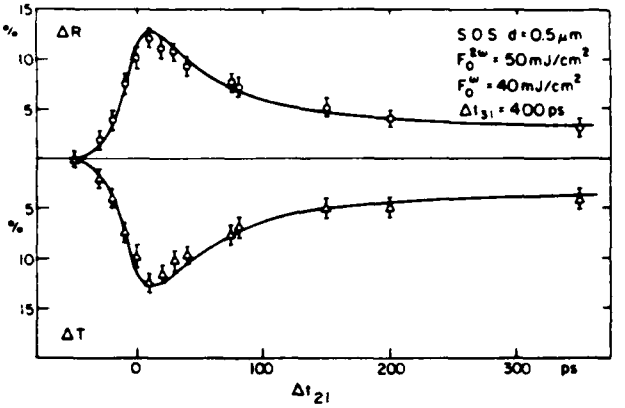

FIG. 2. Relative changes of reflectivity and transmission probed after 400 ps, induced by a second pulse at 1064 nm with a fluence $F_0^{\omega} = 40$ mJ/cm². The ΔR and ΔT values are measured as a function of its delay time Δt_{21}.

nique are reported. The first pulse, with a fluence of 50 mJ/cm² in the visible ($\lambda = 530$ nm) of 20-ps duration, creates the carrier plasma. A second pulse at $\lambda = 1.06\ \mu$m of 30-ps duration adds energy to the plasma by the free-carrier absorption processes without changing its density. A third pulse ($\lambda = 530$ nm) probes the resulting changes in reflectivity and transmission of a 0.5-μm-thick silicon-on-sapphire (SOS) sample. Details of the experimental geometry have been given in Ref. 5.

The time delay between the first two pulses is kept fixed, $\Delta t_{21} = 100$ ps. Then the reflectivity and transmission as a function of Δt_{31}, the time delay of the probe pulse, is shown in Fig. 1 for two cases. The drawn lines are valid in the absence of the second pulse. This behavior has been explained previously[5] in terms of decaying plasma density and with the asymptotic values of R and T indicating the change in lattice temperature. The dotted lines are valid when the IR plasma heating pulse of 25 mJ/cm² is applied. The data give the variations ΔR and ΔT, due to the change in lattice temperature. There is no evidence for an increase in N/m^* due to the second pulse. The data indicate that the energy relaxation time τ_w of the carriers with the lattice is faster than impact ionization.

In Fig. 2 the probe pulse is fixed at $\Delta t_{31} = 400$ ps. The change in reflectivity ΔR is measured as a function of Δt_{21}. It therefore measures the variation in the lattice temperature. Clearly, the additional heating by the second pulse of 40 mJ/cm² is maximum for $\Delta t_{21} = 10$ ps and decays as the plasma density created by the first pulse decays.

These data are consistent with a model in which the energy relaxation time τ_w between carriers and lattice is taken to be short compared to the pulse duration. In fact, we have put $\tau_w = 0$. Instantaneous thermal enhancement of the indirect absorption at 0.53 μm is assumed. Thus the generation rate of electron-hole pairs experiences a significant increase[6] during the picosecond excitation at 0.53 μ. With these assumptions, the highest possible plasma densities in the absence of impact ionization are calculated. The results for a fluence level of $F_0^{2\omega} = 100$ mJ/cm² are shown in Fig. 3, where the plasma density at the surface N_s and the surface

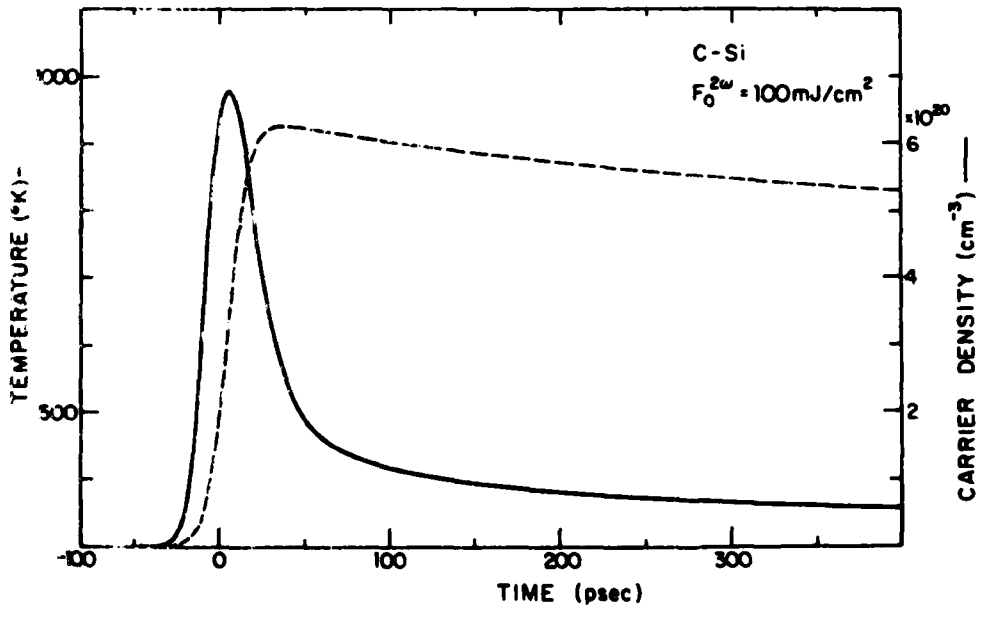

FIG. 3. Calculated temporal profile of the plasma density $N = N_e = N_h$ and lattice temperature at the surface of silicon during and following a 20 ps, 0.1 J/cm² pump pulse at 0.53 μm.

temperature T_s are plotted versus time. The plasma density reaches the maximum with $\sim 6.7\times 10^{+20}\,\mathrm{cm}^{-3}$ a few picoseconds after the intensity maximum of the Gaussian temporal excitation profile centered at $\Delta t = 0$. The plasma density is strongly reduced by Auger recombination ($\gamma = 4\times 10^{-31}$). The rise and peak of the lattice temperature are retarded with respect to the plasma features.

Optical probing of the plasma generated at this fluence level yields an upper limit of N/m^* values with $N/m^* = 4\times 10^{48}\,\mathrm{g}^{-1}\,\mathrm{cm}^{-3}$.[3,4,7] The maximum possible value of the optical mass at this fluence level is $m^* < 0.18\ m_0$. Thus, the data are consistent with a nearly constant reduced optical mass $m^* = (m_e^{-1} + m_h^{-1})^{-1} = 0.15\ m_0$, expected for a plasma in thermal equilibrium with the lattice.

The solid lines in Fig. 2 are calculated on the basis of this model with the free-carrier absorption cross section at 1.06 μm taken to be $\sigma = 2.3\times 10^{-17}\,(T/300)$. This coefficient is four times larger than that reported at lower carrier concentrations.[8] The carrier momentum relaxation times τ_e and τ_h, occurring in Eq. (2), are drastically reduced at high temperatures and high plasma densities; alternatively, the Drude model does not adequately describe the absorption. A more complete theoretical discussion will be presented elsewhere.

In conclusion, the three-pulse experiments support the picture that the carrier plasma rapidly cools off by transferring energy to the lattice. Plasma heating by free-carrier absorption does not lead to significant impact ionization. The "simple heating" model equations yield the correct plasma density and temperature on a picosecond time scale. The real part of the dielectric constant is consistent with a low value of the effective mass, and the imaginary part indicates a shortening of the momentum relaxation times.

This work was supported by the U. S. Office of Naval Research under contract No. 0014-83K-0030. One of us (H.K.) would like to acknowledge partial support from the Alexander von Humboldt Foundation, Bonn, R. R. Germany.

[1] D. H. Auston, C. M. Surko, T. N. C. Venkatesan, R. E. Slusher, and J. A. Golovchenko, Appl. Phys. Lett. **33**, 437 (1978).
[2] J. M. Liu, R. Yen, H. Kurz, and N. Bloembergen, Appl. Phys. Lett. **39**, 755 (1981); R. Yen, J. M. Liu, H. Kurz, and N. Bloembergen, Appl. Phys. A **27**, 153 (1982).
[3] J. M. Liu, H. Kurz, and N. Bloembergen, Appl. Phys. Lett. **41**, 643 (1982).
[4] D. von der Linde and N. Fabricius, Appl. Phys. Lett. **41**, 991 (1982).
[5] L. A. Lompré, J. M. Liu, H. Kurz, and N. Bloembergen, Appl. Phys. Lett. **43**, 168 (1983).
[6] A. Lietoila and F. Gibbons, Appl. Phys. Lett. **40**, 624 (1982).
[7] H. van Driel, L. A. Lompré, and N. Bloembergen (unpublished).
[8] K. G. Svantesson, J. Phys. D **12**, 425 (1979).

Appendix 7

Picosecond time-resolved reflectivity and transmission at 1.9 and 2.8 μm of laser-generated plasmas in silicon and germanium

H. M. van Driel,[a] L.-A. Lompré,[b] and N. Bloembergen
Gordon McKay Laboratory, Division of Applied Sciences, Harvard University, Cambridge, Massachusetts 02138

(Received 24 October 1983; accepted for publication 14 November 1983)

We have observed plasmon resonances with 1.9-μm and 2.8-μm probe pulses in silicon and germanium, excited by 25-ps pulses up to 40 mJ/cm^2 at 0.53 and 1.06 μm, respectively. Firm values of N/m^* are derived.

PACS numbers: 72.30. + q, 71.45.Gm, 52.25.Ps, 52.50.Jm

The kinetics of laser-generated electron-hole plasmas in semiconductors and their possible influence on phase transitions have been of considerable interest, particularly in the area of laser annealing of ion-implanted materials.[1] One of the most direct techniques which can be used to obtain the carrier density and its temporal and spatial evolution involves time-resolved free-carrier infrared spectroscopy[2] with the ambipolar plasmas probed in reflection and/or transmission. This technique has been used[3,4] in nanosecond and picosecond time scales to observe transient plasmon resonances at 5.4 and 10.6 μm in Ge, Si, and GaAs for plasma densities of 10^{19}–10^{20} cm^{-3}. To investigate higher densities in Si, several researchers have used high picosecond or femtosecond excitations with probe pulses at wavelengths ≤ 1.06 μm.[5] Although a free-carrier induced drop in the reflectivity is observed in all cases, the enhanced reflectivity associated with the plasmon resonance is not. Due to a lack of knowledge of the detailed dielectric function at high excitation levels, it is difficult to extract quantitative information about the plasma parameters from such experiments. However, even assuming the validity of Drude–Zener formalism, optical measurements allow only the evaluation of N/m^*, where N is the plasma density and m^* the electron-hole reduced conductivity effective mass.[6] From previous experiments employing a 1.06-μm picosecond probe a normalized density of $N/m^* = 3.4\times10^{48}$ g^{-1} cm^{-3} has been found for a 0.53-μm, 25-ps, 100-mJ/cm^2 excitation pulse.[6] According to the Drude model the plasmon resonance would therefore be expected at a wavelength of

$$\lambda = c/e(m^*/N_p)^{1/2}(\pi\epsilon_\infty)^{1/2} \simeq 2\,\mu m, \tag{1}$$

where $\epsilon_\infty = 11.8$ is the high-frequency dielectric constant.

In this letter we report the direct observation of the plasmon resonances by using picosecond probe pulses at 1.9 and 2.8 μm. A firm value of N/m^* is derived.

A passively mode-locked Nd:yttrium aluminum garnet laser was used to produce single 30-ps, 1.06-μm pulses which had Gaussian spatial and temporal profiles. These pulses were respectively focused to spot sizes of 800-μm diameter (e^{-1} intensity points) on (111) surfaces of nearly intrinsic Ge and Si wafers. The back surface of these samples was optically diffuse and so prevented undesired interference effects. The generated plasmas were probed in reflection (R) and in transmission (T) using 1.9 and 2.8-μm pulses which were derived from a portion of the initial 1.06-μm pulse by the stimulated Raman scattering in 50-cm-long cells containing 50 atmospheres of H_2 and CH_4, respectively. The first Stokes component from the H_2 gas and the second Stokes component from the CH_4 gas were selected using interference filters. The pulse widths, although not measured, are estimated[7] to be less than 30 ps. The probe pulses, whose spatial profile was measured to be close to diffraction limited, were

[a] Permanent address: Department of Physics and Erindale College, University of Toronto, Toronto, Canada, M5S 1A7.
[b] Permanent address: C.E.N./Saclay, DPh.G./S.P.A.S., 91191 Gif-sur-Yvette Cedex, France.

 0003-6951/84/030285-03$01.00

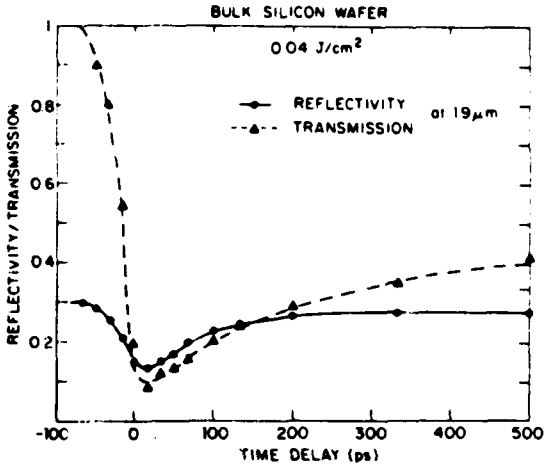

FIG. 1. Reflectivity and transmission of bulk Si at 1.9 μm as a function of probe time delay after a 0.53-μm pump pulse at 0.04 J/cm^2.

focused to spot sizes of $<200\,\mu$m at the center of the excitation region; their fluence was kept less than 1 mJ/cm^2 to avoid undesired heating effects. Three PbS detectors were used to measure reflected, transmitted, and reference probe pulse energies, while a calibrated vacuum photodiode was used to monitor pump energies. The signals from all four detectors were handled by a computer-automated data acquisition system. Standard picosecond pump and probe techniques were used to determine R and T as a function of time.

Figures 1–3 display typical results for the time-resolved reflectivity and transmission signatures in silicon and germanium for different pump fluences. The curves accompanying the data are guides to the eyes. The pump fluence was kept below the threshold fluence for melting (200 mJ/cm^2 in Si at 0.53 μm, 75 mJ/cm^2 in Ge at 1.06 μm) to avoid any contributions from metallic or molten regions. Complete theoretical interpretation of these results will be given elsewhere.[8] Here we wish to illustrate the salient features for

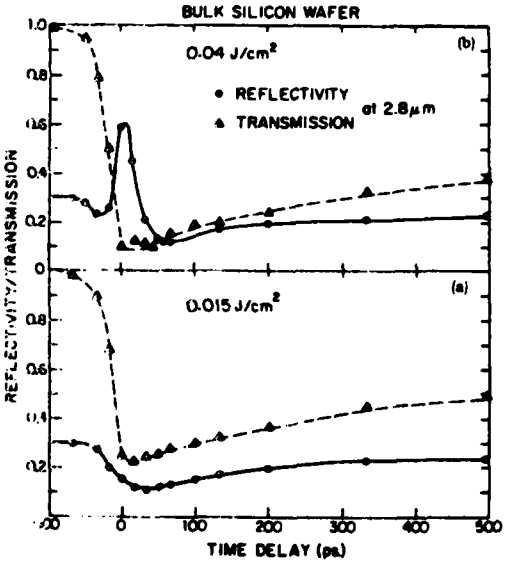

FIG. 2. Reflectivity and transmission of bulk Si at 2.8 μm as a function of probe time delay after a 0.53-μm pump pulsed at (a) 0.015 J/cm^2 and (b) 0.04 J/cm^2.

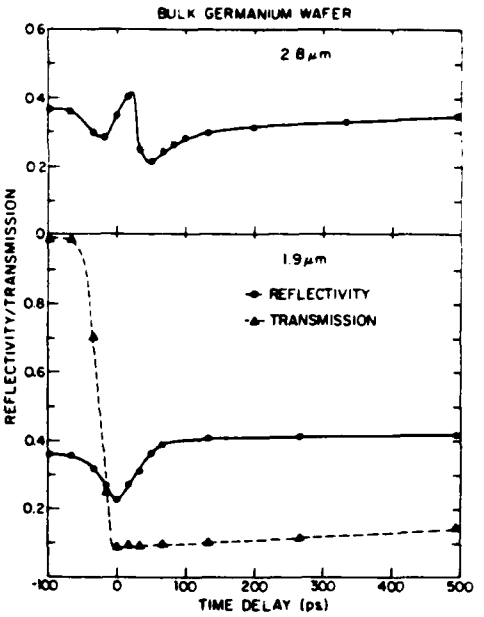

FIG. 3. Reflectivity and transmission of bulk Ge at 1.9 μm and 2.8 μm as a function of probe time delay after a 1.06-μm pulse of fluence 50 mJ/cm^2.

different excitations and probe conditions. Figure 1 shows the reflectivity R at 1.9 μm as a function of time for Si for a 40-mJ/cm^2 pump fluence. At 40 mJ/cm^2, and below, the transient R shows a broad single minimum. Within the Drude–Zener model, the true minimum is reached when the real part of the dielectric constant is unity, which occurs at a critical density $N_c = (1 - 1/\epsilon_\infty)N_p$, where N_p is given by Eq. (1). The value of the reflectivity at the minimum, $R = 0.12$, is determined by the plasma damping mechanism and the temporal width of the probe pulse. The nonzero width of the probe pulse unfortunately partially washes out the actual transient optical response of the plasmon resonance. However, at least for the broad minimum in R, at low fluences, these effects are small. Assuming that the convolution effects do not change the value of the minimum reflectivity, a value of $N/m^* = 3.6\times10^{48}\,\mathrm{g}^{-1}\,\mathrm{cm}^{-3}$ is derived. If one assumes for the effective mass, $m^* = 0.123m_0$, (the low density value) where m_0 is the free-electron mass, the plasma density would be 4×10^{20} cm^{-3} at the pump fluence of 40 mJ/cm^2. Theoretical considerations[9] indicate that m^*, and consequently N, may be up to factor 2 higher at this level of irradiation.

The transmission data, normalized to the bulk transmission of an unexcited sample, provides complementary information to that of the reflectivity, since it is sensitive to the total number of carriers in the bulk. The normalized transmission T is given by

$$T(t) = (0.7)^{-1}[1 - R(t)]\exp\left(-\sigma\int_0^\infty N(x)dx\right), \qquad (2)$$

where 0.7 is the surface transmission of the unexcited sample. This equation is justified if σ, the free-carrier absorption cross section, is independent of depth x. The transmission drops to a minimum of 10% at 40 mJ/cm^2. This transmission minimum is located at a slightly positive time delay between the excitation and the probe pulses. This is a direct

consequence of the temporal integration (nonzero probe pulse width). The free-carrier induced transmission change recovered more slowly than the corresponding reflectivity trace, due to the fact that the plasma density at the surface is higher than the average density in the bulk.

Figure 2 shows typical experimental results obtained at 2.8 μm, where the plasmon resonance is easily observed. The 15-mJ/cm^2 data are similar to that of Fig. 1 and show a broad single minimum. At 40 mJ/cm^2, the transient R shows two shallow minima on both sides of a peak near the zero time delay. During the leading and the trailing edge of the pump pulse, the carrier surface density passes twice through the critical density N_c. Deconvolution of the data with respect to the nonzero probe pulse width indicates that the peak reflectivity is >0.9. The slower decay of R at 2.8 μm is as expected, since the reflectivity at the longer wavelength is more sensitive to a given density of carriers. The clear experimental observation of the plasmon resonance at 2.8 μm indicates that the N/m^* value passes twice through the value of 1.8×10^{48} g^{-1} cm^{-3} on each side of the maximum value of 3.6×10^{48} g^{-1} cm^{-3} at the same fluence of 40 mJ/cm^2. Apart from discrepancy near zero delay, where large fluctuations were noted, the transmission data at 40 mJ/cm^2 are consistent with Eq. (2) with $\sigma = 5\times10^{-7}$ cm^2.[10]

The data taken with the Ge sample are interesting, since they reveal apparent saturation of the carrier generation rate which has been the subject of speculations over the past few years.[11,12] Figure 3 shows R and T data at 1.9 and 2.8 μm for Ge at 50 mJ/cm^2, 30% below the threshold for bulk melting. With a pump absorption depth of 0.7 μm, the carrier generation rate at 1.06 μm is higher than that of 100 mJ/cm^2 at 0.53 μm in Si. Also the Auger recombination coefficient[13] of 2×10^{-31} cm^6/s is a factor of 2 smaller than in Si, as is the reduced effective mass. However, as shown, the plasmon resonance is not observed at 1.9 μm and is barely discernible at 2.8 μm. Theoretical considerations for germanium indicate that the reduced effective mass is not more than 20% greater than its low density value $m^* = 0.08m_0$. A detailed fit of the data shows that the maximum density obtained is $N = 2.5\times10^{20}$ cm^{-3}, while $N_p = 2.0\times10^{20}$ cm^{-3} for 2.8 μm. The observations at 2.8 μm are consistent with those at 1.9 μm where no reflectivity peak is observed, as this would require a density at the surface of 4.5×10^{20} cm^{-3}. The low densities are indicative of intravalence band absorption[12,14] or saturation of the valence-conduction band transition due to the Burstein–Moss effect. A model which neglects these processes would lead to a larger carrier density at the surface ($>10^{21}$ cm^{-3}), which is not observed. The low minimum value of the transmission, shown here only for 1.9 μm, also indicates a stronger plasmon damping, due to the added contribution of intravalence band transitions. Lastly, it should be noted that the melting threshold of Ge at 1.06 μm is consistent with the absorption coefficient and the known melting temperature of 1210 K.

In summary, we have shown experimentally that the plasmon resonances are located between 1.9 and 2.8 μm for picosecond excitation pulses of 40 mJ/cm^2 on silicon and of 50 mJ/cm^2 on germanium. In silicon the maximum plasma density at the surface is 4×10^{20} cm^{-3} if variation of the effective mass is negligible, although both may be up to a factor of 2 higher. In germanium the maximum carrier density is about $2\text{–}3\times10^{20}$ cm^{-3} before melting occurs. These data show that fast infrared transient spectroscopy of Si and Ge is a valuable technique.

This research was supported by the Office of Naval Research under contract N00014-83-K-0030 and the Joint Service Electronics Program under contract N00014-75-C-00648.

[1]See, for example, articles in *Laser and Electron Beam Interactions with Solids*, edited by B. R. Appleton and G. K. Celler (North-Holland, Amsterdam, 1982); *Laser-Solid Interactions and Transient Thermal Processing of Materials*, edited by J. Narayan, W. L. Brown, and R. A. Lemons (North-Holland, Amsterdam, 1983).
[2]W. G. Spitzer and H. Y. Fan, Phys. Rev. **106**, 882 (1957).
[3]G. N. Galkin, L. M. Blinov, V. S. Vavilov, and A. G. Solomatin, Pisma Zh. Eksp. Teor. Fiz. 7, 93 (1968) [JETP Lett. 7, 69 (1968)]; S. A. Jamison, A. V. Nurmikko, and H. J. Gerritsen, Appl. Phys. Lett. **29**, 640 (1976); A. J. Alcock, P. B. Corkum, and P. J. James, Can. J. Phys. **57**, 1280 (1979).
[4]P. C. Hein, M. I. Gallant, and H. M. van Driel, Solid State Commun. **39**, 601 (1981); M. I. Gallant and H. M. van Driel, Phys. Rev. B **26**, 2133 (1982); J. S. Preston and H. M. van Driel, Phys. Rev. B (unpublished).
[5]J. M. Liu, H. Kurz, and N. Bloembergen, Appl. Phys. Lett. **41**, 643 (1983); D. von der Linde and N. Fabricius, Appl. Phys. Lett. **41**, 991 (1983); C. V. Shank, R. Yen, and C. Hirliman, Phys. Rev. Lett. **50**, 454 (1983).
[6]H. Kurz, L.-A. Lompré, and J. M. Liu, in Proc. of MRS-Europe Meeting, Strasbourg, 1983 (unpublished).
[7]R. L. Carman, M. E. Mack, F. Shimizu, and N. Bloembergen, Phys. Rev. Lett. **23**, 1327 (1969); R. L. Carman, F. Shimizu, C. S. Wang, and N. Bloembergen, Phys. Rev. A **2**, 60 (1970).
[8]H. M. van Driel, L.-A. Lompré, and N. Bloembergen (unpublished).
[9]H. M. van Driel (unpublished); see also M. Miyao, T. Matsuoka, N. Tatsuaki, and T. Tokuyama, Solid State Commun. **37**, 605 (1981).
[10]M. Balkanski, A. Aziza, and E. Amzallaq, Phys. Status Solidi **31**, 323 (1969).
[11]A. Elci, M. O. Scully, A. L. Smirl, and J. C. Matter, Phys. Rev. B **16**, 191 (1977).
[12]C. Y. Leung and M. O. Scully, Phys. Rev. B **23**, 6797 (1981); A. L. Smirl, A. Miller, G. P. Perryman, and T. J. Boggess, J. de Physique (Paris) C **7**, 463 (1981).
[13]D. H. Auston, C. V. Shank, and P. Lefur, Phys. Rev. Lett. **35**, 1022 (1975).
[14]R. B. James, IEEE J. Quantum Electron. **QE-19**, 709 (1983).

Appendix 8

Picosecond Photoemission Study of Laser-Induced Phase Transitions in Silicon

A. M. Malvezzi, H. Kurz and N. Bloembergen

Division of Applied Sciences, Harvard University, Cambridge, MA 02138

Summary

Pulsed laser-induced phase transitions in semiconductors are characterized by an ultrafast energy transfer from the generated electron-hole plasma to the phonons. Time-resolved optical measurements provide ample evidence that the thermal equilibrium between carriers and phonons is established within a few picoseconds [1]. However, optical techniques mainly explore the evolution of plasma density and lattice temperature. Direct information about the energy content of the electron-hole plasma and the energy loss due to phonon interaction cannot be obtained. Picosecond photoemission provides a direct approach to this problem.

According to the well-known generalized Fowler-DuBridge theory [2,3], the electron emission current is composed of photoelectric and thermionic contributions. Under high excitation levels multiphotoelectric emission is readily observable. Its power law dependence is characterized by the number of photons necessary to bridge the energy gap between the ground state and the vacuum level in intrinsic silicon. A variation of the photoelectric yield is expected as soon as the incident laser pulse induces structural changes on the surface of the semiconductor. The thermionic contribution is extremely sensitive to the energy content of a thermalized carrier distribution characterized by a temperature $T_c = T_e = T_h$. Picosecond excitation provides a stringent test for anomalous heating in which the carriers are no longer in equilibrium with the lattice phonon. Due to the small specific heat of the electron-hole plasma, T_c should be much higher than the lattice temperature T_L as soon as the energy is not transferred to the phonons instantaneously.

In this contribution we report on picosecond photoemission of silicon, with photon energies corresponding to the second harmonic (E = 2.33 eV) and fourth harmonic (E = 4.66 eV) of a Nd:YAG laser pulse. The photoelectric response is studied as a function of laser fluence up to $2F_{th}$, where F_{th} is the threshold value for phase transition. This work extends the previous analysis of Liu et al. [4] to laser fluences four orders of magnitude below F_{th}, to study explicitly the power laws of photoemission and to monitor the occurrance of anomalous heating even at low carrier densities. In this context we used exclusively 4.66 eV pulses to create carriers with large excess energies. Specific attention has been paid to the emission of positive ions, which starts in the vicinity of F_{th} and exhibits an extremely nonlinear fluence dependence. It is clear that this emission is intimately correlated to the structural change of the surface taking place at F_{th}.

The experiments were performed in a vacuum of 5×10^{-8} Torr. Both Si(111) and Si(100) have been irradiated. A vacuum diode configuration was used to measure the electric charges. A 1 mm diameter wire placed at 2.5-3 mm from the sample surface acted as a charge collector. Both sample and wire were electrically insulated from the body of the vacuum chamber and

could be independently biased up to $\pm$ 4 kV. Two configurations for the measurements are possible. One can measure either the charges collected on the wire or the ones escaping from the sample. Both methods have been shown to give similar results.

The fluence dependence of the photoelectric emission can be genarally divided into three distinct regimes. In the case of UV-irradiation (E_{ph} = 4.66 eV), a superposition of linear and quadratic effects can be observed below $F(4\omega) = F_{th}(4\omega)/15 \sim 2$ mJ/cm^2 (regime I). The amount of collected charges is completely independent of the collector potential. Clearly, at this fluence level we operate in the saturation regime, colecting all electrons emitted from the surface. The value of the linear photoelectric yield in electrons per absorbed photons, $Y_1 = 8 \times 10^{-7}$, is in agreement with published data for silicon exposed to air [6]. The experimental value for the quadratic effect, 3×10^{-32} cm^2 s is consistent with results obtained by Bensoussan et al. in picosecond experiments at lower photon energies [7]. In regime I the nonlinear emission dominates the electron emission over a wide range of fluences (10^{-5}-10^{-3} J/cm^2). The data are highly reproducible and the quadratic quantum yield is completely insensitive to surface cleaning treatments.

Above $F(4\omega) = F_{th}(4\omega)/15$ the collected charge signal starts to be dependent on the collector potential. We enter the space charge limited regime (II) of the vacuum diode, where the applied field is screened by a cloud of electrons in front of the surface [5]. The nonlinear emission is masked by this space charge effect. The electron emission is limited to the leading edge of the picosecond pulse. At $F(4\omega) = 25$ mJ/cm^2, where the first structural changes at the surface are observed, the electron emission exhibits an extremely nonlinear increase in this regime (III). The space charge field is lowered by the simultaneous emission of positive ions. Above $2F_{th}(4\omega)$ equal amounts of electrons and positive ions can be collected with the $\pm$ 4 kV applied on the wire. The space charge fields are completely neutralized above this fluence level. We attribute the sharp increase of photoelectrons and the simultaneous apearance of positive ions to a structural change of the surface. The threshold for photoemission is abruptly changed to lower values and positive ions can be extracted from the highly disordered phase by the space charge field developed in front of the surface. This picture is consistent with melting of the surface. Similar behavior has been observed in the case of VIS-irradiation (E_{ph} = 2.33 eV).

The photoelectric emission at 2.33 eV is determined by a strong two-quantum process and weak higher order contributions. In contrast to the 4.66 eV irradiation, the quadratic quantum yield depends strongly on the surface condition, as expected from a near-threshold excitation. Because of the lower photoelectric current density below the fluence threshold for phase transition, space charge effects are less pronounced than in the case of UV-irradiation.

The lower quadratic quantum yield at 2.33 eV is preferable for the study of possible thermionic contributions. Application of the Richardson-Dushmann equation in the regime I gives an upper limit of 2200 K for the carrier temperature up to fluence levels of 100 mJ/cm^2. At this VIS fluence the lattice temperature is raised to ~ 800 K and the carrier density N is limited to 6×10^{20}, as the optical measurements show [8]. This maximum

splitting between the carrier temperature T_c and the lattice temperature T_L confirms that most of the energy deposited into the electron-hole plasma is transferred to the phonons.

This research was supported by the U. S. Office of Naval Research under contract N00014-83K-0030.

REFERENCES

1. L.A. Lompré, J.M. Liu, H. Kurz and N. Bloembergen, Appl. Phys. Lett. 44, 3 (1984).

2. R.H. Fowler, Phys. Rev. 38, 45 (1931).

3. L.A. Du-Bridge, Phys. Rev. 43, 727 (1933).

4. J.M. Liu, R. Yen, H. Kurz and N. Bloembergen, Mat. Res. Soc. Symp. Proc. 4, 23 (1982).

5. I. Langmuir, Phys. Rev. 21, 419 (1923).

6. R.M. Broudy, Phys. Rev. B 1, 3430 (1970).

7. M. Bensoussan, J.M. Moison, B. Stoesz and C. Sebenne, Phys. Rev. B 23, 992 (1981).

8. L.A. Lompré, J.M. Liu, H. Kurz and N. Bloembergen, in Mat. Res. Soc. Symp. Proc., Boston 1983.

Appendix 9

Second Harmonic Generation in Reflection from Crystalline GaAs under Intense Picosecond Laser Irradiation

A.M. Malvezzi
Division of Applied Sciences, Harvard University,
Cambridge, Massachusetts 02138

J.M. Liu
GTE Laboratories Incorporated
40 Sylvan Road
Waltham, MA 02254

N. Bloembergen
Division of Applied Sciences, Harvard University,
Cambridge, Massachusetts 02138

Abstract: The emission of second harmonic radiation in reflection from crystalline GaAs irradiated with 20 ps, 530 nm laser pulses has been measured for incident laser fluences far exceeding the threshold fluence F_{th} for permanent reflectivity changes. The results are consistent with the occurrence of surface melting during the laser pulse. Detailed analysis of the second harmonic signals reveals an upper limit of 2 ps for the structural transition associated with the melting of the surface.

The intensity of second harmonic generation (SHG) from non-centrosymmetric crystals such as GaAs should show a drastic decrease when a transition to a centrosymmetric phase occurs. This has been observed with nanosecond resolution by S.A. Akhmanov et al.[1] when the laser fluence exceeds a threshold value for melting.

In this letter we present the results of SHG study on GaAs with picosecond excitation. In simple single shot experiments, the SHG dependence of the incident laser fluence is monitored under appropriate geometrical conditions. The deviation from the quadratic power law is analyzed by model calculations based on the assumption of a transition to a centrosymmetric phase as soon as a critical fluence during the 20 ps laser pulse is accumulated on the surface of GaAs.

In our analysis we use mainly (110) surfaces excited with single picosecond pulses at 532 nm with the direction of the electric field parallel to a <111> crystal direction. The second harmonic from a passively mode-locked Nd:YAG laser system is focussed on the GaAs surface at an angle of 45° of incidence. The pulse duration is τ = 12.5 ps at the 1/e points of the Gaussian temporal profile. The second harmonic signal at 266 nm is detected in the direction of specular reflection by a photomultiplier tube. The reflected exciting radiation is suppressed by a combination of filters. Second harmonic signals down to ≈200 photons are detected. The inherent fluctuations in the pulse duration of the laser pulse are monitored by standard SA-techniques[2] Accidental double pulses are rejected. Both precautions yield a significant smoothing of the SHG data.

Generally, two separate SHG regimes are observed. Below the critical fluence of 30 mJ/cm^2 at 532 nm, where melting and subsequent amorphization of the surface occur, the signal exhibits the expected quadratic power law dependence $I_s = \eta_o I_g^2$, where I_s is the intensity of the second harmonic pulse and I_g is the intensity of the exciting green pulse. Figure 1 shows a log-log plot of the absolute SHG energy emitted from a (110) surface as a function of the excitation fluence F. The data in this figure are integrated signals over space and time. The excitation pulse is focussed to a spot size of 200 μm in diameter. The SHG energy increases with slope 2 up to a fluence level of F_{th} = 30 mJ/cm^2. The SHG efficiency is not sensibly affected by the generation of a dense electron-hole plasma or by lattice heating up to the melting point. A value of $\eta_o = 2.5 \times 10^{-18}$ cm^2/W is derived from the experiment. Above F_{th} the SHG signal grows more slowly. The non-centrosymmetric GaAs structure is obviously changed during the excitation pulse. The threshold fluence value of 30 mJ/cm^2 is in excellent agreement with calculated fluence levels necessary to melt GaAs surfaces[3]. The solid curve in Figure 1 represents calculated SHG values where a cutoff in the SHG efficiency is assumed as soon as the critical fluence F_{th} is assumulated during the pulse. The integration over the Gaussian space and time profiles smooths the sharp drop of SHG emission considerably. At fluences far above the threshold value, F_{th}, for melting the UV signal increases again. This puzzling behavior has been carefully examined by looking at the angular and time dependence of the signal. For pump fluences exceeding $\approx 3F_{th}$ an additional UV signal is detected, whose fully isotropic angular distribution is in marked constrast to the specular SHG beam. This radiation, which is

accompanied at high fluences by a readily observed blue spark at the surface, exhibits a decay time of ≈ 1μs, while the duration of the SHG signal is limited by the time constant (10 ns) of the photomultiplier tube. To analyze the growth of this additional signal, the emission from a (100) GaAs surface is studied, where the polarization of the excitation beam is kept parallel to a <001> axis. Under these conditions, the SHG signal is zero and the background UV emission can be measured as a function of the exciting 532 nm pulse fluence. As shown in Figure 1, this new emission does not affect the SHG signal at fluences below $5F_{th}$. However, due to the extreme nonlinear behavior, it is responsible for the unexpected increase of the UV emission at higher fluences. A further study of this new emission process, which is closely related to the evaporation and plasma formation in front of the surface is beyond the scope of this letter. Here, we restrict our interest to the time scale on which the surface structural changes on GaAs occur. For this purpose, this isotropic contribution at high pump fluences is simply subtracted from the total UV signal on (110) surfaces.

To enhance the deviation from the quadratic power law above F_{th} the spatial resolution of the experimental setup is improved by inserting a diaphragm in the path of the specular SHG beam. In Figure 2, the energy dependence of the SHG emitted by the central portion (120 μm in diameter) of the excited area on the surface is shown. Clearly, the saturation of the time integrated SHG signal in the vicinity of F_{th} is more pronounced. These data are now compared with model calculations, where the transition from an ordered non-centrosymmetric structure to a disordered liquid phase is simulated by a SHG efficiency decaying with a time constant τ_s. The SHG intensity is given by:

$$I_s(r,t) = \eta(r,t)\, I_g^2(r,t),$$

where

$$\eta(r,t) = \begin{cases} \eta_o & \text{for } t<t_m(r) \\ \eta_o \exp\left(-\dfrac{t-t_m(r)}{\tau_s}\right) & \text{for } t > t_m(r). \end{cases}$$

At each point r on the surface, η starts to decay as soon as the initial fluence F_{th} is reached

$$\int_{-\infty}^{t_m(r)} I_g(r,t)\, dt = F_{th}.$$

The solid curve in Figure 2 corresponds to a stepwise truncation of the SHG emission by setting $\tau_s = 0$. Around the threshold value for melting, when the phase transition still occurs on the trailing edge of the excitation pulse, the data are well described by the curve. However, at higher fluences, when F_{th} is reached during the leading part of the excitation pulse, the SHG data points are slightly above the calculated curve.

In order to further elucidate the temporal behavior of the transition to the disordered phase the data of Figure 2 are represented in a linear scale in Figure 3 and compared with the model calculations with different time constants τ_s. Despite the scattering of the data points the solid curves of Figure 3 show clearly that the SHG emission drops with a time constant $\tau_s < 2$ ps as soon as the energy necessary for melting is locally delivered. In

Figure 3, the calculation for τ_s = 5 ps is also shown, demonstrating the sensitivity of the SHG emission process towards a slightly delayed phase transition.

In conclusion, the SHG results obtained with a single beam technique indicate that an ultrafast transition to a centrosymmetric phase occurs in crystalline GaAs under picosecond laser irradiation. The SHG emission follows the usual quadratic power law up to the threshold fluence for melting. Above this level the data are consistent with an ultrafast transition to a disordered phase within 2 ps.

We would like to thank R. Yen and J.Y. Tsao for providing the (110) GaAs samples, H. Kurz and D. von der Linde for illuminating discussions. This research was supported by the Office of Naval Research under contract No. 0014-83K-0030 and the Joint Service Electronic Program under contract No. N00014-75-C-0648.

References

1. S.A. Akhmanov, N.I. Koroteev, G.A. Paition, I.L. Shumay, M.F. Guljautdinov, I.B. Khaibullin, and E.I. Shtyrkov, Optics Comm. 47, 202 (1983).

2. W.L. Smith and J.H. Bechtel, J. Appl. Phys. 47, 1065 (1976).

3. A. Lietoila and J.F. Gibbons in "Laser and Electron-beam Interactions with Solids" ed. by B.R. Appleton and G.K. Celler (North-Holland, New York, 1982), p. 163.

Figure Captions

Figure 1 Energy of the specular emission at 266 nm vs incident laser fluence (λ = 532 nm) on GaAs. The laser spot diameter is 200 μm. Closed dots refer to $(1\bar{1}0)$ surface, laser electric field parallel to the $[1\bar{1}1]$ crystal axis. Open dots refer to (100) crystal surface, laser electric field parallel to the [001] crystal axis. The solid curve represents calculated SHG energy with $\tau_s = 0$ as discussed in the text.

Figure 2 Same as Figure 1, but limiting the collection of the SHG signal from a disk of 120 μm in diameter centered on the incident laser spot.

Figure 3 Plot of the data of Figure 2 on linear scales. The solid curves refer to calculations with the values of τ_s shown.

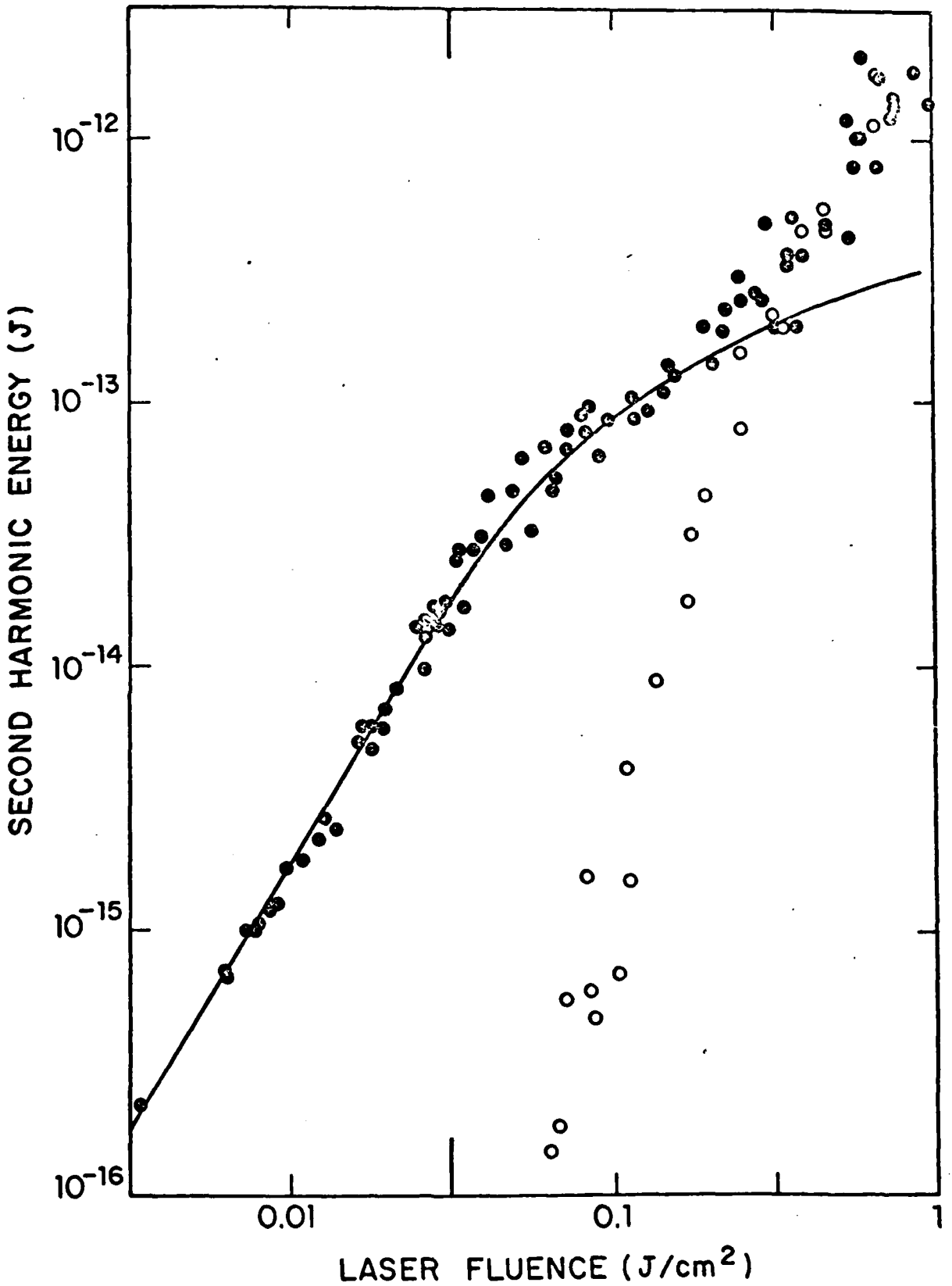
SECOND HARMONIC ENERGY (J)
10^{-12}
10^{-13}
10^{-14}
10^{-15}
10^{-16}
0.01
0.1
1
LASER FLUENCE (J/cm^2)

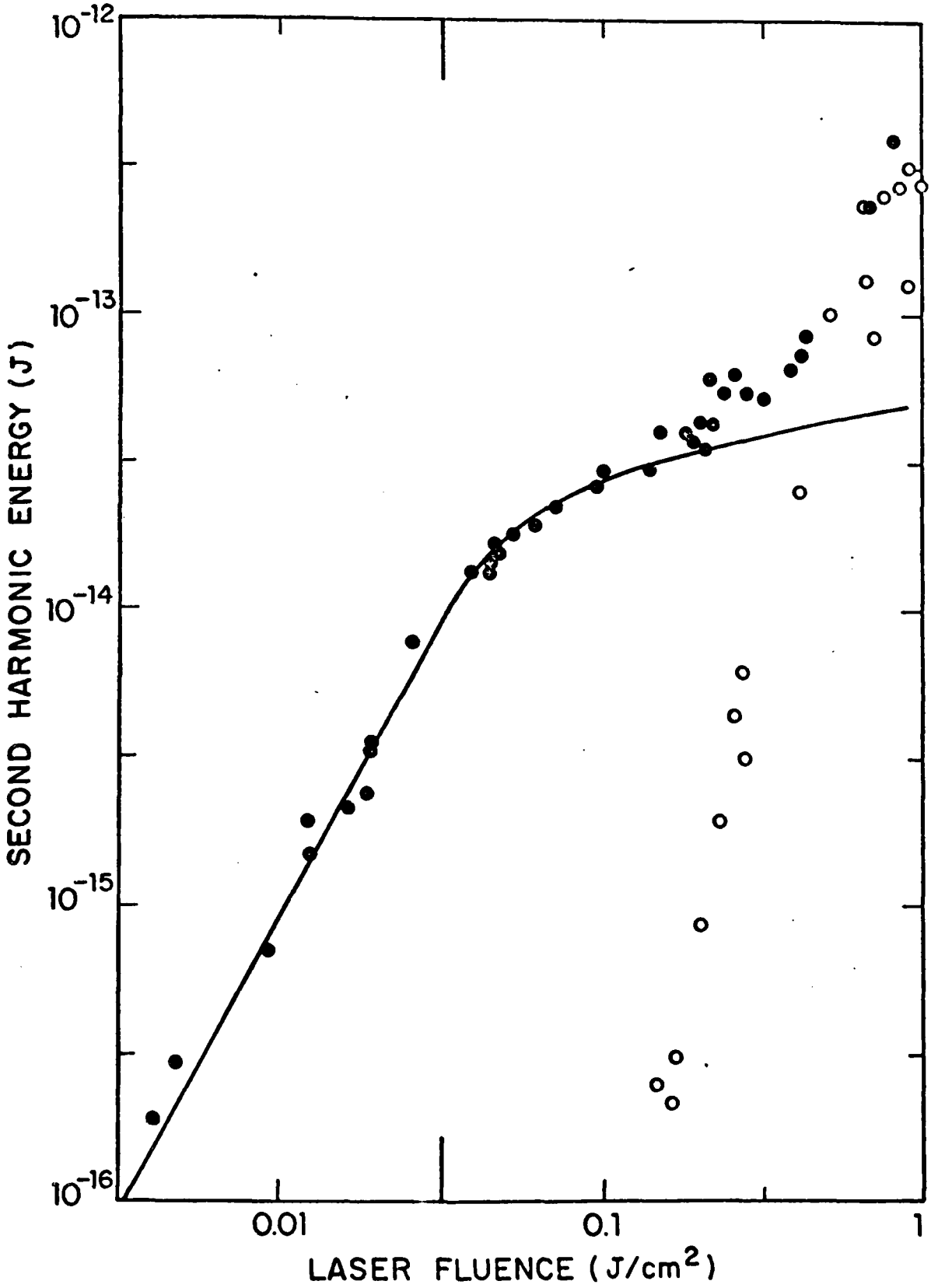
10^{-12}
10^{-13}
10^{-14}
10^{-15}
10^{-16}
SECOND HARMONIC ENERGY (J)
0.01
0.1
1
LASER FLUENCE (J/cm^2)

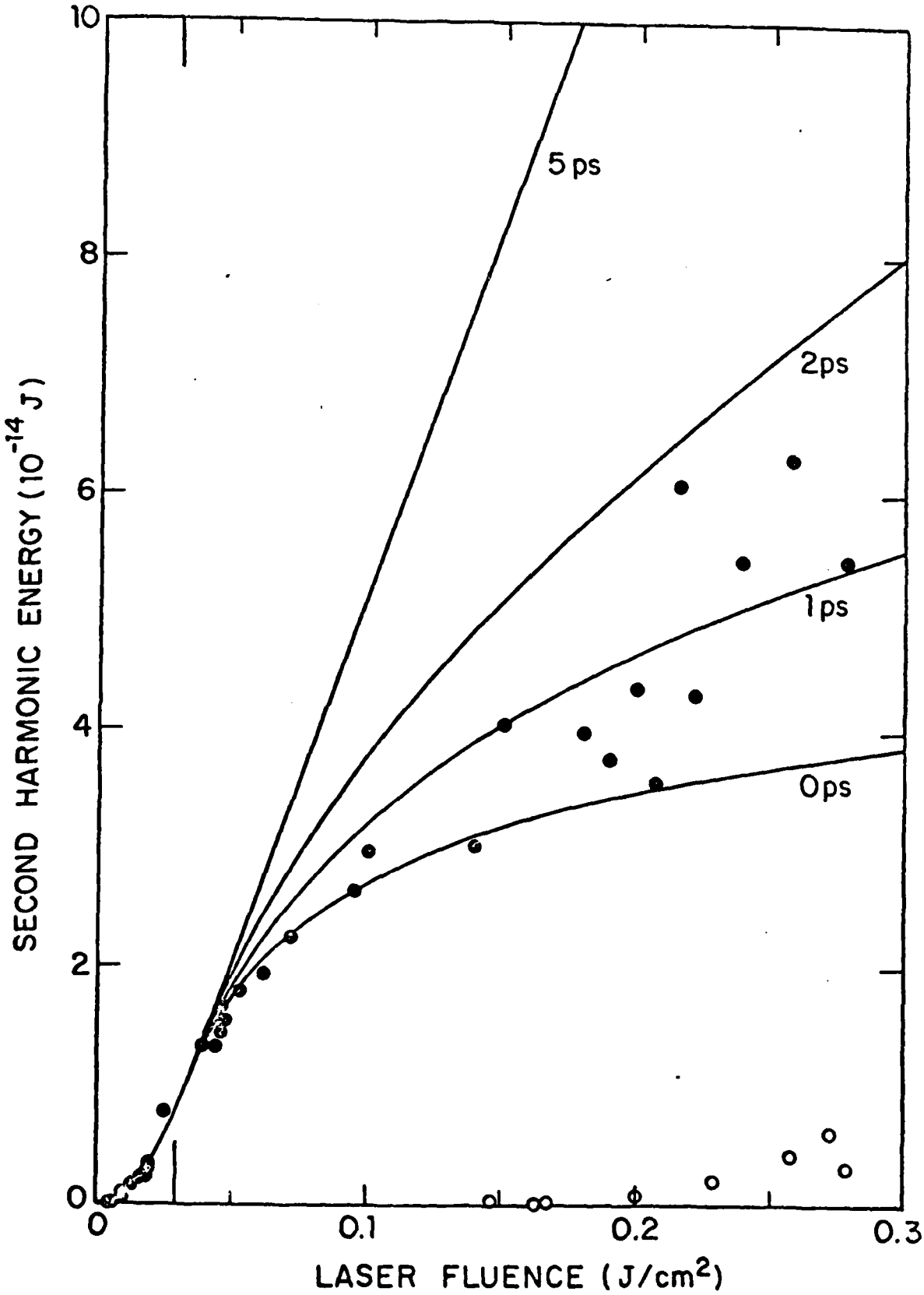
10
8
6
4
2
0
0
0.1
0.2
0.3
5 ps
2ps
1ps
0ps
SECOND HARMONIC ENERGY (10^{-14} J)
LASER FLUENCE (J/cm^2)

Appendix 10

Nonlinear Photoemission from Picosecond Irradiated Silicon

A.M.Malvezzi, H.Kurz and N.Bloembergen
Division of Applied Sciences, Harvard University, Cambridge
Massachusetts 02138, USA

Three distinctly different regimes of photoelectric emission are observed over a wide fluence range of UV-laser pulses irradiating single-crystal silicon samples. The role of the electron-hole plasma in the nonlinear photoemission is demonstrated by temporal correlation measurements. The diffusion properties of hot carriers are analyzed by investigating the influence of energy transport by hot carrier diffusion on the fluence threshold for melting with UV photons.

Pacs numbers: 79.60.-i
64.70.Dv

Pulsed laser-induced modifications of semicondutor surfaces find growing technical interest for the development of novel material processing technologies. In recent times much experimental effort has been devoted to studying laser-induced morphology changes by optical techniques [1]. The formation and relaxation of electron-hole pairs, the kinetics of the ambipolar solid state plasma and the energy transfer to the lattice phonons has been investigated by pump and probe experiments with ps and fs pulses [1,2,3,4].

Charged particle emission measurements provide an alternative approach to the study of the fundamental process at the surface of laser irradiated material. Contrary to optical measurements, where bulk processes are dominant and the interpretation is complicated by spatial gradients of the parameters to be studied, here one probes the outermost layer of the surface. The strict power law of single- and multiple-quantum excitation, described by the generalized Fowler-DuBridge theory [5], can be modified by thermal broadening of the energy distributions of the carriers in the ground or excited states. At very high carrier temperatures the high energy tail of the energy distribution reaches the vacuum level, and pure thermionic electron emission, as described by the generalized Richardson-Dushman equation, occurs. Nonlinear photoemission of silicon has been observed under nanosecond laser excitation [6], The underlying mechanisms, however, could not be clarified. In recent picosecond photoemission experiments the Richardson-Dushman equation has been used to determine the upper limit of the electron temperature of picosecond-irradiated silicon at laser fluences much below [7] and above [8] the threshold values

for melting.

In this paper we present for the first time a plausible explanation of the nonlinearity of photoemission in picosecond irradiated silicon. By using correlation photoelectric techniques, we have been able to reveal the dominant role of the electron-hole plasma in a two-step, single-photon sequence. In addition, by taking advantage of the extremely small penetration depth of the laser frequency used ($\alpha' = 5 \times 10^{-7}$ cm), the distance L, which hot carriers are able to diffuse before they transfer their energy to the lattice phonons, is estimated at the critical laser fluence for melting.

In our experiment the fourth harmonic ($h\nu$ = 4.66 eV) of a 30 ps Nd:YAG laser pulse is focused on a crystalline silicon target placed in 10^{-9} torr vacuum. The emitted charges are collected by a diode configuration as described in [7,8]. A bias voltage of 4 kV is applied to ensure the collection of the total amount of charges emitted. The dependance of the collected charge density (Coulombs/cm^2) on the incident laser fluence is show in Fig. 1.

Three distinctly different photoelectric regimes are observed. In regime I below 1 mJ/cm^2 UV-laser fluence, a superposition of linear and quadratic response is observed independent of the applied collector voltage. The electron current density $J(\underline{r},t)$ can be expressed in this regime by

$$J(\underline{r},t) = k_1\, I(\underline{r},t)\, e/h\nu + k_2\, (I(\underline{r},t)\, e/h\nu)^2 \qquad (1)$$

where e is the electron charge, $h\nu$ the laser photon energy, $I(\underline{r},t)$ the space- and time-dependent laser intensity on the sample surface. Integration of (1) over a space and time gaussian profile results in

$$Q/\pi\rho^2 = k_1 (e/h\nu) F + 2^{-3/2} \pi^{-1/2} k_2 (e/h\nu)^2 F^2 \qquad (2)$$

where Q is the total emitted charge, ρ is the 1/e radius of the laser beam on the surface, τ its 1/e time duration and F the laser fluence (J/cm^2). The observed linear quantum yield of $8 \pm 2 \times 10^{-7}$ electrons per absorbed photon is in fair agreement with published data of silicon exposed to air [9]. The value of the coefficient for the quadratic process, $k_2 = 3.6 \times 10^{-13}$ $cm^2s/Coul$ is consistent with extrapolated data obtained in nanosecond experiments [6]. The dashed line of Fig. 1 shows the calculated charge density using these yield data. In regime II the photoemission deviates from the calculated behavior and is progressively reduced by space charge effects. The collected charge density is dependent upon the applied voltage. By the rapid accumulation of electrons in front of the surface, the applied field is screened and the collector current drops. In regime III the electron emission exhibits a strong increase again as soon the critical laser fluence for melting, $F_{th} = 25$ mJ/cm^2 is reached. The sharp rise in the electron emission is accompanied by the emission of positive ions, which are collected when the bias voltage is reversed. The space charge field which inhibits the electron emission in regime II, is neutralized by the injection of positively charged particles. Thus,

the collection of electrons above the threshold for melting is governed by the availability of positive ions to remove the space charge field. Therefore, nearly the same amount of electrons and ions is collected at higher fluences independently of the magnitude of the applied field.

In order to explore the temporal evolution of the photoemission process, we used a time correlation technique in which two consecutive ps pulses are focused on the same area of the sample. The synergetic effects on the photoemission are measured as a function of time delay τ between the two pulses.

To begin with, this double pulse technique is applied for a general survey of regime I and II. In Fig. 2 the ratio of total collected charge Q to the sum of laser energy $E_t = E_1 + E_2$ is plotted versus the sum of laser fluences $F_t = F_1 + F_2$ (J/cm^2). The $\tau = \infty$ condition is simulated by spatially separating the two laser spots. The solid line in Fig. 2 illustrates the behavior under this condition. Below F = 3 mJ/cm^2 the quantum efficiency increases linearly, as expected from a quadratic process. At 7 mJ/cm^2 the maximum efficiency is reached and at higher fluences (regime II) the amount of collected charges drops again.

As soon as the temporal separation of the two laser pulses is less then 100 ps, noticeable changes in the fluence response occur. The slope of the linear increase below 3 mJ/cm^2 increases significantly. The collected charge maximum moves towards smaller fluences, and the drop in the space charge regime is more pronounced. The largest reduction of collection efficiency occurs in this regime if the two pulses strike the surface simultaneously

(τ = 0). In this case the total charge emitted by the two pulses is less than the sum of the charges of two separated pulses, because of increased suppression by the space charge cloud in front of the surface. If the two pulses hit the same area, but are separated by a time interval sufficiently long to remove the space charge generated by the first pulse, then the combined charge emission should be equal to that of two spatially separated pulses. It is estimated from our sample and anode field geometry, that the electron cloud is removed from the illuminated spot in about 10^{-10} s. The data in Fig. 2 appear to confirm these space charge effects. Longer lasting space charges resulting from thermionic emission are negligible.

The main part of our interest, however, is focused on the increase of quantum efficiency at fluences at which space charge effects can be neglected. To explore the origin of the quadratic photoemission process in regime I, we performed a complete time-resolved study of the correlation of the collected charges. In Fig. 3 the linear slopes of Fig. 2 are plotted versus the time delay between the two UV pulses. The data are normalized to the $\tau = \infty$ condition. Despite the large experimental error, the temporal correlation behavior clearly indicates that the first pulse activates the surface for the second. This optical activation persists for times much longer than the pulse duration and is closely correlated to the dynamics of the elctron-hole plasma formed. At a fluence level of 1 mJ/cm^2 no significant lattice heating occurs, and the maximum carrier density generated at the surface is too low for Auger recombination processes to become

dominant in the density equation. The penetration depth of 4.66 eV photons ($\alpha' = 5 \times 10^{-7}$ cm) is much smaller than the diffusion length $L_a = (D_a \tau_p)^{1/2}$ on a picosecond time scale. Under these conditions, an analytical solution of the density at the surface N(0,t) can be derived using solutions of the surface heating problem [10]. Under irradiation with a laser pulse with gaussian temporal profile, the density time-dependance is given by:

$$N(0,t) = \frac{I_m (1-R)}{(D_a)^{1/2}} \tau_p^{1/2} \eta(t/\tau_p) \qquad (3)$$

where $I_m(1-R)$ is the reflection corrected incidence irradiance, τ_p the *1/e half width of the laser pulse*, D_a the ambipolar diffusion coefficient and $\eta(t/\tau_p)$ a strictly time-dependent form factor, which is developed in [9]. With $D_a = 20$ cm^2/s, a maximum density of 5×10^{18} cm^{-3} is reached after 0.55 τ_p under the excitation levels used in this correlation experiment. The temporal decay is solely determined by $\eta(t/\tau_p)$. The striking resemblance between the temporal behavior of the photoelectric correlation signal and temporal shape of η leads us to the conclusion that the nonlinearity of the photoemission regime I is caused by the presence of the electron-hole pairs. It is basically a two-step single-photon excitation process, where in the first step electrons are excited via direct transitions into high-lying conduction bands. Rapid intercarrier collisions ensure thermalization of the

carrier distribution, and phonon assisted inter- and intravalley relaxation processes lead to the accumulation of a large carrier density in the vicinity of conduction band minima. Because of the lack of sufficient electron-hole recombination channels, their accumulation is mainly determined by the relaxation rate from the higher-lying states and diffusion into low-density regions. From the intermediate excited states, as well as from the final reservoir in the conduction band minimum, the electrons are reexcited by a second single-photon absorption process to final states above the vacuum level.

A second point of interest in this paper concerns the diffusion properties of hot carriers during UV excitation. The rise in lattice temperature during UV excitation at higher fluence levels depends sensitively upon the distance L over which carriers have diffused into the bulk before substantial energy is transferred to the phonons. In a simple approximation this distance L can be treated as a diffusion length [11]

$$L = (D_a \tau)^{1/2} \qquad (4a)$$

with the diffusion coefficient in the classical model given by

$$D_a = \frac{2 k T_c \tau_e \tau_h}{m^*_e \tau_h + m^*_h \tau_e} \qquad (4b)$$

In these equations all quantities refer to hot carriers. In

(4a) τ is the energy relaxation time for such carriers, and in eq. (4b) τ_e and τ_h are the momentum relaxation times; m^*_e and m^*_h are the effective carrier masses, and T_e is the temperature of the hot carriers. As a consequence of hot carrier diffusion, the heating rate at the surface by UV pulses is reduced by a factor $(L\,\alpha + 1)^{-1}$, where α is the UV absorption coefficient.

In numerical model calculations the influence of the critical hot carrier diffusion length L on the heating rate and the laser fluence necessary to melt the surface have been analyzed. The laser fluence required to raise the surface lattice temperature to the melting point has been computed as a function of L. Comparison with the experimental value F_{th} = 25 mJ/cm^2 to melt silicon with UV photons indicates a hot carrier diffusion length of $L = 1 \times 10^{-6}$ cm or a $D_a\tau$ product of 10^{-12} cm^2. From optical investigations it is known that the energy relaxation time τ is in the order of 1 ps. As an immediate consequence the threshold value analysis reveals a rather low ambipolar diffusion coefficient $D_a \approx 1$ cm^2/s for the hot carriers (comparable to that in metallic conductors). This should be compared with the room temperature value at low densities (D_a = 20 cm^2/s). In agreement with transport measurements at high carrier densities [12], but in disagreement with a series of theoretical predictions [11], the ambipolar diffusion of hot carriers is lower than the room temperature value. A drastic

decrease of the momentum relaxation times $\tau_{e,h}$ down to 1×10^{-15} s occurs in UV laser-induced electron-hole plasmas at fluences close to the melting threshold, outweighing the linear dependance of D_a on the electron temperature T_c. This momentum relaxation time is two orders of magnitude lower then the value determined by carrier -lattice scattering ($\approx 2 \times 10^{-13}$ s). Similar low values have been found in optical investigations of the free carrier absorption cross sections at high excitation level [13]. These extremely short momentum relaxation times are consistent with the fast energy losses of the electron-hole plasma to the phonons observed in earlier investigations using 2.33 eV excitation. Whether this reduction of the hot carrier diffusion mobility is due to the extremely high excess energy of the initially-created electron-hole pairs or to a density-dependent phenomenon like electron hole scattering cannot be answered conclusively at the present state of the investigation. More theoretical work on the basis of the data presented in this paper is necessary to clarify this point.

In conclusion, three distinct regimes in the photoemission are observed in ps experiments using 4.66 eV photons. The quadratic photoelectric response is closely related to the formation of an electron-hole plasma during the pulse providing the intermediate states from where electrons are more easily excited into the vacuum level. The distance which the initially hot carriers can travel before they lose their energy to the lattice phonons indicates extremely short momentum relaxation times under excitation levels

close to the threshold fluence for melting.

Acknowledgements

This work was supported by the U.S. Office of Naval Research under contract N00014-83K-0030 and by the Joint Services Electronics Program of the U.S. Department of Defense under contract N00014-75-C-0648.

References

[1] J.M.Liu, H.Kurz and N.Bloembergen, Appl. Phys. Letters 41,693 (1982)

[2] L.A.Lompre, J.M.Liu, H.Kurz and N.Bloembergen, Appl. Phys. Letters 44, 3 (1984)

[3] C.V.Shank, R.Yen, and C. Hirlimann, Phys. Rev. Letters, 50,454,(1983)

[4] C.V.Shank,R.Yen and C.Hirlimann, Mat. Res. Soc. Symp. Proc. 23, 53 (1984)

[5] J.H.Bechtel, W.Lee Smith and N. Bloembergen, Phys. Rev. B 15, 4457 (1977)

[6] M.Bensoussan, J.M.Moison, B.Stoesz and C.Sebenne, Phys. Rev. B 23, 992 (1981)

[7] A.M.Malvezzi, J.M.Liu and N.Bloembergen, Mat. Res. Soc. Symp. Proc. 23, 135 (1984)

[8] J.M.Liu, H.Kurz and N.Bloembergen, Mat. Res. Soc. Symp. Proc. 4, 23 (1982)

[9] R.M.Broudy, Phys. Rev. B 1, 3430,(1970)

[10] J.M.Bechtel, J.Appl. Phys. 46, 7585 (1975)

[11] E.Yoffa, Phys. Rev. B 21, 2415 (1980)

[12] F.Berz, R.W.Cooper and S.Fagg, Solid State Electronics 22, 293 (1978)

[13] H.Kurz, A.M.Malvezzi, L.A.Lompre, Proc. of the 17th International Conference on Physics of Semiconductors, S.Francisco, Ca, August 1984

Figure Captions

Fig. 1 Emitted charge density versus fluence at 266 nm for Si(111) samples. The dashed line refers to the calculated linear and quadratic photoelectron effect with the coefficients given in the text.

Fig. 2 Ratio Q/E_n of the negative charge emitted by Si(111) over total laser energy at 266 nm versus total laser fluence for two pulses separated by the interval τ shown.

Fig. 3 Correlated photoelectron signal versus daly time τ for 266 nm illumination of Si(111) in region I. The data are normalized to the $\tau = \infty$ results.

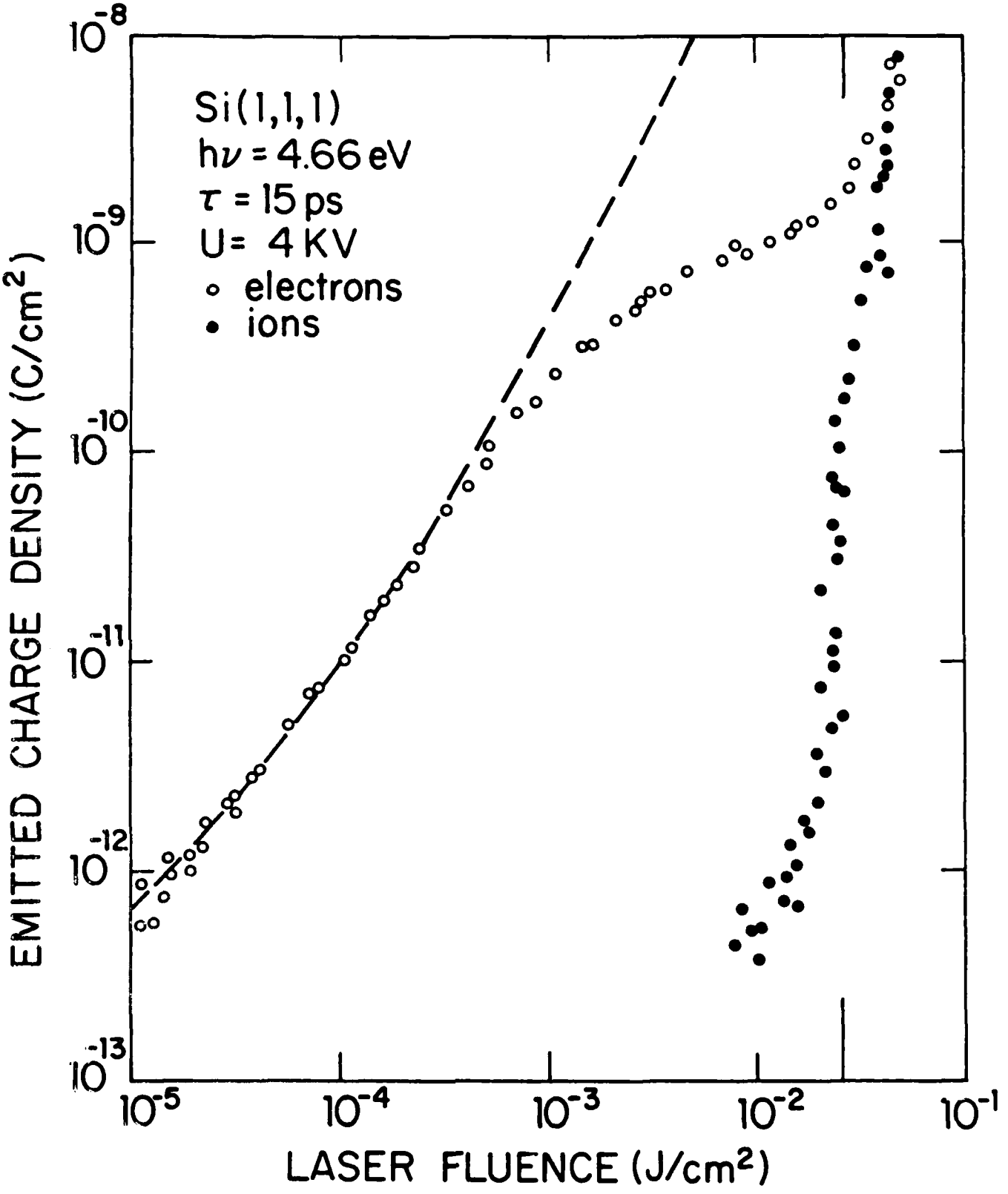
Si(1,1,1)
hν = 4.66 eV
τ = 15 ps
U = 4 KV
electrons
ions
EMITTED CHARGE DENSITY (C/cm²)
LASER FLUENCE (J/cm²)
10⁻⁸
10⁻⁹
10⁻¹⁰
10⁻¹¹
10⁻¹²
10⁻¹³
10⁻⁵
10⁻⁴
10⁻³
10⁻²
10⁻¹

Figure 1

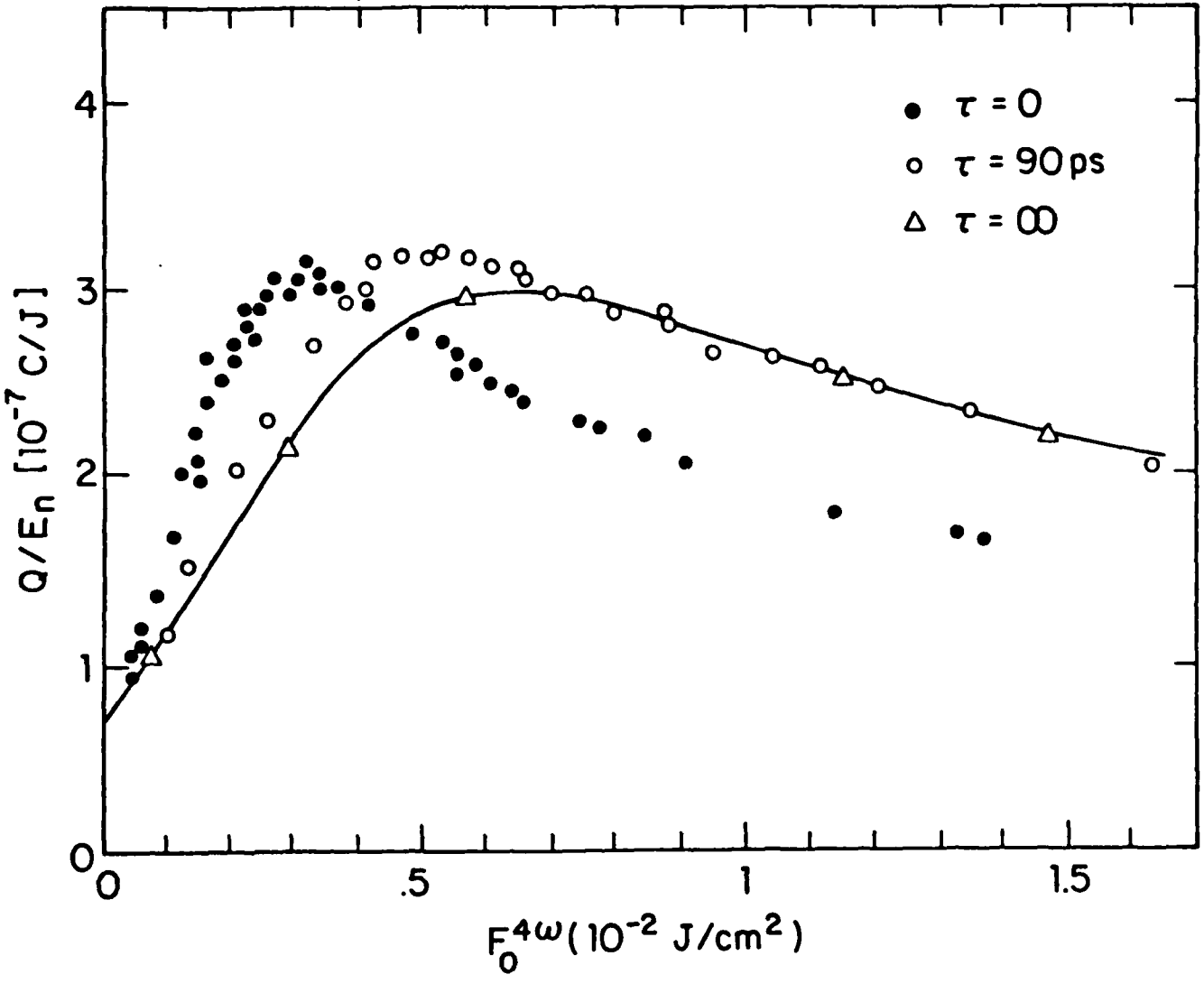

Figure 2

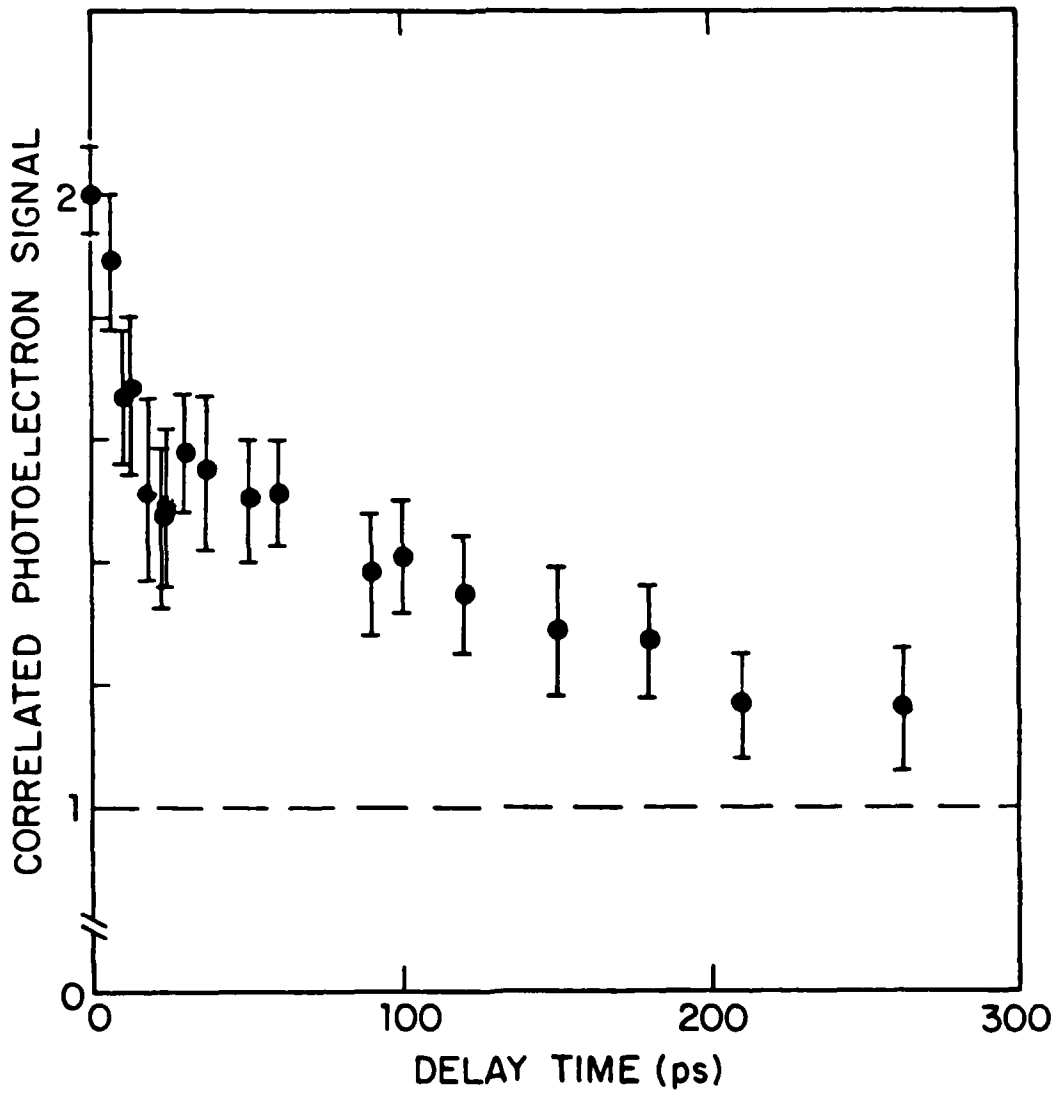
CORRELATED PHOTOELECTRON SIGNAL
2
1
0
0
100
200
300
DELAY TIME (ps)

Figure 3

Appendix II

Journal of Non-Crystalline Solids 61 & 62 (1984) 767-772
North-Holland, Amsterdam

PICOSECOND PULSED LASER-INDUCED MELTING AND GLASS FORMATION IN METALS

Chien-Jung LIN, Frans SPAEPEN and David TURNBULL

Division of Applied Sciences, Harvard University, Cambridge, Mass. 02138*

Irradiation of a solid surface by a picosecond laser pulse leads to melting of a thin overlay, and subsequent quenching at rates of 10^{12}K/s or higher. This technique is also one of the few available for superheating a crystal above its melting temperature. The ultra-fast quenching rates permit the formation of new metallic glasses. Work on the Fe-B and Ni-Nb system is reviewed, and new results on the Mo-Ni, Mo-Co and Nb-Co systems are reported. In all cases, glasses are formed below the T_0-line, indicating that partitionless crystallization is usually at least partially diffusion controlled due to the change in short range order upon crystallization; only in the simplest structures, such as disordered f.c.c. solutions, are the partitionless crystallization kinetics fast enough to preclude glass formation.

1. INTRODUCTION

When a solid metallic surface is irradiated by a laser pulse of duration t_p, the energy is deposited in a layer of thickness α^{-1}, where α is the absorption coefficient; for metals, α^{-1} is on the order of 100Å. During the pulse, a layer of thickness $(2D_{th}t_p)^{1/2}$ is heated up by thermal conduction, where D_{th} is the thermal diffusivity. For metals D_{th} is on the order of 0.5cm^2/sec, which, for a 30ps pulse, corresponds to an initial heated layer of about 500Å thick. For a typical laser fluence of about 0.5 J/cm^2 and a metallic reflectivity, the temperature rise in this (molten) layer is estimated to be several thousand degrees. The fraction of the energy lost due to evaporation is small ($< 10^{-3}$) since it is limited by the evaporation kinetics and the short duration of the process. The rest of the energy is conducted into the bulk, leading to further melting to a total depth on the order of 1000Å. Further cooling then leads to resolidification of this layer, either by crystallization or glass formation. Heat flow calculations and direct observations of melting (e.g. in Si, using time-resolved reflectivity) show that the total lifetime of the melt for a 30ps pulse is about 1ns;[1] given that the temperature drop is on the order of 10^3K, this corresponds to an average cooling rate during solidification on the order of 10^{12}K/s. Since most "conventional" quenching techniques, such as melt spinning, produce cooling rates of about 10^6K/s, it is expected that pulsed laser quenching can lead to the formation of new metastable phases. A review of the fundamentals of pulsed laser interactions with solid surfaces has been given by

*This work has been supported by the Office of Naval Research under Contract No. N00014-83-K-030.

Bloembergen.[2]

2. MELTING AND SOLIDIFICATION KINETICS

The general formalism of these transformations has been reviewed by Spaepen and Turnbull.[3,4] The velocity of the crystal-melt interface, u, may be approximated by:

$$u \simeq u_0(T_M - T_i)/T_i \tag{1}$$

where T_M is the melting temperature and T_i the temperature at the interface; u_0 is a velocity determined by the kinetics of the melting or crystallization process: for pure metals, when these processes are collision-limited, u_0 is approximately equal to the speed of sound, u_s; for alloys, where diffusive rearrangements may be important $u_c \approx D/\lambda$ (D: diffusivity; λ: interatomic distance).

The heat flow associated with melting or solidification leads to a second expression for u:

$$u = -\kappa \bar{V} \nabla_i T/\Delta H_c \tag{2}$$

with κ: thermal conductivity; $\bar{V}$: molar volume; $\nabla_i T$: temperature gradient at the interface; ΔH_c: molar heat of crystallization. The combination of eqs. (1) and (2) then leads to a determination of the interface temperature, T_i. If the interface kinetics are fast compared to the rate of heat removal (or heat supply, for melting), as is the case in most conventional metal processing, the process is called *heat flow limited*, and T_i is only slightly different from T_M. If, however, the interface kinetics are slow (e.g. if limited by diffusional rearrangements), and the rate of heat removal (or supply) is fast (e.g. due to the very steep thermal gradients in ps pulsed laser annealing), the process becomes *interface limited*, and T_i is very different from T_M.

If the kinetic processes at the interface are collision-limited, as in crystallization of pure metals, T_i differs from T_M by only a few tens of degrees even in ps pulsed laser quenching. It should be noted that the thermal gradients during the melt-in phase following the pulse are much steeper than during solidification: $\nabla_i T \approx 10^3 K/(2D_{th}t_p)^{1/2} \approx 10^{11} K/m$. According to eq. (2) this corresponds to a heat-flow limited velocity on the order of 2000m/s, i.e., on the same order of u_s. Eq. (1) therefore predicts a substantial overheat at the interface. Consequently, picosecond pulsed laser heating is one of the few methods available for superheating metallic crystals.

For metallic glass formation, it is clear that T_i must fall far below T_M during cooling, and that hence diffusion-limited interface kinetics seem required. The solidification velocity, u, in ps laser quenching can be estimated, from the melt depth ($\sim$ 1000Å) and the lifetime of the melt ($\sim$1 ns),

to be at least 100m/s. The distance that an alloy atom can travel diffusively during the passing of the solidification front, $(D\tau/u)^{1/2}$, is then less than an interatomic distance. The solidification process is therefore a "partitionless" one. Partitionless crystallization is only thermodynamically possible if the temperature drops below the so-called "T_0-line" in Fig. 1, i.e., the line where the free energy of the crystal and the undercooled liquid solutions are equal.[5]

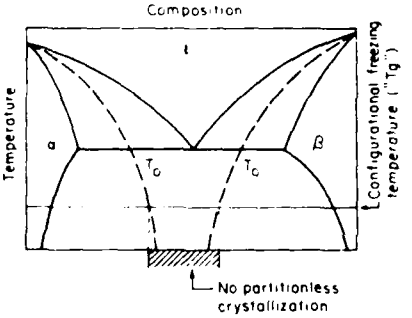

FIGURE 1
Schematic illustration of the T_0-lines (equal free energy for liquid and crystal) in a simple eutectic phase diagram.

This "solute trapping" process has been discussed in detail by Aziz.[6] If the configurational freezing temperature ("T_g") of an alloy lies above the T_0 lines, glass formation is expected if no intermetallic phases can be formed; the complex structure of most of these phases, however, usually requires diffusion-like rearrangements that slow down the crystallization kinetics. Since partitionless crystallization into the primary solutions is often a very fast process, it has been proposed that the T_0-lines represent the limits of glass formation.[7,8] However, as will be demonstrated below, this is only the case for the simplest crystal structures, such as disordered f.c.c. alloys, where the kinetics may approach the collision limit. If, as is often the case, reconstruction of the short-range order is required, the crystallization kinetics are at least partially diffusion-limited and glass formation can occur even below the T_0-lines.

3. EXPERIMENTAL PROCEDURE

The main experimental problem in studying the solidification of binary alloys in the ps pulse regime is obtaining a homogeneous melt in its 1 ns lifetime, since the mixing length corresponding to this time, $(Dt)^{1/2}$, is only 30Å. The phases in the alloy must therefore be dispersed on this scale. We have solved this problem[9,10] by preparing the starting alloy as a ~1000Å thick com-

positionally modulated film with a wavelength shorter than the mixing length. After irradiation, the film is floated off the substrate and is ready for transmission electron microscopy without further thinning. This procedure is also very flexible in that it allows preparation of a continuous range of compositions using only two sources or sputtering targets.

4. RESULTS

In earlier papers[9,10] we showed that Fe-B alloys with a B content as low as 5 at.% can be made glassy by psec laser quenching, whereas "conventional" quenching requires a minimum of 12 at.%B. Below 5 at.%B, the alloys solidify as supersaturated b.c.c. crystals. Estimates of the T_0-line in the Fe-B system, based on regular solution modeling and on the devitrification mechanism, show that all the *new alloys* obtained by laser quenching were formed below the T_0-line.

Similar observations were made for the Ni-Nb system,[11] where glasses were formed by laser quenching in the 23-82 at.%Ni range, with (supersaturated) f.c.c. and b.c.c. crystalline solid solutions outside this range; the glass formation range in "conventional" quenching[12] is only 40-70 at.%Ni, and corresponds roughly to the range between the T_0-lines. Again, laser quenching demonstrated that glasses could still be formed far *below* the T_0-lines.

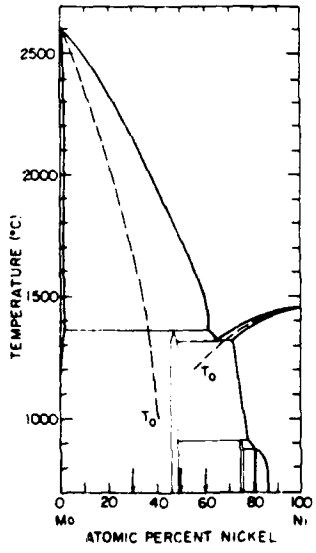

FIGURE 2
Molybdenum-nickel phase diagram, indicating estimated T_0-lines for the primary solid solutions. Glasses have been formed by laser irradiation at the three compositions indicated by arrows.

We also report here new results on glasses formed in the Ni-Mo, Co-Mo and Co-Nb systems. Figure 2 shows the Mo-Ni phase diagrams with estimated T_0-lines for the primary solid solutions. For three compositions, with 30, 50 and 60 at.%Ni, ps laser quenching produced the amorphous phase. Note that in two cases glasses are formed below the T_0-line, and that the δ(MoNi) intermetallic is not formed upon quenching the alloy between the T_0-lines. Similar alloys, with 35, 50 and 65 at.%Ni, had been made amorphous by Liu *et al*[13] by ion mixing of multi-layer films of the

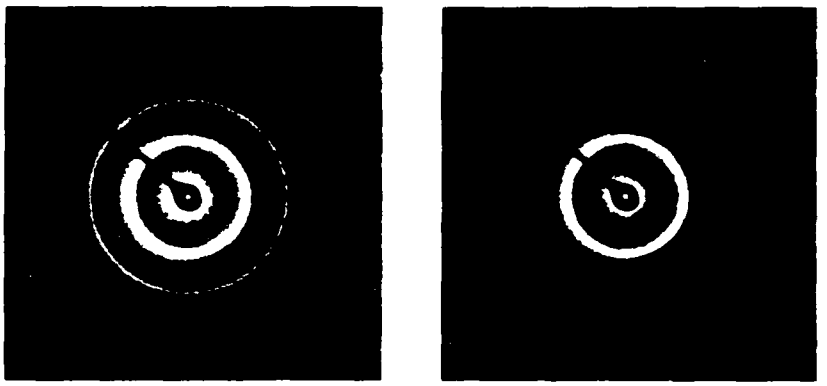

(a) (b)

FIGURE 3
Electron diffraction patterns of an as-deposited (a) and laser-irradiated (b) compositionally modulated film of average composition $Mo_{55}Co_{45}$.

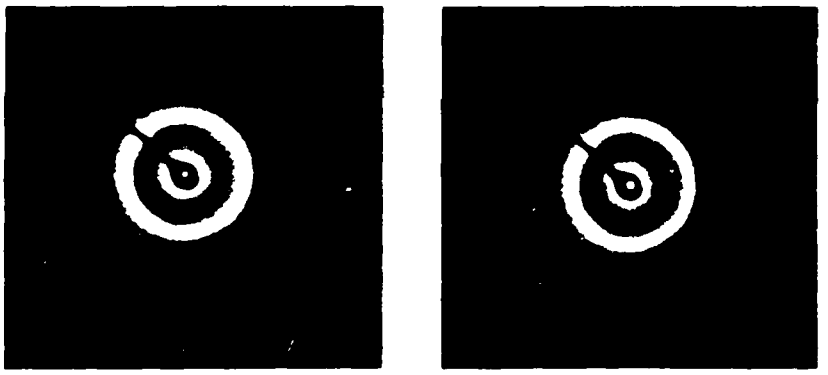

(a) (b)

FIGURE 4
Electron diffraction patterns of an as-deposited (a) and laser-irradiated (b) compositionally modulated film of average composition $Nb_{40}Co_{60}$.

crystalline elements. In the 60 at.%Ni alloy, we observed some microcrystals, but only near the center of the laser-irradiated spot; in the 30 at.%Ni alloy some crystals (b.c.c.) were observed at the edge of the spot, but not in the center; in the 50 at.%Ni alloy the entire spot was amorphous. A possible explanation of the difference in the occurrence of the crystals may be that crystals at the edge in the 30 at.%Ni alloys grow epitaxially on the only

partly melted modulated film (the beam has a Gaussian intensity profile), whereas in the 60 at.%Ni alloy the higher quench rate at the edge suppresses growth while at the slower cooling center new crystals can nucleate on the substrate. Figures 3 and 4 show the diffraction patterns of as-deposited and irradiated $Mo_{55}Co_{45}$ and $Nb_{40}Co_{60}$ alloys. In both cases, fully glassy phases are formed upon irradiation. To our knowledge, Co-Mo amorphous alloys had so far not been produced by liquid quenching; Liu *et al.*[13] have produced amorphous alloys with 65 and 35 at.%Co by ion mixing. It is interesting that the as-deposited modulated Nb-Co film is entirely amorphous, whereas the as-deposited Mo-Co film is entirely crystalline, although both were prepared by sequential sputter deposition of the crystalline elements. Since both systems are clearly glass formers, and since the sputter-induced mixing is probably similar for both films, the occurrence of the as-deposited amorphous film may be the result of enhanced solid state interdiffusion between the layers, as observed in La-Au.[14]

REFERENCES

1) J.M. Liu, Thesis, Harvard University, 1982.

2) N. Bloembergen, in: Laser-Solid Interactions and Laser Processing, eds. S.D. Ferris, H.J. Leamy and J.M. Poate (Academic Press, New York, 1979) p. 1.

3) F. Spaepen and D. Turnbull, ibid., p. 73.

4) F. Spaepen and D. Turnbull, in: Laser Annealing of Semiconductors, eds. J.M. Poate and J.W. Mayer (Academic Press, New York, 1982) p. 15.

5) J.C. Baker and J.W. Cahn, in: Solidification, eds. T.J. Hughel and G.F. Bolling (ASM, Metals Park, Ohio, 1971) p. 23.

6) M.J. Aziz, J. of Appl. Phys. *53*, 1158 (1982).

7) T.B. Massalski, in: Proc. 4th Int. Conf. on Rapidly Quenched Metals, eds. T. Masumoto and K. Suzuki (Jap. Inst. Metals, 1982) p. 203.

8) W.J. Boettinger, ibid., p. 99.

9) C.-J. Lin and F. Spaepen, Appl. Phys. Lett. *41*, 721 (1982).

10) C.-J. Lin and F. Spaepen, in: Chemistry and Physics of Rapidly Solidified Materials, eds. B.J. Berkowitz and R. Scattergood, TMS-AIME Symposia Proc., in press.

11) C.-J. Lin and F. Spaepen, submitted to Acta Met.

12) R.C. Ruhl, B.C. Giessen, M. Cohen and N. Grant, Acta Met. *15*, 1693 (1967).

13) B.X. Liu, W.L. Johnson, M.A. Nicolet and S.S. Lau, Appl. Phys. Lett. *42*, 45 (1983).

14) R.B. Schwarz, W.L. Johnson, and B.M. Clemens, this volume.

Appendix 12

PARTITIONLESS CRYSTALLIZATION AND GLASS FORMATION IN Fe-B ALLOYS DURING PICOSECOND PULSED LASER QUENCHING

Frans Spaepen and Chien-Jung Lin*
Division of Applied Sciences, Harvard University, Cambridge, MA 02138

Résumé - La vitrification, par trempe au laser à durée de picosecondes, des alliages Fe-B contenant au moins de 5 at.% B est expliquée quantitativement par une transition d'une croissance cristalline limitée par collision atomique, à une croissance limitée par diffusion atomique. La ligne T_o pour la solidification de la phase c.c. dans le liquide, sans rédistribution des constituants, est calculée utilisant la théorie des solutions régulières et le diagramme de phases.

Abstract - Glass formation in picosecond laser quenching of Fe-B alloys containing a minimum of 5 at.% B is explained quantitatively by a transition from collision-limited to diffusion-limited crystal growth. The T_o line for partitionless growth of the fcc phase from the liquid is calculated from regular solution theory and the equilibrium phase diagram.

1 - INTRODUCTION

The process of energy deposition, heating and colling in pulsed laser processing has been discussed in detail by Bloembergen [1] and others [2-4]. Figure 1 illustrates

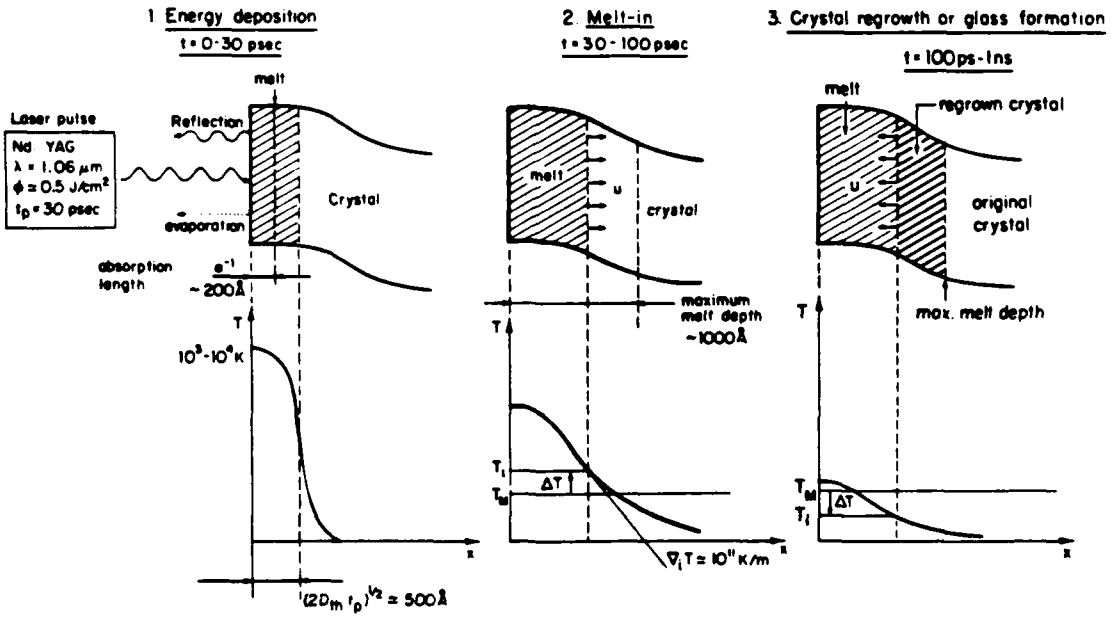

Fig. 1 - *Schematic diagrams illustrating the mechanism of pulsed laser quenching.*

the main stages of this process in a typical picosecond pulsed laser experiment: (i) energy deposition in a layer on the order of the absorption depth (200 Å), which spreads by heat conduction over a layer of thickness $(2D_{th}t_p)^{1/2}$ of about 500 Å

(D_{th}: thermal diffusivity; t_p: laser pulse length); since energy losses due to evaporation are negligible [4], this layer melts and its temperature rises to several thousand degrees; (ii) during the melt-in period, this overheat is spent as heat of fusion of more substrate crystal to a total thickness of about 1000 Å; due to the very high thermal gradients, the estimated melt-in velocity is extremely large (~1000 m/s); (iii) when the maximum melt depth is reached, the crystal melt interface reverses direction; depending on the relative rates of crystal growth and heat removal, the molten layer solidifies as a regrown crystal or a glass. The competition between the latter processes are analyzed in detail in this paper for the Fe-B system.

2 - THERMAL PARAMETERS

Although a number of sophisticated analyses of the heat flow during laser quenching are available, the order of magnitude of most of the relevant quantities can easily be estimated from essentially dimensional arguments. They are listed in Table I, together with the corresponding values for melt spinning. The starting point is

Table I

THERMAL PARAMETERS IN MELT QUENCHING

		Laser Quenching	Melt Spinning
Melt temperature	T_m(K)	10^3	10^3
Melt thickness	d(m)	10^{-7}	5×10^{-5}
Temperature gradient	∇T(K/m)	10^{10}	2×10^7
Cooling rate	$\dot{T}$(K/s)	10^{12}	4×10^6
Melt lifetime	τ(s)	10^{-9}	not applicable
Isotherm velocity	u_T(m/s)	100	0.2
Heat-flow limited crystal growth velocity	u_h(m/s)	230	0.5

that for both processes the melt temperature, T_m, is on the order of 10^3K, but the melt thickness, d, in laser quenching is much less (1000 Å) than in melt spinning (50 μm). The temperature gradient for heat removal can then be estimated as $\nabla T = T_m/d$, and the cooling rate as $\dot{T} = D_{th}\nabla T/d$ (D_{th}: thermal diffusivity, about 10^{-5} m^2/s for iron its alloys). The lifetime of the melt is then $\tau = T_m/\dot{T}$; this quantity is only relevant for laser quenching, and has in fact been checked experimentally by time resolved reflectivity measurements on Si, which has thermal characteristics similar to those of the metals [5,6]. The velocity of the isotherms in the specimen (the quantity to be compared to the crystal growth velocity later) is $u_T = \dot{T}/\nabla T$.

3 - THERMODYNAMICS AND KINETICS OF CRYSTAL GROWTH

The crystal growth velocity is determined by the balance of the removal of the heat of crystallization, ΔH, and the kinetics of the atomic processes at the interface. The heat flow limited crystal growth velocity is:

$$u_h = \frac{\kappa \bar{V} \nabla T}{\Delta H} \qquad (1)$$

(κ: thermal conductivity; $\bar{V}$ molar volume). Table I lists typical values for Fe, using $\Delta H = 15$ kJ/mole, $\kappa = 50$ W/m·K, and $\bar{V} = 7.1 \times 10^{-6}$ m^3/mole.

The crystal growth velocity depends on the interface kinetics and the thermodynamic driving force as follows [2]:

$$u = u_o\left[1 - \exp\left(\frac{\Delta G}{RT}\right)\right] \tag{2}$$

where ΔG is the free energy difference between crystal and melt, and the prefactor, u_o, depends on the nature of the atomic rearrangement needed for incorporation of a liquid atom into the crystal. If only simple collision of liquid atoms with the crystal surface is required (as in pure metals), the atomic jump frequency is the vibrational frequency in the liquid, so that u_o in this case is close to the speed of sound, u_s, in the liquid. In the analysis below, a rough, estimated value of 3500 m/s, independent of temperature, is used for u_s. If incorporation of the atoms in the crystal requires diffusional jumps (i.e., changes of nearest neighbors), u_o is approximately equal to D/λ (D: diffusivity in the liquid; λ: jump distance, taken as 2.6×10^{-10} m in Fe-based alloys). Note that diffusion-limited crystal growth does not necessarily imply long-range atomic transport; changes in short-range order that require changes in coordination can also only occur by diffusional jumps. The diffusivity used in the analysis below has the Fulcher-Vogel form, typical of liquid metal alloys:

$$D = D_o \exp\left(-\frac{B}{T-T'_o}\right) \tag{3}$$

with $D_o = 1.4 \times 10^{-8}$ m^2/s, $T'_o = 581$K, and $B = 1300$K.

The value of B is a rough estimate, similar to that observed in measurements on other metallic glasses and consistent with the free volume model [7]. D_o and T'_o were then calculated by assuming $D = 5 \times 10^{-9}$ m^2/s at the melting point of iron (1807K), and $D = 10^{-16}$ m^2/s at the crystallization temperature of B-rich Fe-B glasses (650K) [8].

Since the isotherm speed is several 100 m/s in the ps laser quench, the crystal growth velocity, u, must be at least this high to prevent glass formation. The time required to crystallize a monolayer at this speed, λ/u, is less than 1 ps. The distance an atom can diffuse in that amount of time, $(D\lambda/u)^{1/2}$, is then less than an interatomic distance. Crystallization must therefore be *partitionless*, i.e., without change in composition. In alloys, partitionless crystallization at a particular composition is thermodynamically possible only below a temperature, T_o, at which the free energies of melt and crystal are equal.

Assuming a simple regular solution model for both melt and crystal, the driving free energy for partitionless crystallization of an Fe-B alloy melt to a supersaturated b.c.c. phase is

$$\Delta G = G_c - G_\ell = x_{Fe}\Delta\mu^o_{Fe} + x_B\Delta\mu^o_B + x_{Fe}x_B(\varepsilon_c - \varepsilon_\ell) \tag{4}$$

(G_c, G_ℓ: free energies of crystal and liquid, respectively; x_{Fe}, x_B: atom fractions of Fe and B; ε_c,ε_ℓ: regular solution interaction parameters).

The standard free energy difference can be approximated by:

$$\Delta\mu^o_i = \mu^o_{i,c} - \mu^o_{i,\ell} = \Delta S_{f,i}(T - T_{M,i}) \tag{5}$$

($\Delta S_{f,i}$: entropy of fusion, and $T_{M,i}$: melting temperature of element i). The T_o temperature is found by setting ΔG equal to zero, which gives:

$$T_o = \frac{x_{Fe}x_B(\varepsilon_c-\varepsilon_\ell)+x_{Fe}T_{M,Fe}\Delta S_{f,Fe}+x_BT_{M,B}\Delta S_{f,B}}{x_{Fe}\Delta S_{f,Fe}+x_B\Delta S_{f,B}} \quad (6)$$

The interaction parameters can be determined by equating the chemical potentials of Fe and B at the equilibrium liquid and crystal compositions, which can be found on the phase diagram. For the Fe-B systems, $\varepsilon_c - \varepsilon_\ell$ was calculated to be -92 kJ/mole, independent of temperature. The other parameters can be found in all standard references [9]: $\Delta S_{f,Fe} = 7.6$ J/K mole; $\Delta S_{f,B} = 21.8$ J/K mole; $T_{M,Fe} = 1807$K; $T_{M,B} = 2300$K. The result is shown in Fig. 2. Note that only the b.c.c. phase is

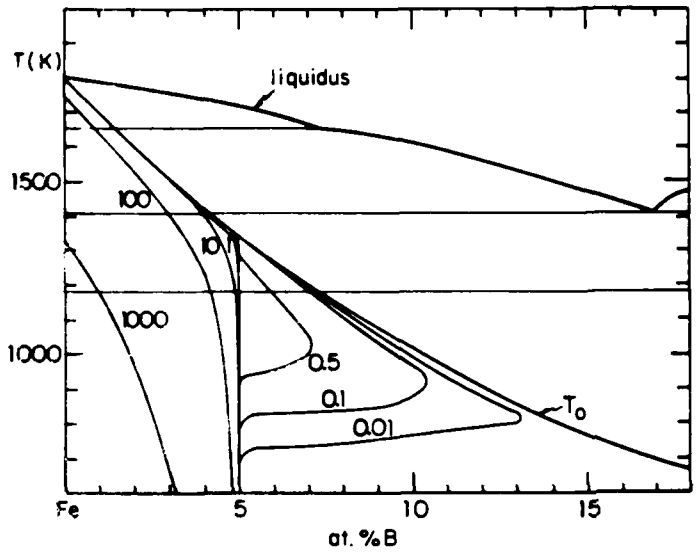

Fig. 2 - *The Fe-B phase diagram. The T_o line corresponds to the liquid→b.c.c. transition. The contours represent the crystal growth speed (in m/s) as a function of composition and interface temperature.*

being considered here; the f.c.c. Fe phase does not nucleate or grow. Inserting Eq. (6) into Eq. (4) gives an expression for the driving force.

$$\Delta G = (x_{Fe}\Delta S_{f,Fe} + x_B\Delta S_{f,B})(T - T_o) \quad (7)$$

Some authors [10,11] have assumed that partitionless crystallization is always a very fast process, and that therefore glass formation below the T_o line is prohibited. The Fe-B system is one of many in which this has experimentally been disproved.

4 - EXPERIMENTAL RESULTS

Fe-B glasses have been prepared by melt spinning in the 12-28 at.%B range [8,12,13]. Below 12 at.%B a b.c.c. supersaturated solution is formed. It is interesting to note that upon heating glasses with less than 18 at.%B first crystallize to the metastable b.c.c. solution, which then converts to the stable phase mixture of α-Fe and Fe_3B [8]. Our calculation shows that the composition corresponding to $T_o = 660$K (the crystallization temperature for an 18 at.%B glass) is 16 at.%B. Considering the approximate nature of the regular solution models, this agreement is quite satisfactory.

Glass formation in the Fe-B system has been studied under ps laser quenching conditions, using the following experimental technique [14,15]. On a copper substrate, first coated with a 1 μm thick Al film, a 1000 Å thick compositionally modulated film consisting of alternate layers of Fe and $Fe_{76}B_{24}$ was deposited by dual target

DC sputtering. The repeat length of the modulation was about 20 Å. By varying the relative thicknesses of the Fe and $Fe_{76}B_{24}$ layer, films with average compositions between 0 and 24 at.%B were prepared. These samples were irradiated with a 30 ps Nd:YAG ($\lambda = 1.06$ μm) laser pulse, with a beam diameter of about 100 μm and an average fluence of about 0.8 J/cm^2. The composition modulation wavelength was chosen on the order of the mixing length $(D\tau)^{1/2}$ in the liquid during the lifetime of the melt ($\tau = 1$ ns, Table I), to ensure homogeneity. After dissolution of the Al film in dilute NaOH, the irradiated film could be investigated directly by transmission electron microscopy without further thinning.

These experiments showed that ps laser quenching results in glass formation in alloys containing at least 5 at.%B. Alloys containing less than 5 at.%B crystallized as a b.c.c. solid solution. The solidification morphology of the 4 at.%B contained a small amount of glass/crystalline mixture near the top surface of the film [16]; this could have been the result of an interfacial instability that became possible at the last stages of solidification due to the decrease in the crystal growth velocity [17]; the associated redistribution of B then could result in glass formation in the B-rich regions.

5 - ANALYSIS

The sharp transition from partitionless crystal growth to glass formation at 5 at.%B can most easily be explained by a transition from a collision-controlled to a diffusion-controlled crystal growth mechanism. The short-range order in a metal-metalloid glass such as Fe-B, and hence also in the very undercooled melt, is known to be quite strong: each metalloid is surrounded by metal atoms only, in a coordination shell similar to that found in the intermetallic compounds [18,19]. The short-range order around the B atom in the b.c.c. solution, either substitutional or interstitial, is clearly very different. Reconstruction of the cluster containing the B atom therefore requires diffusive jumps. The formation of a glass with a minimum of 5 at.%B suggests that the size of this cluster is 20 atoms (i.e., each B atom and 19 of its nearest neighbors, which corresponds to the first and about half the second coordination shell of the B-atom [20]). The Fe atoms outside these clusters are assumed to make collisional jumps. The kinetic factor in Eq. (2) for the crystal growth speed can therefore be written for $x_B \leq 0.05$:

$$u_o = (20\ x_B)\ \frac{D}{\lambda} + (1-20\ x_B)u_s \quad . \tag{8}$$

For $x_B \geq 0.05$, the crystal growth speed is equal to the diffusive speed D/λ.

Figure 2 shows contours of the crystal growth speed, u, as a function of interface temperature and composition. The abrupt transition at 5 at.%B is obvious. Figure 3 shows as a function of composition, the total distance grown by the crystal if cooled at a constant rate form the liquidus temperature to 600K. The scale on the left hand side is for the "master curve" representing the product of this distance and the cooling rate. On the right hand side, the actual growth distances in melt spinning and laser quenching are shown. At 5 at.%B, the growth distance in ps laser quenching is on the order of 10 Å; most of a 1000 Å thick layer is therefore transformed to a glass, as observed in our experiments. At 12 at.%B, the growth distance in melt spinning is on the order of 1 μm, consistent with the experimentally observed glass formation in 50 μm thick ribbons. Figure 4 illustrates the same points in a slightly different way. For pure Fe and the 4 at.%B alloy, the crystal growth velocity rises above the isotherm velocity in ps laser quenching, thus preventing glass formation. For 5 at.%B, the crystal growth velocity rises above the isotherm velocity in melt spinning, but remains below the one in laser quenching. This is consistent with glass formation at this composition under the latter conditions, and failure to form a glass under the former. The crystal growth velocity for the 12 at.%B alloy lies below the isotherm velocity for melt spinning, in agreement with the observations.

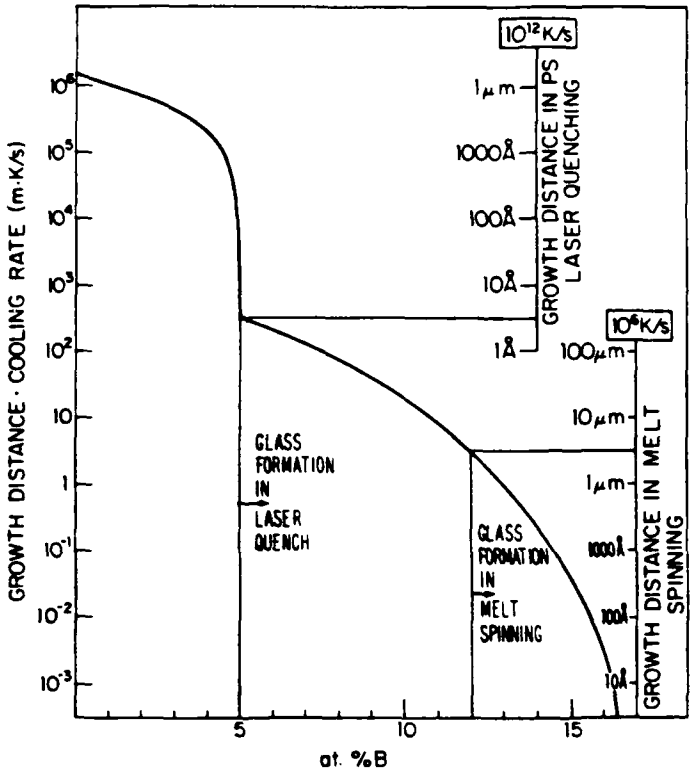

Fig. 3 - *Crystal growth distance upon continuous cooling of an* Fe-B *alloy, as a function of composition (see text for explanation of scales).*

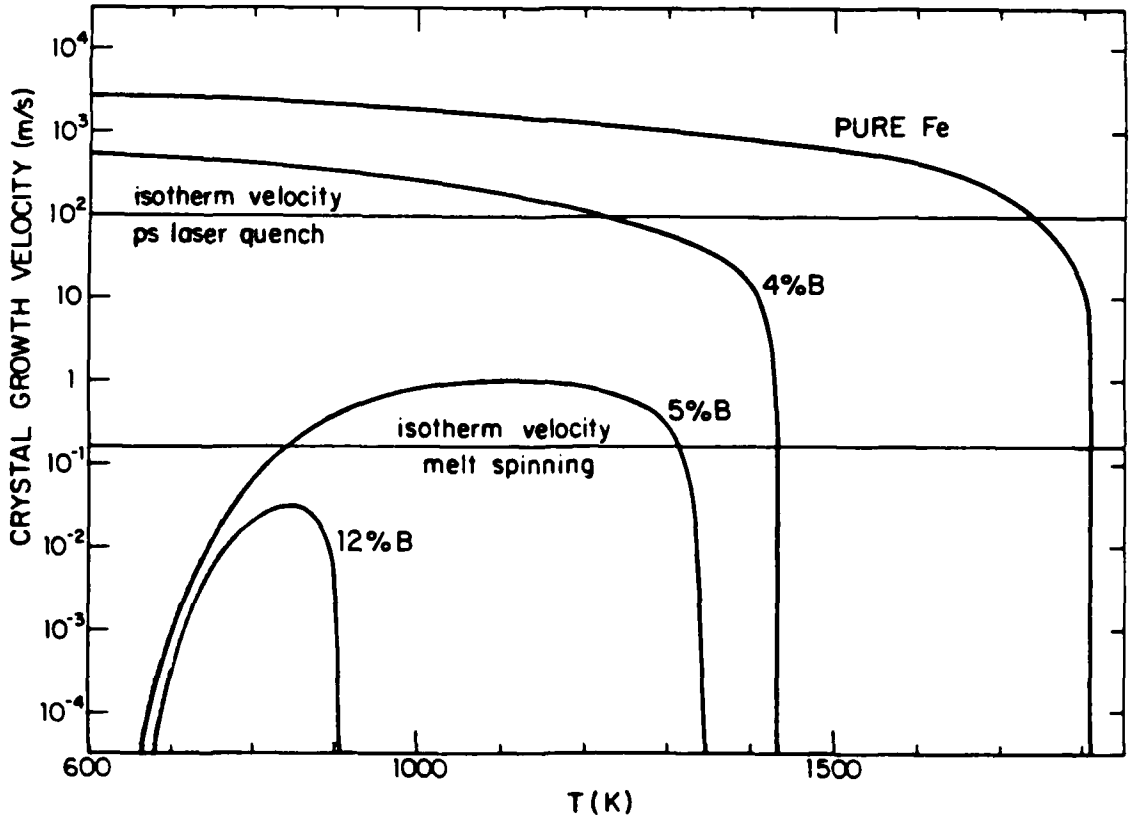

Fig. 4 - *Crystal growth velocity as a function of interface temperature for four compositions in the* Fe-B *system.*

There exists experimental support for the very large growth velocities for pure Fe shown on Fig. 4. In ps laser annealing experiments on pure Fe, the original sputtered film had a grain size of 500 Å. After irradiation the grain size was 1 μm or more [15,21]. Since these grains had to grow within the 1 ns lifetime of the melt, the lateral growth velocity must have been at least 500 m/s; the velocity may in fact be considerably larger yet, since the lateral growth is limited to the very early stages of the crystallization. Coriell and Turnbull [22] also found a very large kinetic factor, on the order of the speed of sound, in their analysis of dendritic growth velocity measurements in very undercooled Ni melts.

6 - CONCLUSIONS

The ps laser quenching experiments on Fe-B alloys have demonstrated that metallic glasses can be formed far below the T_o-line. This has also been observed in the Ni-Nb, Mo-Ni and Mo-Co systems [3]. Partitionless crystallization is therefore not necessarily a fast mechanism that forestalls glass formation as some authors have claimed [10,11]. For the Fe-B system, the glass formation range can be qualitatively accounted for by a transition from collision-controlled to diffusion-controlled crystallization at 5 at.%B. The analysis gives sensible values for the glass formation range in melt spinning as well. Detailed quantitative agreement on the latter process cannot be claimed, however, since the results at low temperature depend rather sensitively on the choice of the parameters in the Fulcher-Vogel equation for the diffusion coefficient. Crystal nucleation, which is probably more important in melt spinning than in laser quenching, has not been considered here. Unless the conditions are right for copious homogeneous nucleation (including the transient effects [23]), taking into account nucleation effects will result in a decrease of the fraction crystallized.

ACKNOWLEDGMENTS

This work has been supported by the Office of Naval Research under Contract No. N00014-83-K-0030.

REFERENCES

*Present address: IBM Research Laboratory, 5600 Cottle Road, San Jose, CA 95193.

1. N. Bloembergen, in "Laser-Solid Interactions and Laser Processing," eds. S.D. Ferris, H.J. Leamy, and J.M. Poate, AIP, N.Y. (1979), p. 1.

2. F. Spaepen and D. Turnbull, in "Laser Processing of Semiconductors," eds. J.M. Poate and J.W. Mayer, Academic, N.Y. (1982), p. 15.

3. C.J. Lin, F. Spaepen, and D. Turnbull, J. Non-Cryst. Solids, 61/62, 767 (1984).

4. C.J. Lin and F. Spaepen, in "Rapidly Solidified Metastable Materials," eds. B.H. Kear and B.C. Giessen, MRS Symp. Proc., North-Holland, Amsterdam (1984), in press.

5. J.M. Liu, Ph.D. Thesis, Harvard University (1982).

6. A.L. Lompré, J.M. Liu, H. Kurz, and N. Bloembergen, in "Energy Beam-Solid Interactions and Transient Thermal Processing," eds. J.C.C. Fan and N.M. Johnson, MRS Symp. Proc., North-Holland, Amsterdam (1984), in press.

7. F. Spaepen and A.I. Taub, in "Amorphous Metallic Alloys," ed. F.E. Luborsky, Butterworths, London (1983), p. 231.

8. R. Hasegawa and R. Ray, J. Appl. Phys., 49, 4174 (1978).

9. R. Hultgren, P.D. Desai, D.T. Hawkins, M. Gleiser, K.K. Kelley, and D.D. Wagman, "Selected Values of the Thermodynamic Properties of the Elements," ASM, Cleveland (1973).

10. T.B. Massalski, Proc. 4th Int. Conf. on Rapidly Quenched Metals, eds. T. Masumoto and T. Suzuki, Jap. Inst. Metals, Sendai (1982), p. 203.

11 W.J. Boettinger, *ibid.*, p. 99.

12. R. Ray and R. Hasegawa, Sol. St. Comm., 27, 471 (1978).

13 F.E. Luborsky and H.H. Liebermann, Appl. Phys. Lett., 33, 233 (1978).

14. C.J. Lin and F. Spaepen, Appl. Phys. Lett., 41, 721 (1981).

15. C.J. Lin and F. Spaepen, in "Chemistry and Physics of Rapidly Solidified Materials," eds. B.J. Berkowitz and R. Scattergood, TMS-AIME, N.Y. (1983), p. 273.

16. C.J. Lin and F. Spaepen, Scripta Met., 17, 1259 (1983).

17. J.W. Cahn, S.R. Coriell, and W.J. Boettinger, in "Laser and Electron Beam Processing of Materials," eds. C.W. White and P.S. Peercy, Academic, N.Y. (1980), p. 89.

18. G.S. Cargill III, Solid State Physics, 30, 227 (1975).

19. P.H. Gaskell, in "Glassy Metals II," eds. H. Beck and H.J. Güntherodt, Springer, Berlin (1983), p. 5.

20. E. Nold, P. Lamparter, H. Olbrich, G. RAiner-Harbach, and S. Steeb, Z. Naturforsch., 36A, 1032 (1981).

21. C.J. Lin, Ph.D. Thesis, Harvard University (1983).

22. S.R. Coriell and D. Turnbull, Acta Met., 30, 2135 (1982).

23. K.F. Kelton, A.L. Greer, and C.V. Thompson, J. Chem. Phys. 79, 6261 (1983).

Appendix 13

AN ION BEAM SPUTTERING APPARATUS FOR FABRICATION OF COMPOSITIONALLY MODULATED MATERIALS

F. Spaepen, A.L. Greer,* K.F. Kelton and J.L. Bell

Division of Applied Sciences, Harvard University,
29 Oxford Street, Cambridge, Massachusetts 02138, U.S.A.

August 1984

*Present address: Department of Metallurgy and Materials Science, University of Cambridge, Pembroke Street, Cambridge CB2 3QZ, U.K.

AN ION BEAM SPUTTERING APPARATUS FOR FABRICATION OF COMPOSITIONALLY MODULATED MATERIALS

F. Spaepen, A.L. Greer,* K.F. Kelton and J.L. Bell
Division of Applied Sciences, Harvard University, Cambridge, MA 02138

1. INTRODUCTION

Compositionally modulated materials are fabricated by repeated alternate deposition of very thin layers of different composition. Materials with composition modulation repeat lengths between a few Å and about 100Å are of interest for a number of scientific and technical applications as semiconductor devices, as x-ray mirrors, as samples for the study of diffusion at low temperature [1], and as starting materials for alloying in the liquid state following very fast pulsed laser heating [2]. Some of their physical properties, such as their elastic moduli [3] and magnetic properties [4], are unusual.

These materials have been produced by a variety of methods: molecular beam epitaxy [5] (mainly for semiconductors), vapor deposition [6,7], D.C. and R.F. sputtering [8,9], and chemical vapor deposition [10]. In this paper, we report on a new method that employs ion beam sputtering. Its main advantages, as will be explained below, are its simplicity, its flexibility (e.g. metals, semiconductors and insulators can be deposited under identical conditions), and convenient control.

---

*Present address: Department of Metallurgy and Materials Science, University of Cambridge, Pembroke Street, Cambridge CB2 3QZ, U.K.

2. DESCRIPTION OF THE APPARATUS

2.1 Overall design

The apparatus consists of a vacuum chamber containing two ion guns, one aimed at the target, the other aimed at the substrate. The target assembly contains four different targets that can be selected externally by a stepping motor. The deposition rate is monitored by a crystal oscillator. A feedback system from the deposition monitor to the target selection stepping motor controls the sequential deposition for the fabrication of compositionally modulated materials.

2.2 Chamber

The chamber is a vertical cylinder, 45cm tall and 41cm in diameter, made entirely of stainless steel. Figure 1 shows a view from the top of the cylinder. The bottom plate is connected to the vacuum system. The top plate contains the mechanical feedthroughs for the shutters and the target assembly, and the electrical feedthroughs for the ion probes in the gun shutters.

The substrate is placed on a water cooled support block on a removable flange. This flange also supports the crystal sensor and a second substrate holder; the latter is a cylinder that allows external insertion of a heating element. The centers of the targets of the substrate and of the substrate flange, and the ion beams are all in the same plane. The centers of the crystal sensor or the hot substrate can be placed in the same plane by rotating the substrate flange by 72° or 144° (2 or 4 boltholes), respectively. The substrate flange also contains a shutter by which the substrate or the crystal can be exposed, either separately or together.

The target assembly consists of a hollow 4-inch stainless steel cube

attached to a 2-inch vertical stainless steel tube that goes through a Ferrofluidics SC2000C hollow rotary feedthrough in the top plate of the chamber. The targets are 4-inch square plates that are screwed to the vertical faces of the cube. Cooling water is brought in through a 1-inch stainless steel tube inside the 2-inch tube and is removed through the space between the tubes. Outside the chamber, flexible hoses are used to conduct the cooling water, thus allowing 360°C rotation of the target assembly. The target assembly is surrounded by a shield that minimizes the spread of sputtered material around the chamber.

All the shutters in the chamber are moved through Ferrofluidics SB250AN086 1/4-inch rotary feedthroughs. Viton O-rings are used for all flanges, except for the flanges holding the ion guns, which are of the Conflat type with copper gaskets.

2.3 Ion guns

The two ion guns were obtained from Ion Tech, Inc. (Ft. Collins, Colorado), Model 2.5-1500-125. Both have 2.5cm diameter grids and are run by 2.5-1500-125EL power supplies. Both can be closed off by shutters containing ion probes. So far, only argon has been used as a sputter gas in either gun.

The gun aimed at the target is typically run at a beam voltage of 1500V and a current of 70-100mA. A feedback system (MKS 250B) that regulates the gas supply to the guns keeps the beam current constant. The chamber pressure during the run is between 5×10^{-5} and 2×10^{-4} torr.

The gun aimed at the substrate is used mainly for sputter cleaning prior to deposition, usually at a beam voltage of 300V and a current of 30mA. The gas flow to this gun is regulated by a three channel controller (MKS 254) that makes it possible to inject a mixture of three gases, which could be used for

controlled reaction with the sputtered species at substrate.

2.4 Vacuum system

The system is pumped by a 6-inch diffusion pump, separated from the chamber by a liquid nitrogen filled cold trap. The pressure is read by an ionization gauge located just below the vacuum post of the chamber. Without baking out the system, a base pressure of 3×10^{-7} torr is obtained.

2.5 Deposition control system

Figure 2 shows a schematic of the feedback system used to produce compositionally modulated films. The sputtering rate is monitored by an Inficon crystal sensor (vertical model IPN7504061) connected to an XTC monitor. The latter is connected via an RS-232 port, set at 1200 baud (bits per second), to an IBM-PC with 128K of memory and one double-sided/double-density disk drive. The PC program has as input parameters the total thicknesses and densities of the alternating layers. When the thickness of a layer reaches the preset value, the PC sends a set of pulses to a stepping motor translator (Superior Electric Slo-Syn type ST103), which makes the stepping motor (Slo-Syn M093-FC11, geared down by 8.5 using a toothed belt) turn the target assembly by 90° to the other target. This rotation takes 0.7 seconds, and requires no ramping of the speed. The instantaneous deposition rates, total sample thickness, deposition time, and the deposition rates averaged over a preset time interval, are continuously monitored and calculated, and are periodically printed out on a CRT monitor and a printer.

The PC has also been programmed to alternate targets based on preset time intervals; this is useful for very short modulation repeat lengths (1-2Å), for which the resolution of the crystal monitor is insufficient.

3. EXPERIMENTS

3.1 Deposition rates

A typical deposition rate, as measured at the sensor position, for pure copper, sputtered at a beam voltage and current of 1500V and 70mA, respectively, and a chamber pressure of 5×10^{-6} torr, is 2.5Å/sec. The deposition rate at the substrate position, which could be measured quite accurately from the x-ray modulation peak of the modulated films, was found to be between 10% and 30% greater than at the sensor position. The thickness variation across the substrate was also investigated by the x-ray technique and found to be less than 1%/cm at the center of the substrate.

3.2 Deposition of homogeneous films

Binary metal alloys were deposited from composit targets. An arrangement consisting of horizontal strips (1/4 to 1/2-inch wide) of one metallic component stretched across a 4-inch square backing plate of the other component was found to give the most reproducible results. Electron microprobe analysis showed the composition across the 2-inch substrate to be uniform.

Amorphous metal films of composition $Ni_{50}Zr_{50}$, $Cu_{82}Zr_{18}$ and $Cu_{65}Zr_{35}$ have been produced. $Cu_{90}Zr_{10}$ and $Nb_{93}Si_{7}$ films were microcrystalline.

Amorphous Si and Ge films were produced from 4-inch square cast polycrystalline targets that were, respectively, 0.5mm and 2mm thick. Best results were obtained by glueing these targets to an aluminum backing plate with a silver-epoxy conducting glue (Ablestik). The conductivity of the targets was high enough to make neutralization of the beam was unnecessary.

The argon incorporation, measured by electron microprobe analysis, was 1%

or less in most films. Contamination by stainless steel sputtered from the shield around the target assembly could be avoided by keeping the accelerator voltage around 100V, which limits the beam divergence.

The structure of the films was determined by a combination of x-ray diffraction, electron diffraction, and differential scanning calorimetry.

3.3 Compositionally modulated films

3.3.1 Metallic films. Films of Cu/Al, Cu/Ni, and Cu/Zr with repeat lengths between 10 and 100Å were produced from pure targets on glass or Si substrates. In most of the films the thicknesses of the two types of alternating layers were equal. The Cu/Al and Cu/Ni films, and the Cu/Zr films with repeat lengths above 65Å were polycrystalline. The Cu/Zr films with repeat lengths less than 65Å were amorphous; which is a manifestation of the formation of the amorphous phase by interdiffusion in the solid state between the pure elements observed, for example, in the La-Au, Ni-Zr and Ni-Nb systems [11-13] It is also an indication of a substantial amount of interdiffusion during the deposition process. Lin et al. [14] noticed a similar effect in the D.C. sputter deposition of Nb/Co films. Nevertheless, the amorphous Cu/Zr films were still compositionally modulated, as indicated by the presence of the characteristic x-ray peak. As made, the Cu/Al films showed a very strong first-order x-ray (000) modulation peak; the weakness of the second-order peak and absence of higher order peaks is further evidence of substantial rounding of the composition profile due to interdiffusion during deposition After five months of storage at room temperature, the intensity of the modulation peak in the Cu/Al films had decreased to a tenth of its original value; this is to be expected for polycrystalline non-textured layers, in which mixing can be enhanced substantially at low temperatures by grain boundary diffusion

along moving boundaries [7].

3.3.2 Metal-semiconductor films. Two sets of Nb/Si films were produced. Their average compositions and repeat lengths were, respectively: $Nb_{75}Si_{25}$, 32Å; and $Nb_{81}Si_{19}$, 48Å. The composition was adjusted by changing the relative thicknesses of the two layers. This method allows much better control of the average composition than sputtering from a composite target. Our technique is therefore quite useful for producing starting materials for laser mixing.

The Nb in the as-deposited films is polycrystalline with very small grains; the Si is amorphous.

3.3.2 Semiconductor films. Amorphous Si/amorphous Ge films, with equal layer thicknesses for both components were produced by sputtering from pure polycrystalline targets, with repeat lengths of 26, 47 and 64Å. They all showed strong first order modulation peaks. The full width at half maximum of this peak for the 64Å film, for example, was 0.25° (using Cr Kα radiation). This corresponds to a 10% variation in the layer thickness over the course of the deposition. The second and third order peaks in this sample were, respectively, 20 and 50 times less intense than the first peak; this again indicates substantial rounding of the profile due to interdiffusion during deposition. Nevertheless, these samples are very well suited for the study of interdiffusion in the a-Si/a-Ge system by further annealing. The sharpness of the composition profile can be improved by lowering the deposition rate; the width of the modulation peak can be decreased by improving the stability of the crystal sensor.

4. CONCLUSION

The system described in this paper provides a new method for producing

compositionally modulated films. Its advantages are:

(i) simple and relatively inexpensive design;

(ii) flexibility, in that it allows deposition of metals, semiconductors and insulators, without changes in the system; it also serves to deposit alloy films of good uniformity from inexpensive composite targets;

(iii) convenience of control, since the crystal oscillator feedback system makes it possible to ''dial in'' the required layer thicknesses.

Section 3 was intended as a survey of the capabilities of the system. Further details on the characterization and the physical properties of the materials discussed will be presented in separate papers.

5. ACKNOWLEDGMENTS

We thank P. Reader of Ion Tech, Inc. for his assistance with the design, and G. Pisiello and E. Sefner of the Harvard Scientific Instrument Shop for their skillful construction of the chamber. The sample preparation discussed in Section 3 is part of the research of R.C. Cammarata (NiZr, CuZr), C.A. MacDonald (Cu/Ni), T. Mizoguchi (Cu/Zr), S.M. Prokes (Si/Ge) and W.K. Wang (Nb/Si).

6. REFERENCES

1. For a review see ''Synthetic Modulated Structure Materials'', edited by L. Chang and B.C. Giessen, Academic Press, N.Y., in press.
2. C.J. Lin and F. Spaepen, Appl. Phys. Lett., 41, 716 (1982).
3. D. Baral in ''Modulated Structure Materials'', ed. by T. Tsakalakos, NATO ASI Series, Applied Science, Nijhoff, The Hague, in press.

4. G. Dublon, M.P. Rosenblum and W. Vetterling, IEEE Trans. Mag. 16, 1126 (1980).

5. L.L. Chang, L. Esaki, W.E. Howard, R. Ludeke, and G. Schul, J. Vac. Sa. Technol. 10, 655 (1973).

6. J. DuMond and J.P. Youtz, J. Appl. Phys., 11, 357 (1940).

7. H.E. Cook and J.E. Hilliard, J. Appl. Phys., 40, 2191 (1969).

8. M.P. Rosenblum, F. Spaepen and D. Turnbull, Appl. Phys. Lett., 37, 184 (1980).

9. A.H. Eltoukhy and J.E. Greene, Appl. Phys. Lett., 33, 343 (1978).

10. B. Abeles and T. Tiedje, Phys. Rev. Lett., 51, 2003 (1983).

11. R.B. Schwarz, K.L. Wong, and W.L. Johnson, J. Non-Cryst. Solids 61/62, 129 (1984).

12. B.M. Clemens, W.L. Johnson and R.B. Schwarz, J. Non-Cryst. Solids 61/62, 817 (1984).

13. C.C. Koch, O.B. Cavin, C.G. McKamey and J.O. Scarbrough, Appl. Phys. Lett., 43, 1017 (1983).

14. C.J. Lin, F. Spaepen and D. Turnbull, J. Non-Cryst. Solids, 61/62, 767 (1984).

FIGURE CAPTIONS

Figure 1. Schematic diagram of the ion beam sputtering chamber, viewed from the top.

Figure 2. Feedback system for the deposition of compositionally modulated materials.

Figure 3. Photograph of the ion beam sputtering system (left: power supplies; center: chamber and vacuum system; right: crystal monitor, computer, printer, monitor translator).

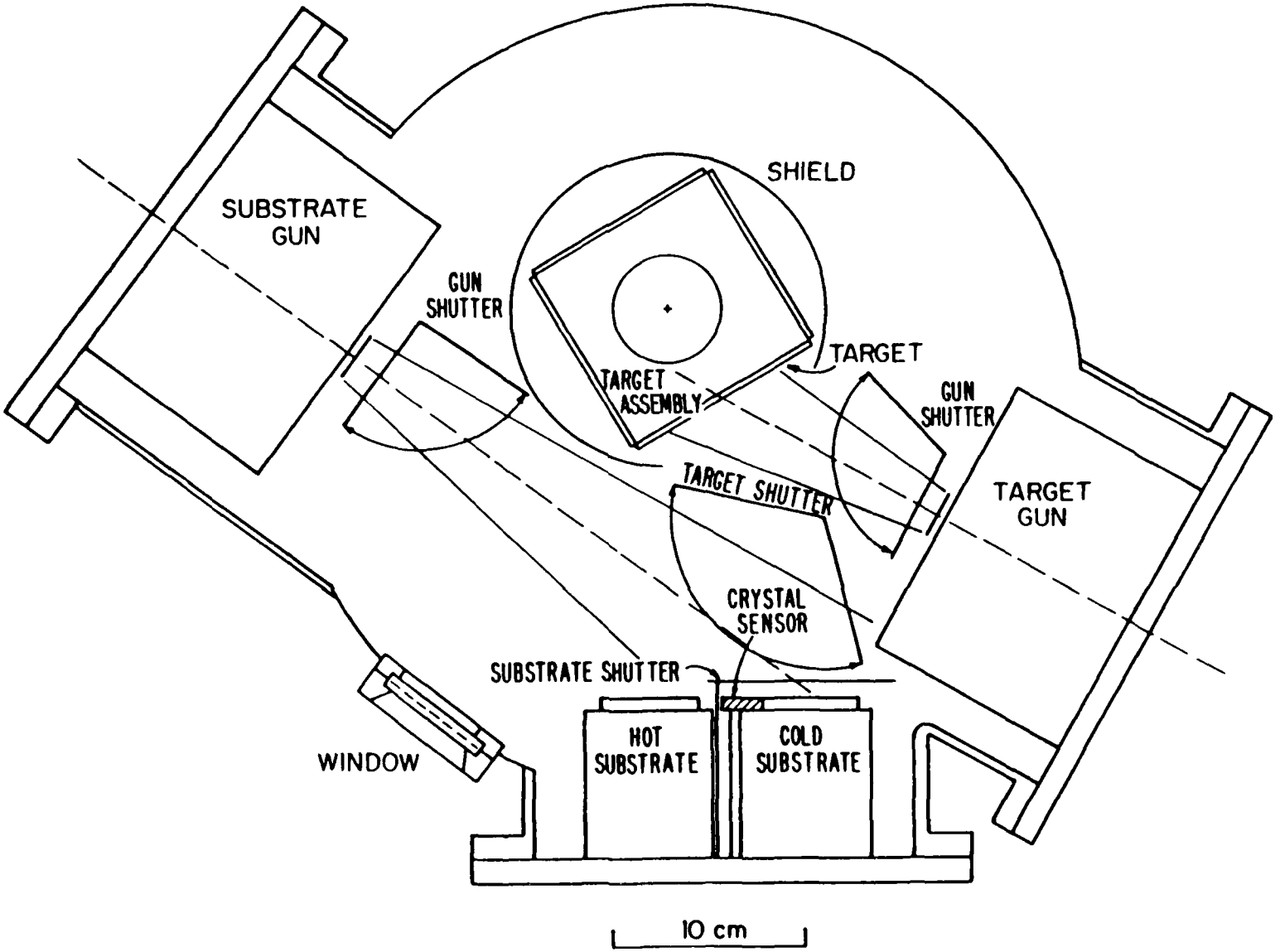

Figure 1. Schematic diagram of the ion beam sputtering chamber, viewed from the top.

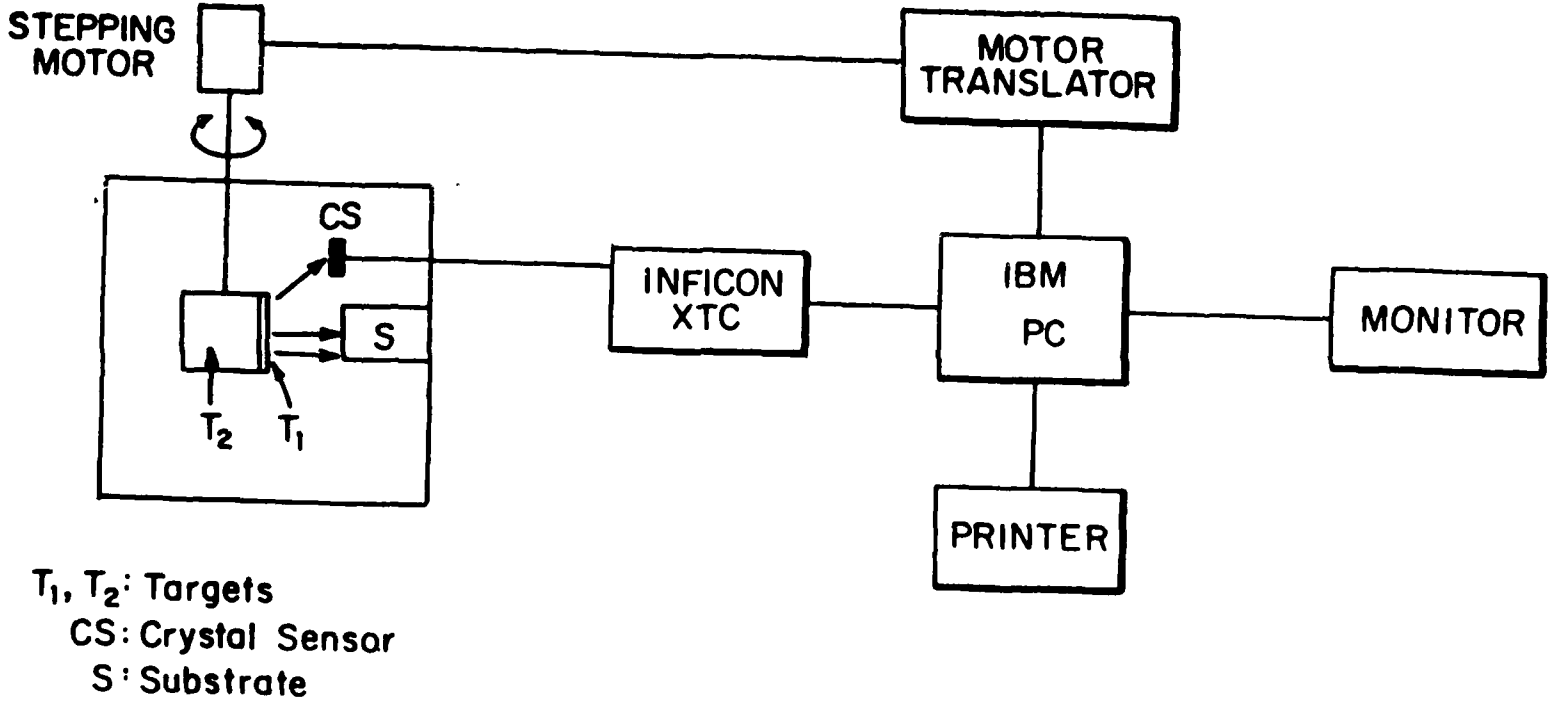

Figure 2. Feedback system for the deposition of compositionally modulated materials.

Figure 3. Photograph of the ion beam sputtering system (left: power supplies; center: chamber and vacuum system; right: crystal monitor, computer, printer, monitor translator).

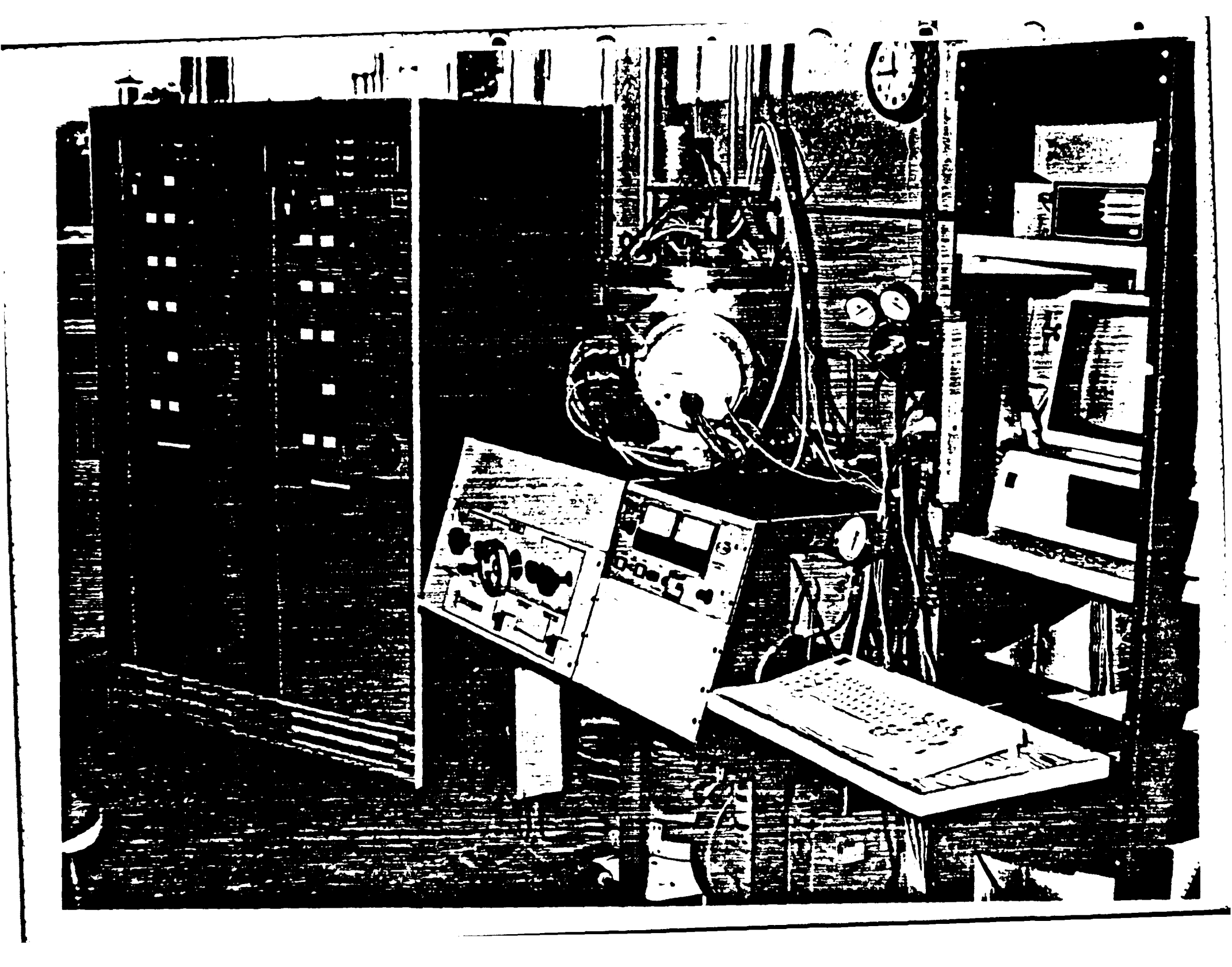

Figure 4. Photograph of the chamber (the target gun is on the right, the substrate flange is the center, the substrate gun on the left).

AD-A149 112 PICOSECOND LASER PULSE INTERACTIONS WITH METALLIC AND SEMICONDUCTOR SURFACES(U) HARVARD UNIV CAMBRIDGE MA DIV OF APPLIED SCIENCES N BLOEMBERGEN ET AL. 01 NNV 84 2/2

UNCLASSIFIED N00014-83-K-0030 F/G 20/5 NL

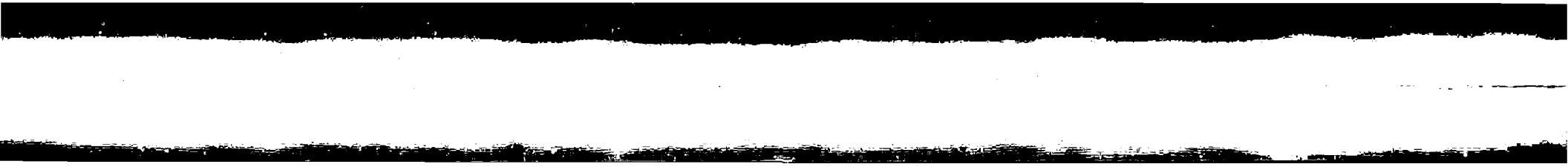

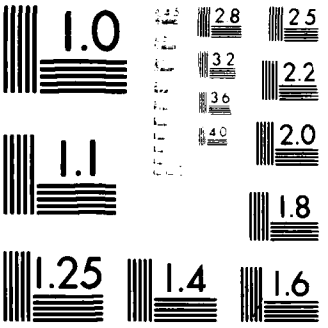

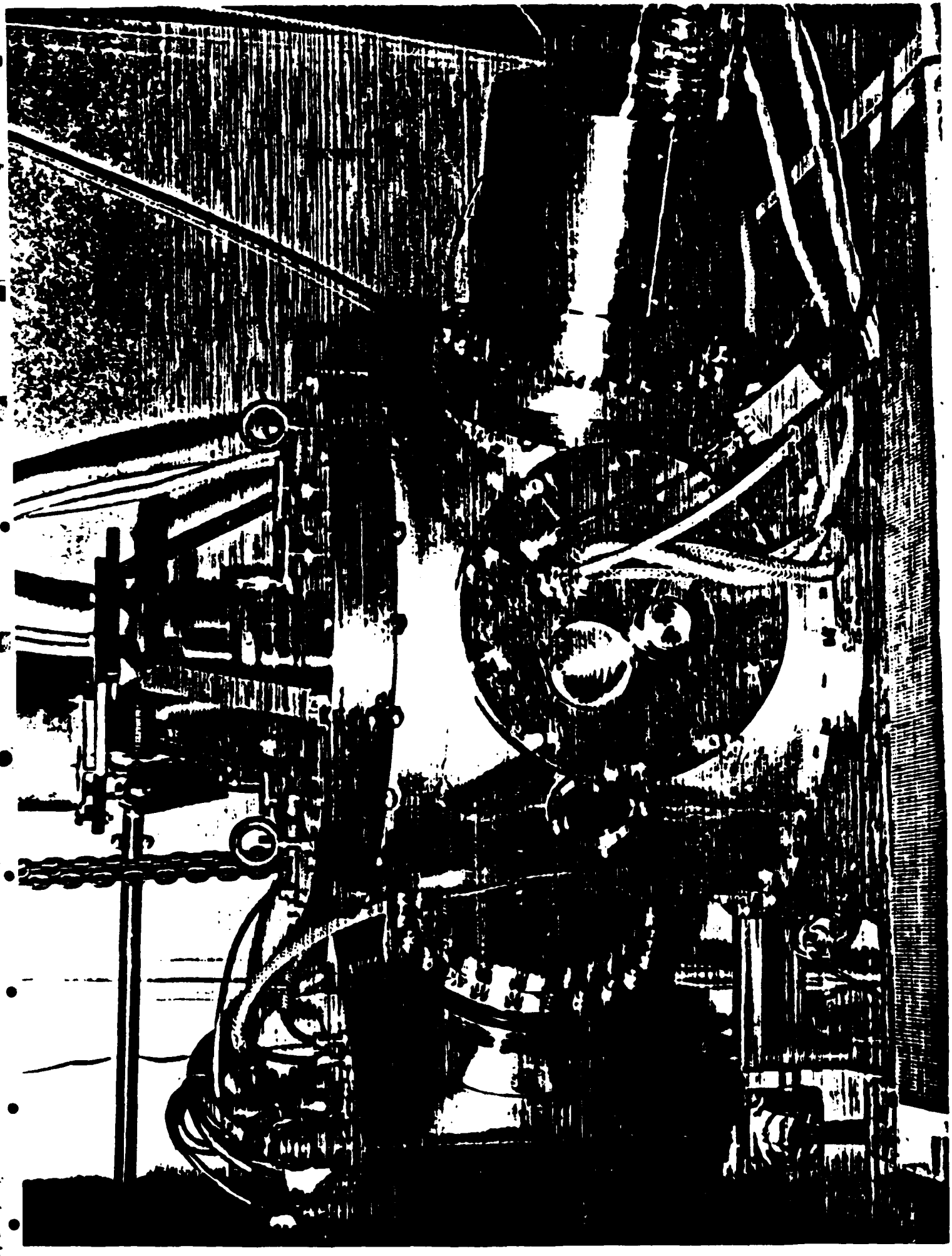

END

FILMED

2-85

DTIC